1972

Studies on rheo-optical properties of ethylene-propylene random copolymers.

Kenichi Baba
University of Massachusetts Amherst

STUDIES ON RHEO-OPTICAL PROPERTIES
OF
ETHYLENE-PROPYLENE RANDOM COPOLYMERS

A Dissertation Presented

By

KENICHI BABA

Submitted to the Graduate School of the
University of Massachusetts in
partial fulfillment of the requirements for the degree of

MASTER OF SCIENCE

June 1972

Major Subject: Polymer Science & Engineering

STUDIES ON RHEO-OPTICAL PROPERTIES OF ETHYLENE-PROPYLENE RANDOM COPOLYMERS

A Dissertation Presented

By

KENICHI BABA

Approved as to style and content by:

Richard S. Stein
(Chairman of Committee)

Roger L. Porter
(Head of Department)

(Member)

R. S. Porter
(Member)

June 1972
(Month) (Year)

A C K N O W L E D G E M E N T S

The auther wishes to express his sincere thanks to Prof. R. S. Stein, thesis director, for his invaluable guidance, for his warm encouragement and for his personal help during the stay in the U. S. A.

The auther expresses his deepest gratitude to Mitsui Toatsu Chemicals, Inc. for the financial support for this work.

The auther extends his gratitude to the thesis committee members, Prof. F. P. Price, Prof. F. E. Karasz and Prof. R. S. Porter who substituted for Prof. F. E. Karasz for their kind advice and suggestions.

The auther further extends his thanks to the faculties and staffs of Polymer Science & Engineering department and to the staff of the Polymer Research Institute.

The auther wishes to thank Dr. Z. Wilchinsky in Esso Research & Engineering Co. for providing the ethylene-propylene copolymers.

DEDICATED

TO

MY FATHER, YOSHIICHI BABA

AND

MY MOTHER, TSUGIKO BABA

for their love and their toils in the field for us, their four sons and a daughter.

TABLE OF CONTENTS

ABSTRACT viii

I. INTRODUCTION 1

II. EXPERIMENTAL 5

1. Materials 5

2. Sample Preparation 5

3. Experimental Procedure 6

(1) Measurement of viscoelastic properties 6

(i) Measurement procedure 6

(ii) Data processing for viscoelastic measurement 7

(2) Measurement of crystallinity 8

(i) Procedure of crystallinity measurement 8

(ii) Data processing for measurement of crystallinity 9

(iii) Calculation of crystallinity 11

(3) Young's modulus, stress and strain optical coefficients measurement 13

(i) Procedure for Young's modulus, stress and strain optical coefficients measurement 13

(ii) Data processing for Young's modulus, stress and strain optical coefficients measurement 14

(4) Measurement of orientation function 15

(i) Procedure of orientation function measurement 15

(ii) Data processing of orientation function measurement 17

(5) Photographic measurement of small angle light scattering 18

(6) Estimation of form birefringence 19

(i) Procedure for estimation of form birefringence 19

(ii) Data processing for form birefringence estimation 20

III. RESULTS AND DISCUSSION 22

1. Viscoelastic Properties 22

2. Crystallinities of the Copolymers 27

3. Superstructures of the Copolymers 36

4. Orientation of Crystallites under Deformation 40

(1) X-ray diffraction measurement of orientation functions of various temperature 40

(2) Orientational behavior in small angle light scattering 44

5. The Emerging Scattering Lobes under Deformation 49

6. Young's Modulus, Strain and Stress Optical Coefficients 53

(1) Young's modulus of the copolymer 53

(2) Strain and stress optical coefficients 59

7. Estimation of Form Birefringence 72

IV. CONCLUSIONS AND FUTURE WORKS 76

1. Conclusions 76

2. Future Works 78

APPENDIX 81

BIBLIOGRAPHY 93

CAPTIONS FOR TABLES 100

CAPTIONS FOR FIGURES 101

A B S T R A C T

The mechanical and rheo-optical properties of two ethylene-propylene random copolymers containing 77 and 68 mole percent of ethylene were studied.

The viscoelastic properties were measured by "Vibron" at four different frequencies.

The crystallinities of the copolymers were measured by x-ray diffraction method in the temperature region from room temperature to the melting temperature of the copolymers.

The orientation functions of the (110) normals were also measured by x-ray diffraction method.

The Young's modulus and the birefringence of the samples were measured at the same time using the Instron tester equipped with a Babinet compensator and a light source. By combining the mechanical and the birefringence measurements, the anisotropy of the statistical unit in the amorphous phase was discussed on the basis of the statistical rubber elasticity theory.

The form birefringence of the copolymers was estimated by measuring the variation in birefringence of the stretched sample with swelling.

The superstructures of the crystallites in the copolymers were studied by small angle light scattering method.

The anisotropies caused by the strain field around the crystallites were studied by small angle light scattering

method and polarized microscope.

I. INTRODUCTION

The unique properties of rubbery materials have drawn the attention of many scientists from an early date. The discovery of vulcanization has resulted in rubbery materials becoming among the most important materials in practical use. Chemical structures of these materials have been studied together with their physical properties.

The thermodynamic approach[1-4] has revealed that most of the restoring force of the stretched rubber is attributable to an entropy decrease. It was soon realized that the application of the statistical theory[5] to the material could lead to quantitative expressions for the mechanical properties of the materials. The development of this aspect of the subject has in fact been in many ways the most impressive feature of the statistical theory.

Kuhn[5] showed that the elastic modulus could be directly related to the number of network chains per unit volume of the material, or alternatively, to the mean molecular weight between crosslinks. The first explicit treatment of the network was given by James and Guth.[6,7] Alternative methods of attack on the same problem which led to essentially the same conclusion were published in the same period by Wall[8-10] and by Flory and Rehner.[11,12]

Nowadays, comprehensive theories capable of giving a quantitative description of the elastic properties of a

rubber for any type of deformation is available. The theory had also been successfully applied to the treatment of the swelling phenomena[13] and, by a slight modification, to the rheo-optical properties of rubbers.[5,13,14]

The development of stereospecific catalysts[15-18] in the 1950s has opened a new field in polymer physics. Various highly crystalline polymers have emerged, one after another. Crystalline structures of these new polymers have been studied extensively ever since.

One of the general structural features found in the bulk state of these polymers is that they have spherulitic superstructures. Microscopic studies on these structures have revealed that the spherulite consists of crystalline fibriles radiating from the center, twisting and intertwining with each other.[19-24]

The discovery of single crystals[25,26] from solutions of polyethylene has given a clue to solve the finer structures of fibriles in spherulites.

The crystalline lattice structure has been studied by x-ray, electron, and neutron diffraction methods. Even the positions of atoms in the lattice has been determined in some cases.[27]

In addition to morphorogical studies, the response of the crystalline lattice, fibriles, and spherulite to mechanical and electrical stimuli has been studied by various methods.

In contrast to rubbery and highly crystalline polymers, the study of low crystalline polymers has been left behind because of the inapplicability of those materials for practical use, and because of their lack of clear-cut structures. But there are some interesting features in these polymers. In low crystalline polymers, the strong interactions between crystallites found in highly crystalline polymers[28] may be reduced drastically. By changing the crystallinity, the intensity of interactions between crystallites may be changed, revealing the various aspects of interactions in the polymer.

There are several ways to attain low crystallinity. One of the most effective methods is to copolymerize the different monomers randomly. Monomers which do not cocrystallize must be used. The advantage of this method is that one can attain very wide ranges of crystallinity. In addition to this, if one attains equilibrium, crystallinity may not change drastically by orienting the amorphous chains under deformation, because of the irregularities in the polymer chain.

In ethylene copolymers it has long been recognized that the introduction of propylene units decreases the crystallinity and also some of the propylene units are accommodated into crystalline phase, expanding the cell dimensions.[29,30] In this study ethylene-propylene copolymers are chosen because of the reasons mentioned above, and because

of their availability.

As has been pointed out in the work from this laboratory, it is possible to study the response of crystal lattice, fibriles and spherulites to static and dynamic mechanical stimuli by birefringence,[31,32,33] light scattering[34] and x-ray scattering[35,36,37] measurements. For low crystalline polymers used in this study, it may be difficult to apply x-ray and light scattering techniques because of the weak intensities of diffracted rays by their crystalline portion. For low crystalline polymers it may be appropriate to apply static and dynamic birefringence measurements to study the behavior of crystalline and amorphous part.

As has been shown, the birefringence of a crystalline polymer may be resolved into three parts, amorphous and crystalline contributions and form birefringence.[38] If the structure and orientation of the crystalline phase are known, it is possible to estimate the crystalline contribution. Combining the measurements of crystallinity and orientation function, it is possible to calculate the amorphous contribution. The amorphous contribution can be discussed on the basis of well established statistical rubber elasticity theory.[13,14] In addition to this, the light scattering measurement give a clue of interactions between crystalline and amorphous phases.

II. EXPERIMENTAL

1. Materials

Two ethylene-propylene random copolymers of different ethylene content were provided by Esso Research & Engineering Co. Those samples were laboratory preparations synthesized in heptane (solution or slurry depending on solubility) at about 25°C in a continuous stirred tank reactor with a Ziegler-Natta type homogeneous catalyst.[39] For this catalyst the reactivity ratio product was about 0.5. The copolymers were heterogeneous in both composition and molecular weight. This in part was due to the presence of more than one active catalyst species. However 98 % of the polymer was within 10 weight percent ethylene of the stated average value. These statements are based on column elution fractionation data and on studies on the kinetics of the polymerization processes. Some of the properties of those samples, which were given together with the samples by the company, are shown in Table 1.

The samples contain approximately 1 % calcium stearate, 0.01 % catalyst residue, and 0.1 % inhibitor.

2. Sample Preparation

The copolymers were used without further purification. Sheets of about 12.5 cm x 15.1 cm x (3-30)mil were molded in a laboratory press. Samples were pre-heated for five

minutes at 375°F (190°C) between metal plates with covers of cellophane film prior to pressing under the force of 20,000 pounds for another 8 minutes. After the pressing, the temperature of the sample was decreased rapidly to room temperature in about 15-20 minutes by passing water through the cooling system of the press. After the molding, the sheets were melted at a temperature of 250°F (121°C), under the pressing force of 20,000 pounds, and slowly cooled over about 12 hours without using cooling water.

The heat treated sheets prepared by the above method were then covered through the same procedure as that of initial pressing. The samples were then left at room temperature at least more than 3 days before using them.

3. Experimental Procedure

(1) Measurement of viscoelastic properties.

(i) Measurement procedure. The viscoelastic properties of the ethylene-propylene copolymers were measured by the "Rheovibron" made by Toyo Measuring Instruments Co., Ltd. (Tokyo, Japan).

A specimen of dimensions of 18.5 mil x 157.5 mil x 1.02 inch was cut from the press sheet. The specimen was attached to the clamps of the equipment. Zero adjustment and calibration were done before attatching the sample.

The temperature was lowered to approximately -150°C, using liquid nitrogen. Dried nitrogen gas was sent into

sample chamber during the experiment. The temperature was then raised, first without heating. When the temperature reached approximately -50°C, the heating chamber was heated by electric power so that the temperature rise was approximately 1.5°C/min. Measurement was continued to as high a temperature as the equipment permitted.

One specimen was used to measure at each specific frequency. Viscoelastic properties were measured at the frequencies of 110 c/s, 35 c/s, 11c/s and 3.5 c/s.

(ii) Data processing for viscoelastic measurement. The absolute value of complex modulus was calculated according to the following equation.

$$E = 2.0 \times 10^9 \times L / (A \times D_i \times S) \qquad (1)$$

where

E = the absolute value of complex modulus (dynes/cm^2)

S = cross section of the sample (cm^2)

A = constant given in Appendix I

D_i = the value of dynamic force dial

L = the length of the sample (cm).

The dynamic storage modulus E' and loss modulus E" were given by the following equations.

$$E' = E \cos \delta \qquad (2)$$

$$E'' = E \sin \delta \qquad (3)$$

where

δ = phase angle

A computer program was used to perform these calculations and is shown in Appendix II.

(2) Measurement of crystallinity.

(i) Procedure of crystallinity measurement. The crystallinity of the sample was measured by transmission x-ray diffraction method. The dynamic x-ray diffractometer was used[35] to measure the diffracted intensities at various Bragg angle (2θ) without adding strain to the sample. An x-ray beam was passed normally through the sample. Intensities of diffracted x-ray were measured every 1° of 2θ in the region of 5° to 15°. From $15^{\circ}$to 17°, they were measured at 0.5° intervals, and from 17° to 24°, at every 0.2°. From 24° to 28° , they were measured at every 0.5°, and from 28° up to 32°, every 1° respectively.

After the scanning was over, the temperature was raised. The diffracted intensities were measured again. This was repeated until the melting occured. The intensities of diffracted x-rays at various Bragg angles were corrected by the procedure described in II. 3. (2). (ii) and plotted against the Bragg angle. The crystalline and amorphous peakes were resolved by the method described in II. 3. (2). (iii)

The areas of these peakes were measured by planimeter.

(ii) Data processing for measurement of crystallinity. The correction of x-ray intensity was done according to the following equation.

$$I_{corr} = C_{pol} \cdot K_{abs} \cdot (I_{exp} - I_{bkg}) - I_{compt} \quad (4)$$

where

I_{corr} = corrected intensity

I_{exp} = experimental intensity

I_{bkg} = background intensity

I_{compt} = Compton effect (incoherent) intensity

C_{pol} = polarization correction factor

K_{abs} = correction factor for sample absorption and changes in scattering volume.

The Compton intensity is given by

$$I_{compt} = C_{compt} \cdot F_{incoh} \quad (5)$$

$$F_{incoh} = \sum_{i=1}^{N} x_i \cdot (Z_i - \sum_{j=1}^{Z_i} f_{ij}^{\,2}) \quad (6)$$

where

x_i = mole fraction of atom type i

Z_i = atomic number of atom type i

f_{ij} = scattering factor for the j^{th} electron of the i^{th} atom

C_{compt} = experimentally determined constant

N = number of types of atom.

In a previous report from this laboratory,[40] C_{compt}

was evaluated by assuming that at a sufficiently high 2θ value (50° was used), the entire sample scattering intensity consists of Compton scattering. However, Krimm and Tobolsky[41] did not assume that the coherent intensity vanishes at large 2θ. Though the theoretical work done by A. H. Compton[42] is in favor of Krimm and Tobolsky, the method developed in our laboratory was chosen for its simplicity in this work. Then the value of C_{compt} is given by the following equation.

$$C_{compt} = \frac{I(50^\circ)}{F_{incoh}(50^\circ)} \qquad (7)$$

where

$I(50^\circ)$ = intensity of diffracted x-rays at 50° of Bragg angle

$F_{incoh}(50^\circ)$ = the value of F_{incoh} at 50° of Bragg angle.

The intensity of incoherent scattering at various Bragg angles is then calculated using Equation (5). The atomic scattering factors used in equation are taken from Compton's book[42] and are compiled as part of the computer program.

The polarization correction factor is given by the following equation.

$$C_{pol} = 2 / (1 + \cos^2 2\theta) \qquad (8)$$

The absorption correction depends on the angle of incidence of the x-ray beam relative to the polymer film

surface. Gingrich[43,44] has shown that for the incident beam normal to the film surface, K_{abs} is given by the following equation.

$$K_{abs} = \frac{\mu t(\sec 2\theta - 1)}{1 - \exp\left[-\mu t(\sec 2\theta - 1)\right]} \qquad (9)$$

where

μ = linear absorption coefficient

t = the thickness of the sample film.

The linear absorption coefficient of the polymer is given by the following equation.

$$\mu = \rho \sum w_i \left(\frac{\mu_i}{\rho_i}\right) \qquad (10)$$

where

ρ = density of the sample

ρ_i = density of the i^{th} element

w_i = weight fraction of i^{th} element

μ_i = linear absorption coefficient of i^{th} element.

A computer program for correction of diffracted intensities of x-rays is shown in Appendix III. The calculated value was plotted against Bragg angle and is shown in Figure 1 in schematic fashion.

(iii) Calculation of crystallinity. The crystalline and the amorphous diffraction peaks were resolved according to the method reported by Z. Wilchinsky.[39] The procedure for resolving the two contributions will be described with reference to Figure 1. A straight base line ab is

drawn from $2\theta = 7^\circ$ to $2\theta = 32^\circ$. The area above this base line may now be considered to consist of diffractions from crystalline and amorphous parts. The height I_a of the amorphous halo above the base line is determined, and the points c and d on the diffraction trace at $(7/8)I_a$ and $(1/4)I_a$ are marked to establish the line cd. The average value of $A_a"/ A_a'$ was found to be 0.119, the standard deviation being 0.006 in the work of Z. Wilchinsky[39] on the same samples used in this work. Thus, from measurement of A_a' and $A_a" + A_c'$, one can determine A_a $(=A_a' + A_a")$ and A_c $(=A_c' + A_c")$.

The crystallinity was determined by an adaption of the procedures reported by Weidinger[45] and Hermans.[46] The weight fraction X_c of the polymer in the crystalline phase is thought to be proportional to A_c and the fraction X_a in the amorphous phase to be proportional to A_a. These relations may be written as follows.

$$X_c = K_c A_c \tag{11}$$

and

$$X_a = 1 - X_c = K_a A_a \tag{12}$$

where K_c and K_a are the respective proportionality factors. By combining these equations, one may obtain the following equation.

$$1 = K_c A_c + K_a A_a \tag{13}$$

Dividing Equation (11) by Equation (13) one obtains

$$X_c = 1 / \left[1 + K \left(A_a / A_c \right)\right] \qquad (14)$$

where $K \left(= K_a / K_c \right)$ is a constant independent of the intensity scale factor used. The value of K for the polymers used in this work was reported to be given by the following equation.[39]

$$K = 0.55\ A_c / \left(A_c + A_a \right) + 0.54 \qquad (15)$$

Substituting the values of A_c and A_a into Equation (15), values of K were calculated. These values were again substituted into Equation (14) to calculate crystallinity.

(3) Young's modulus, stress and strain optical coefficients measurement.

(i) Procedure for Young's modulus, stress and strain optical coefficients measurement. Stress and birefringence were measured simultaneously using a table model Instron tester equipped with a light source, polarizer and a Babinet compensator.[47] The set-up of the equipment is shown in Figure 2 in schematic fashion. Measurements were made with monochromatic light from a mercury lamp at a wavelength of 5461 Å.

Specimens of the dimensions of 1.5 inch x 300 mil x 17 mil were cut from the press film. They were clamped to the equipment. About 10 minutes after the sample was clamped, the initial length between the clamps was meas-

ured. After another 10 minutes (so that the temperature of the sample be the same to that of sample chamber,) retardation of the sample was measured. The sample was stretched stepwise, 0.01, 0.02, 0.03, 0.04, 0.05, 0.06, 0.08 and 0.1 inch. Measurements of retardation and stress at each step was made 10 minutes after the stretching of the sample. For measurement at lower temperature than room temperature, nitrogen gas cooled by passing through liquid nitrogen was introduced directly into the sample chamber.

(ii) Data processing for Young's modulus, stress and strain optical coefficients measurements. The strain optical coefficient was calculated from the initial slope of the reading of the compensator versus strain plot according to the following equation.

$$S_r = C_1 \lambda \xi_1 / t \qquad (16)$$

where

S_r = strain optical coefficient

C_1 = waves per turn of Babinet compensator scale

λ = wave length of the light

ξ_1 = initial slope of reading of Babinet compensator versus strain plot.

The Young's modulus of the sample was calculated according to the following equation.

$$E_Y = 9.8 \times 10^{5} \xi_2 / (t \times W) \qquad (17)$$

where

ξ_2 = initial slope of total force versus strain plot (kg)

W = width of the sample (cm).

The stress optical coefficient (S_{oc}) will be given by the following equation.

$$S_{oc} = S_r / E_y \qquad (18)$$

A computer program for calculating these coefficients is shown in Appendix IV.

(4) Measurement of orientation function.

(i) Procedure of orientation function measurement. Orientation functions were measured using the dynamic x-ray diffractometer.[35] A schematic diagram of the set-up is shown in Figure 3. A specimen of the dimension of 17 mil x 2 cm x 2.5 in. was cut from the press film and was clamped to the equipment. After setting the azimuthal angle to zero, the intensity of diffracted x-rays at various Bragg angles was measured. The position of the (110) diffraction peak and the amorphous peak were determined by this Bragg angle scanning. After setting the detector at the Bragg angle of (110) diffraction peak, the intensity of diffracted x-rays at various azimuthal angles was measured. The measurement of the intensity of diffracted rays was covered out at every 5° of azimuthal angle from 0° to 90°.

Assuming that the maximum position of the amorphous

halo is not affected by diffraction peaks due to the crystalline part, and that the amorphous halo is symmetrical with respect to the maximum position, the intensity of the diffracted x-rays by the amorphous part at Bragg angles of (110) diffraction peak was estimated.

The intensity at the Bragg angle which is smaller than the maximum position of halo by the same amount of Bragg angle difference between (110) diffraction peak and that of amorphous halo, was measured.

For evaluation of Compton scattering intensity, the diffracted intensity at 50° was measured,[40] setting the azimuthal angle to zero. As it was not possible to set the detector at 50° of Bragg angle, the x-ray source was tilted 16° from the normal of the surface of the sample and the detector was set at 34° of Bragg angle.

The orientation function was measured over the strain range from 0.0 to 1.0 and at temperatures from 25°C to 80° C for the higher crystalline 1248B sample and from 30°C to 50°C for the lower crystalline 1193A sample.

As it was not possible to stretch the sample from outside the sample chamber, the cover was removed from the sample chamber when the specimen was subjected to stretching. Even though the thermometer reading did not change, there may be some decrease of temperature during this operation. About 10 minutes after putting the cover on to the chamber, the measurement was began. The background was

measured prior to the main experiment.

(ii) Data processing of orientation measurement. The intensities of the diffracted x-rays were corrected by the same data-processing method described in II. 3. (2). (ii). It was reported[48] that orientation function of the (110) normal could be calculated by the following equation. The coordinate system used is shown schematically in Figure 4.

$$f_{110} = (3 \overline{\cos^2 \gamma_{110}} - 1) / 2 \qquad (19)$$

where f_{110} is the orientation function of (110) normals. $\cos \gamma_{110}$ in the equation could be expressed as follows.

$$\cos \gamma_{110} = \cos \theta_{110} \sin \psi_{110} \qquad (20)$$

By combining Equations (19) and (20), one could obtain the following expression.

$$f_{110} = (3 \cos^2 \theta_{110} \overline{\sin^2 \psi_{110}} - 1) / 2 \qquad (21)$$

The value of $\overline{\sin^2 \psi_{110}}$ could be obtained by the following equation.

$$\overline{\sin^2 \psi_{110}} = \frac{\int_0^{\pi/2} I(\psi_{110}) \sin^2 \psi_{110} \cos \psi_{110} \, d\psi_{110}}{\int_0^{\pi/2} I(\psi_{110}) \cos \psi_{110} \, d\psi_{110}} \qquad (22)$$

where $I(\psi_{110})$ is the relative intensity of diffracted x-rays of (110) plane at the azimuthal angle ψ_{110}. The integrals were evaluated using the Simpson's equation.

Though one could not see the (110) normals within the angular region of θ_{110} from the both poles in reciprocal space, this method is accurate at the small strain range, especially when the Bragg angle is small.

A computer program used to calculate the orientation function of (110) normal according to the above mentioned procedure is shown in Appendix V.

(5) Photographic measurement of small angle light scattering. Light scattering patterns in the strain range from 0 to 2.0 were measured at room temperature using the photographic set-up developed in this laboratory.[49] The schematic arrangement for this set-up is shown in Figure 5. The laser provides a parallel monochromatic polarized light beam directly, eliminating the need for auxilliary optical elements except for a guard pinhole to exclude fluorescence from the laser crystal. The beam is passed normally through the sample. It then passes normally through an analyzing Polaroid and finally on a photographic film. Specimen of the dimensions of 1.2 in. x 150 mil x (3-4) mil were used. The specimen was clamped to a stretcher and was put on the stage of the equipment. The sample-to-film distance was set to 21.4 cm so that one could obtain proper size scattering patterns. Exposure times were 1.0 and 1/50 seconds for H_v and V_v scattering patterns respectively. The strain was increased stepwise from 0 to 2.0. After the scattering pattern was taken at a strain of 2.0, the strain

was decreased. Both samples recovered to approximately 1.5 times of their original length. Final pictures were taken at this condition.

To avoid contribution from scattering from surface irregularities, films were held between microscope cover glasses using silicone oil as an immersion fluid. The refractive index of the silicone oil was matched to the refractive index of the polymer by mixing different silicone oils having different refractive indices. The Becke test was used to determine whether the refractive index of the silicone oil was matched or not.

(6) Estimation of form birefringence.

(i) Procedure for estimation of form birefringence.

The swelling method established in this laboratory[38] was applied in this work. The polymers used were swollen so rapidly that the method should be modified to apply to this work. A specimen of the dimension of 1.5 in. x 150 mil x 15 mil was cut from the press film and was stretched about 50 %. It was then fastened to a sample holder shown in Figure 6. Strain of the sample was determined using a travelling microscope by measuring the distance between the two marks put on the surface of the sample. The samples, fastened to a holder, were immersed in a swelling solvent. The solvents used in this work are shown in Table 2 together with the values of their refractive indices and densities. Swollen samples were put in cells shown in

Figure 6 so that the evaporation of the solvent could be suppressed. The birefringence and the weight of the sample were measured by a set-up shown in Figure 7 together with that of the cell. The solvent was evaporated stepwise until the original weight was gained.

(ii) Data processing for form birefringence estimation. Degree of swelling was expressed by the volume fraction of polymer in the swollen state. The volume fraction of polymer was calculated according to the following equation.

$$v_2 = \rho_1 W_2 / \{\rho_1 W_2 + \rho_2 (W_1 - W_0)\} \qquad (23)$$

where

v_2 = volume fraction of polymer

ρ_1 = density of solvent

ρ_2 = density of polymer

W_1 = weight of swollen sample and cell

W_2 = weight of polymer

W_0 = weight of dry sample and cell.

The birefringence of the sample was calculated by the equation shown below.

$$\Delta = C_1 \frac{\lambda}{t} (R_1 - R_0 - R_c) \qquad (24)$$

where

Δ = birefringence of sample

R_1 = reading of Babinet compensator of a swollen

sample in a cell

R_0 = reading of Babinet compensator without sample

R_c = birefringence of a cell expressed in the scale of Babinet compensator.

The birefringence versus volume fraction of polymer was plotted schematically as shown in Figure 8. From this plot, the value of birefringence at 0.9 of volume fraction of polymer was read and plotted against the strain of the sample. As it was difficult to stretch the sample exactly to a specific amount, it was stretched more or less than the strain wanted. The birefringence at the strain was interpolated by a straight line.

In this work, birefringence at 0.5 of strain was determined.

III. RESULTS AND DISCUSSION

1. Viscoelastic Properties

The dynamic storage modulus and dynamic loss modulus of the 1248B and 1193A samples measured at various frequencies are plotted against temperature in Figure 9 and Figure 10 respectively.

The dynamic storage moduli of both samples decrease gradually with increasing temperature in the low temperature region, especially at temperatures lower than the glass transition temperature. They decrease appreciably in the γ-transition region, though the decrease is not so marked as that in the β-transition region. At around -50°C, they decrease very sharply from the 10^{10} dynes/cm^2 to around 10^8 dynes/cm^2. After this β-transition, they continue to decrease with increasing temperature. Again in the α-transition region, they decrease rapidly..

Nielsen[50] has shown that the dynamic storage modulus is strongly dependent on the crystallinity of the material. In some cases, one can estimate the crystallinity of a polymer from its dynamic storage modulus.[51] One could deduce from the results mentioned above that the bigger dynamic storage modulus of 1248B as compared with that of 1193A over the whole temperature range studied could be attributable to higher crystallinity of 1248B.

The notable plateau region, in which the dynamic

storage modulus is of the order of 10^7 dynes/cm^2, lies from -20°C to 50°C for sample 1248B. Though less marked, the same plateau region is found in 1193A. The same flat portion is also found in amorphous polymers. In such cases, it is attributable to the entanglement of the amorphous chains. The bigger the molecular weight of a polymer, the more strongly the plateau persists. In highly crystalline polymers this region is not observed because of the strong constraints in the amorphous phase.

It is thought from those results that the crystallinity is small enough to release the constraint in the amorphous phase but not small enough to permit molecules flow in the copolymers used in this study. In other words, one could assume that crystallites are acting as multifunctional crosslinks. This means that the properties of the copolymers may well be described, or analyzed by the statistical theory, which is well established in the study of rubber elasticity.

Though it is not clear in the plot of dynamic loss modulus against temperature, three transitions were observed for the copolymers. In the plots shown in Figure 11 and Figure 12, one could clearly spot the three transitions designated α, β and γ. A transition, designated by Boyer[52] as the $T_{1,1}$ transition due to the motion in the amorphous phase above the glass transition temperature, was not observed in the polymers studied.

The α-transition is related to a relaxation process in the crystalline phase of the polymers. This becomes very clear when the strong influence of the degree of crystallinity on the magnitude of this dispersion is considered. As is seen in Figure 11 and Figure 12, the magnitude of tanδ is decreased in the lower crystalline 1193A sample as compared to the higher crystalline 1248B sample. Also, the transition temperature of 1193A is appreciably lower than that of 1248B. This result strongly suggests that the mobility of polymer chains in the crystalline phase of 1193A is bigger than in the crystalline phase of 1248B. Compared to the result obtained in polyethylene,[53] the α-transition temperatures of both samples are very low. This extra mobility of the chains of ethylene-propylene copolymers in the crystalline phase may be attributable to defects or imperfection of the crystals. Actually it was observed by x-ray diffraction measurement that the crystalline cell dimensions of the copolymers were expanded. The result will be discussed in the next section.

The β-transition was found around -40°C in both polymers. It has been attributed to the onset of movement of molecular chains in the amorphous phase. This transition is also found in low density polyethylene.[54] In this case, it is found that the transition is due to the branching of the molecule.

It was noticed that the temperature of α-transition

found in linear polyethylene shifts toward the lower temperature at which the β-transition occurs upon introduction of side groups or bulky atoms. This has been noted in copolymers of ethylene-propylene[55] and ethylene-vinylacetate[56] copolymers and chlorinated polyethylenes.[57] The results obtained in methyl-branched polyethylene and ethylene-propylene copolymers are summarized and are shown in Figure 13 together with the results obtained in this work. Introduction of small amount of propylene or methyl-branch decreases the transition temperature drastically. It seems that the reduction of temperature levels-off at about 85 to 95 mole percent of propylene content. The results obtained in this work agree very well with the values found by other researchers.[55,58,59] The same trend has also been found in the variation of magnitude of β-dispersion with propylene content.

The γ-transition of the copolymer is located at a temperature around -120°C. This transition has been thought to be attributable to the onset of cooperative motion of small linear segments containing at least 3 or 4 methylene groups. It was reported that in ethylene-propylene copolymers, the magnitude of the dispersion decreases significantly with increasing propylene content.[55] This tendency was also found in this work, though it is not so marked as found in the lower propylene content region. As has been demonstrated by Flocke[55] and others,[58,59] the

temperature at which γ-transition occurs is not affected by the propylene content.

The dynamic storage modulus, dynamic loss modulus and tanδ increase with increasing frequency. The temperature at which transitions occur become higher with increasing frequency. These phenomena are well understood by applying time-temperature superposition principle.

From the frequency dependence of transition temperature, the apparent activation energy of the process was evaluated. The frequency dependence of the temperature at which dynamic loss modulus maxima locate is tabulated and is shown in Table 3.

The reciprocals of the temperature (^{o}K) are plotted against the logarithm of frequencies. The results are shown in Figure 14 and Figure 15. For both β and γ-transition, straight lines are obtained in both copolymers. The activation energy was calculated according to the following equation.

$$\Delta E = - R / \xi_3 \qquad (25)$$

where ΔE is the activation energy, R is gas constant and ξ_3 is the slope of the straight line in Figure 14 and 15. The values obtained are shown in Table 3. The activation energies of the β-transition in 1193A and 1248B are the same within experimental error. The same conclusion is obtained for γ-transitions of both copolymers.

2. Crystallinities of the Copolymers

The corrected intensities of diffracted x-rays of 1248B and 1193A at various Bragg angles are shown in Figure 16 and Figure 17 respectively. Two diffraction peaks observed in this Bragg angle region agree very well with the amorphous and (110) diffraction peaks of polyethylene. In polypropylene, strong diffraction peaks are found at the Bragg angle of 12.9°, 15.8° and 17.3°,[17] which are located very differently from that of polyethylene. Those diffraction peaks have been indexed to (110), (040) and (130) respectively. None of those diffraction peaks attributable to polypropylene crystallites was observed. This means that the crystalline phase of the copolymers consists of polyethylene chains rather than those of polypropylene. This result could be easily understood on the basis of the monomer reactivity ratio of the catalyst. Usually the Zieglar-Natta type catalysts have larger reactivity to ethylene than to propylene leading to longer and more crystallizable ethylene sequences.

The intensity of the (110) diffraction decreases with increasing temperature. On the other hand the amorphous halo increases its intensity with increasing temperature.

Another interesting point is that the Bragg angles at which amorphous and (110) diffraction intensity maxima occur decrease with increasing temperature. The behavior of

the diffraction peaks could be well explained by the thermal expansions of crystalline lattice and amorphous volume. The locations of the diffraction peak maxima for amorphous halo and (110) plane were measured and are shown in Table 4. (110) spacings at various temperature were calculated using the Bragg's law shown below.

$$d = \lambda / 2 \sin\theta \qquad (26)$$

The calculated values of the (110) spacings were also shown in Table 4. In Figure 18, (110) spacings of both samples obtained are plotted against temperature, together with the results for polyethylene obtained by E. A. Cole and D. R. Holmes.[60]

The expansion coefficient of the (110) spacings of copolymers are substantially bigger than that of Marlex as reported by Cole et al.[60] As has been suggested by him the expansion coefficient becomes bigger with increasing methyl side group concentration. The bigger expansion coefficients in the copolymer may be due to the imperfections of crystallites.

The crystallinities of the copolymers at various temperature are shown in Figure 19. The values obtained by Z. Wilchinsky[39] are also shown in the same figure. The crystallinities of the copolymers at room temperature obtained in this work agree very well with the values reported by Wilchinsky.

The crystallinities of both polymers decrease with increasing temperature. The higher crystalline 1248B melts approximately at 105°C. The lower crystalline 1193A melts at 76°C, about 30°C lower than 1248B. Compared to homopolymers of ethylene, the melting point of the copolymers is lower. Crystallinities of the copolymers are also much lower than that of homopolymers. Melting of copolymers occurs in very wide temperature range compared to homopolymers.

These peculiar behavior of copolymers was studied extensively in theoretical and experimental field. Assuming that one of the comonomer can not be accommodated into crystalline phase, Flory[61] developed a theory concerning the melting point and crystallinity depression in copolymers.

The copolymer was thought to contain crystallites of varing lengths expressed in terms of the number, ζ of repeating unit A in a single chain running from one end of the crystallite to the other. Longitudinal growth of established crystallites will be restricted by the occurence of B units in some of the chains where they protrude from the ends of the crystallites. Lateral growth, however will be restricted only by the availability of sequencies of A units in the amorphous region. It was also assumed that acquisition of an additional chain may be initiated at any site on the lateral surface of a crystallite. Then at equilibri-

um with the crystallites of length ζ, the "concentration" of acceptable A units in the amorphous phase P_ζ^e was calculated. From the value of P_ζ^e one may then caluculate the residual concentration w_ζ^e of sequence of length ζ in the melt. The results are as follows.[61]

$$w_\zeta^e = \zeta D^{-1} \left\{ 1 - \exp(-\theta_1) \right\}^2 \exp(-\zeta\theta_1) \qquad (27)$$

where

$$\theta_1 = \left(\frac{\Delta H_u}{R} \right)\left(1 / T - 1 / T_m \right) \qquad (28)$$

and

$$D = \exp \left(-2\sigma_e / R T \right) \qquad (29)$$

where ΔH_u is the heat of fusion per unit, T_m^o is the melting point of the pure polymer, σ_e is the surface free energy per unit at the end of the crystallites. The residual concentration w_ζ^0 of sequences of length ζ in the copolymer prior to development of crystalline region can be evaluated from the composition of the copolymer.

In case of a copolymer which can be characterized by a unique probability p that an A unit is succeeded by another A unit, this probability being independent of the number of A's preceding the given A unit in the sequence, w_ζ^0 could be expressed by the following equation.

$$w_\zeta^0 = \left(\frac{X_A}{p}\right)\left(1 - p \right)^2 p^\zeta \qquad (30)$$

For a random copolymer the sequence propagation probability p is equal to mole fraction of A unit (X_A), for a block copolymer $p > X_A$; and for a copolymer in which alteration of units is favored $p < X_A$.

Except for copolymers with high alternation, D^{-1} will exceed (X_A / P), hence if $e^{-\theta_1} < p$ the equilibrium distribution lies above w_ζ^0 for low ζ and below it for large ζ. The intersection occurs at

$$\zeta^* = - \left\{ \ln \left(\frac{D\, X_A}{p} \right) + 2 \ln \left(\frac{1 - p}{1 - e^{-\theta_1}} \right) \right\} \frac{1}{(\theta_1 + \ln p)} \qquad (31)$$

The necessary and sufficient condition for crystallization for one or more values of ζ can be given as follows.

$$\left(\frac{X_A}{p} \right) p^{\zeta} > \frac{1}{D} \exp (-\theta_1 \zeta) \qquad (32)$$

In the ordinary case for which (X_A / p) < 1 / D, fulfillment of the condition requires that

$$\theta_1 > \theta_{1m} \qquad (33)$$

where

$$\theta_{1m} = - \ln p \qquad (34)$$

This relation defines the melting point of T_m given by

$$1 / T_m - 1 / T_m^0 = -(R/\Delta H_u) \ln p \qquad (35)$$

If crystallization is conducted by gradual cooling of the melt, the increment of crystallinity owing to a small decrease in temperature must be derived principally from sequences with lengths less than that for which w_ζ^e is already very small, but greater than ζ^*. Hence, the sequences of length j will on the average enter sequences of length ζ such that $(j - \zeta) / \zeta$ is small compared to unity. From these considerations a useful approximation to the degree of crystallinity would be obtained by

$$w^c = \sum_{\zeta^*}^{\infty} (w_\zeta^0 - w_\zeta^e) \qquad (36)$$

Substitution from Equation (30) for w_ζ^0 and from (27) for w_ζ^e gives the final result shown below.

$$w^c = (X_A/p)(1-p)^2 \, p^{\zeta^*} \Big[p/(1-p)^2 - e^{-\theta_1}/(1-e^{-\theta_1})^2 + \zeta^* \{1/(1-p) - 1/(1-e^{-\theta_1})\} \Big] \qquad (37)$$

From consideration of the nature of the curves depicted by Equation (37), the melting depression observed experimentally is expected to be appreciably greater than that calculated according to the equation. Its apparent value will depend on the sensitivity of the method used for determining the disappearance of crystallinity even under ideal conditions of crystallization equilibrium. Some of

the experimental results on ethylene-propylene copolymers reported from other laboratory, and the results obtained in this work are shown in Figure 20 and are compared with the theoretical value obtained by Equation (35). A value of ΔH_u of 960 cal/mole and a value of T_m^o of 137.5°C reported by Quinn and Mandelkern[62] were used for the calculation. The value of p was assumed to be equal to that of the mole fraction of ethylene. The melting points of 1248B and 1193A are much higher than those expected from the theory and the experimental results reported by other workers.[29,63] The melting points reported by Swan[29] and by Richardson and Flory[63] are lower than the values obtained by theory but the deviation is not great in the high ethylene content region. However, the difference between the theory and the experimental results becomes substantial in the lower ethylene content region. As was pointed out by Flory[61] part of deviation of the theory may be attributable to the difficulty to find the true melting point by experiment because of the peculiar melting behavior of copolymers.

The observed exceptionally high melting points of 1193A and 1248B are thought to attributable to the inhomogeneity of compositions of the polymer chains. That is, the polymers are not completely random but rather have long ethylene sequencies within a molecule. This reasoning is further substantiated by comparing the crystallinities of 1193A and 1248B with those obtained by other researchers.[39,

[64,65] In Figure 21, crystallinities of ethylene-propylene copolymers at room temperature are plotted against their ethylene contents. Some of the copolymers whose ethylene contents are about 70 mole percent, among which are 1193A and 1248B, have higher crystallinities than those expected from the extrapolation from the values observed in the region of ethylene content of 85 mole percent to 100 mole percent. These results clearly suggest that the compositions of 1193A and 1248B are not homogeneous.

Another complication in applying Flory's theory to the ethylene-propylene copolymer is that the assumption of unit B's not being incorporated into the crystalline phase is not valid in this case. For ethylene copolymers, it has been shown that propylene is less effective in disrupting crystallinity than the higher normal α-olefins such as butene, pentene or hexene.[65] In addition to this, it is known that branched structure of polyethylene expands the unit cell. It was revealed that small pendent groups, such as the methyl groups can to a large extent be accommodated in the expanded crystalline lattice.[66]

The newly developed method of fuming nitric acid treatment was applied extensively to ethylene-propylene copolymers.[67-71] Keller[68-70] reported that about 75 % of the propylene unit was lost by prolonged treatment with nitric acid. His results show that about 25 % of the propylene units are in the crystalline core, which is not ac-

cessible to nitric acid. Most of the propylene units were shown to be in the amorphous phase and in some defects in crystalline lattice. As was pointed out by Shida,[71] the latter were thought to be in large open defects consisting of highly disordered material or vacancies which might extend to the crystalline surface.

In Figure 22, the (110) spacing reported by Swan[29] is shown together with the results obtained in this work. Swan[29] also showed that the expansion of lattice is most pronounced in the a spacing. b and c spacing do not change very much.

The expansion of crystalline lattice affects the magnitude of the heat of fusion. It is expected that the heat of fusion of ethylene-propylene copolymer is very different from that of homopolymer. From Equation (35), one can derive the following equation.

$$T_m/T_m^0 = \Delta H_u/(\Delta H_u - RT_m^0 \ln p) \qquad (38)$$

Assuming T_m^0 and p to be constant, one may plot T_m/T_m^0 as a function of ΔH_u. The result is shown in Figure 23 in schematic fashion. As could be seen in this result, reduction in ΔH_u leads to an increasing depression of the melting point per unit variation in p. This could also partly account for the deviation of Flory's theory from experiment.

Because of the complexity, no attempt was made to fit the Equation (37) with experiment. This difficulty might

be greatly reduced if one could know the value of p or ΔH_u. It may be difficult to determine the value of p by IR-method developed by Bucci,[72] because of the complication in resolution of absorption bands. The estimation of ΔH_u from the variation of melting temperature on swelling ratio would be a convenient method for those polymers. This experiment was undertaken but because of some minor difficulties in determining the melting point of the polymers and mainly because of the lack of time to solve the problem, it was left behind.

3. Superstructures of the Copolymers

Small angle light scattering patterns of pressed sheet of 1193A and 1248B are shown in Figure 24. The H_v scattering patterns of both samples have 4 scattering lobes orienting 45° at the analyzer and polarizer. V_v scattering patterns are almost spherically symmetrical for both samples. The intensity of V_v scattering is approximately 50 times as strong as that of H_v scattering.

The intensity of scattered light is given by the following equation.[73]

$$I = \sum_i \sum_j A_i A_j \cos \left\{ k \left(\underset{\sim}{r}_{ij} \cdot \underset{\sim}{s} \right) \right\} \qquad (39)$$

where A_i and A_j are the amplitudes of light scattered from the i^{th} and j^{th} volume elements, $k = 2\pi/\lambda$, λ is the wavelength of light in the medium, $\underset{\sim}{r}_{ij} = \underset{\sim}{r}_i - \underset{\sim}{r}_j$ and is the

vector separation of the i^{th} and j^{th} volume elements, $\underset{\sim}{s} = \underset{\sim}{s}_0 - \underset{\sim}{s}_1$, where $\underset{\sim}{s}_0$ is a unit vector along the incident light ray and $\underset{\sim}{s}_1$ is a unit vector along the scattered ray. If it is assumed that the anisotropic volume elements have cylindrical symmetry and the volume element may fluctuate in the values of the average polarizability, in the anisotropy and in the orientation of the principal axis without any correlation between them, one might define correlation functions for fluctuations in average polarizability and in the magnitude of the anisotropy as follows.

$$\gamma(r) = \frac{\langle \eta_i \eta_j \rangle_r}{\langle \eta^2 \rangle_{av}} \qquad (40)$$

$$\psi(r) = \frac{\langle \Delta_i \Delta_j \rangle_r}{\langle \Delta^2 \rangle_{av}} \qquad (41)$$

where η_i is the fluctuations in average polarizability in volume element i, and the Δ_i is the fluctuations in the magnitude of the anisotropy in the i^{th} volume element. $\langle \eta_i \eta_j \rangle_r$ and $\langle \Delta_i \Delta_j \rangle_r$ represent averages over all pairs of volume elements at constant scalar separation r, and $\langle \eta^2 \rangle_{av}$ and $\langle \Delta^2 \rangle_{av}$ is the mean square fluctuations in average polarizability and the magnitude of anisotropy respectively.

If the orientation of the principal axis of the i^{th} volume element is not correlated with the value of the vector $\underset{\sim}{r}_{ij}$ and $\cos^2 \theta_{ij}$, where θ_{ij} is the angle between the principal axes of i^{th} and j^{th} volume elements, depends only

on $|\tilde{r}_{ij}|$, one might introduce an orientation correlation function defined by

$$f(r) = \langle (3 \cos^2\theta_{ij} - 1) / 2 \rangle_r \qquad (42)$$

where the average is taken over all pairs of volume elements separated by a constant scalar distance r. In case the fluctuation in magnitude of anisotropy is caused only by the fluctuations in average polarizability, the intensities of H_v and V_v scattering could be expressed as follows.

$$I_{Hv} = \frac{4}{15}\pi c^2 \delta^2 \int_0^\infty f(r)\, \mu(r)\, \frac{\sin hr}{hr}\, r^2\, dr \qquad (43)$$

$$I_{Vv} = 4\pi c^2 \left\{ \langle \eta^2 \rangle_{av} \int_0^\infty \gamma(r)\, \frac{\sin hr}{hr}\, r^2\, dr \right.$$

$$\left. + \frac{4}{45}\, \delta^2 \int_0^\infty f(r)\, \mu(r)\, \frac{\sin hr}{hr}\, r^2\, dr \right\} \qquad (44)$$

where

$$\mu(r) = 1 + \frac{\langle \Delta^2 \rangle_{av}}{\delta^2}\, \psi(r) \qquad (45)$$

and c is a constant, δ is the average anisotropy, and h is $k|s|$.

The equations obtained show that the V_v component consists of contributions from density fluctuations and and fluctuations of orientation of anisotropic entities and of the magnitude of anisotropy of them.

on the other hand, the H_v component is attributable to scattering by anisotropic entities.

From these conclusions one could notice that the V_v scattering for the copolymers is mainly attributable to density fluctuations. It seems reasonable because the crystallinities of both samples are so small that one could not expect much contribution from anisotropic crystallites.

The above theory leads to an H_v pattern without azimuthal angle dependence. Whereas the observed patterns depend on azimuthal angle, suggesting that orientation fluctuations are non-random.

Another important feature in the light scattering pattern shown in Figure 24 is that the scattering lobes of H_v patterns do not have any maximum in them. That is, the intensity along the scattering lobe decreases with increasing scattering angle. It has been shown that these features of light scattering pattern could arise from anisotropic entities having rod-like or disk-like superstructures.[74] In the study of orientation functions of the copolymers described in the next section, it was found that the (110) normals tend to orient perpendicularly to the stretching direction with increasing strain. This means that c axis, the principal axis of anisotropy, orients parallel to the stretching direction. This result favors the rod-like structures rather than the disk-like structures.

Orientation of scattering lobes of the H_v patterns to 45° to polarizer and analyzer direction shows that the principal axis of anisotropy lies parallel or perpendicular to the axis of the rod. From the above mentioned c axis orientation, one could conclude that the principal axis of anisotropy lies parallel to the rod axis.

4. Orientation of Crystallites under Deformation

(1) X-ray diffraction measurement of orientation functions at various temperature. As described in the previous discussion, the crystallites in the copolymers used in this work have rod-like structure. These crystallites are embedded in a large amount of amorphous matrix which is rubbery at temperatures higher than that of the β-transition. They are thought to be acting as multifunctional crosslinks. As has been pointed out by Kratky,[75,76] the crystallites in those structures may well be described by his "floating rod" model. In the case of uniaxial deformation, one could assume cylindrically symmetric distribution function with respect to stretching direction. If the deformation occurs affinely without changing the volume, one could easily calculate the distribution function at certain extension ratio χ. If the crystallites orient randomly at $\chi = 1$, and the total number of crystallites is N, then the number of crystallites orienting to the

direction of γ and ϕ as shown in Figure 25, at the extension ratio of χ, will be given by the following equation.

$$N(\gamma,\phi)d\gamma d\phi = \frac{N}{4\pi} \frac{\chi^{3/4} \sin\gamma \, d\gamma \, d\phi}{(\chi^{-3/2}\cos^2\gamma + \chi^{3/2}\sin^2\gamma)^{3/2}} \qquad (46)$$

The average value of $\cos^2$ will be given by the following equation.

$$\langle\cos^2\gamma\rangle = \frac{\int_0^{\pi}\int_0^{2\pi} N(\gamma,\phi)\cos^2\gamma \, d\gamma \, d\phi}{\int_0^{\pi}\int_0^{2\pi} N(\gamma,\phi) \, d\gamma \, d\phi} \qquad (47)$$

Then the orientation function will be given by the following equation.

$$f = (3\langle\cos^2\gamma\rangle - 1) / 2$$

$$= \frac{3\chi^3}{2(\chi^3-1)} \left(1 - \frac{\tan^{-1}\sqrt{\chi^3-1}}{\sqrt{\chi^3-1}} \right) - \frac{1}{2} \qquad (48)$$

The orientation functions of (110) normals obtained at various temperature in the copolymers are shown in Figure 26 and Figure 27. The orientation functions of (110) normals of both samples decrease almost linearly with increasing strain. As one could see in Figure 16 and Figure 17, it was not possible to locate (200) diffraction peak in the Bragg angle scanning of both samples.

Because of this unfavourable situation, a and b axes orientation functions could not be determined by the x-ray dif-

fraction method. Since the crystallites in these polymers have rod-like superstructure and are embedded in large amounts of amorphous matrix, it is thought possible to assume that the orientation functions of a and b axes are the same to that of (110) normal. In orthorhombic crystal systems like polyethylene the following equation holds.[48]

$$f_a + f_b + f_c = 0 \qquad (49)$$

where f_a, f_b and f_c are the orientation functions of a, b and c axes. If $f_a = f_b$, one obtains the following result:

$$f_a = f_b = -\frac{1}{2} f_c \qquad (50)$$

The c axis orientation function is given by Equation (48). By substituting Equation (48) into Equation (50), one may calculate the a axis orientation function, which is thought to be equal to the (110) normal orientation function. The calculated values are shown in Figure 26 and Figure 27 and are smaller than experimentally obtained value. This means that the crystallites do not orient as much as expected from the theory. The failure of the theory to predict the orientation behavior of the crystallites may be partly due to the fact that in case of these polymers, there may be many imperfect crosslinks which allow polymer chains to be free to move. These might prevent crystallites from orienting affinely.

The initial slopes of the orientation functions of the (110) normals were measured from Figure 26 and Figure 27 and are shown in Figure 28. The slopes of both samples do not change very much with temperature in the low temperature region. At higher temperatures, especially near melting temperature, the diffracted x-ray intensity is weak, hence the larger error is expected in this region than in lower temperature region. Even though, it seems that the initial slope of orientation function at higher temperature decreases.

In polyethylene, strong dependency of magnitude of orientation function on temperature is observed even at lower temperatures.[28,77] In polyethylene, the c axis orientation function at a given elongation is greater for the sample stretched at a higher temperature than at a lower temperature. It was revealed that this behavior in polyethylene is the clear manifestation of strong interactions between crystallites. That is, the increased temperature accelerates the movement of crystallites by releasing the constraint acting on them. The marked contrast between the copolymers and the polyethylene in orientational behavior suggests that in copolymers, the interactions between crystallites are minimized because of the large amount of amorphous phase. The orientation functions of the copolymers are decreased because the destruction of crystallites acting as crosslinks allows the molecules between crystal-

lites to flow. One could confirm that this flow process is occurring at the temperatures at which orientation function decreases, by looking at the viscoelastic properties of the copolymers shown in Figure 9 and Figure 10.

(2) Orientational behavior in small angle light scattering. The small angle light scattering patterns of the copolymers observed at various strains are shown in Figure 29, 30, 31 and 32. The variation of the light scattering patterns with increasing strain are almost the same for 1193A and 1248B.

H_v scattering patterns of these copolymers have 4 scattering lobes orienting 45° to the analyzer and polarizer directions. Upon elongation of the sample, the 4 scattering lobes move toward the horizontal direction.

At a strain of about 20 %, there develop 4 new scattering lobes. These new scattering lobes lie near the meridian. With increasing strain they also move toward horizontal direction. The intensity of the new scattering lobes increases with increasing strain. If the sample is relaxed, the directions of the 8 scattering lobes return toward the original directions. The intensity of newly developed lobes decreases with decreasing strain.

H_v scattering patterns having 8 lobes were observed in stretched polyethylene films heat treated under constraint.[78] In this case, 4 lobes developing during heat treating, were found to be due to the new crystallites grown, ori-

enting differently from the original crystallites. This conclusion was further confirmed by x-ray diffraction technique. In the case of the copolymers, the amorphous phase consists of uncrystallizable chains so that one could not expect further crystallization under the strains applied in this work. As one could see in the x-ray scattering patterns shown in Figure 33 and Figure 34, no crystallites orienting differently from the original were found in these polymers under various strains.

Other cases one observes 8 lobed H_v scattering patterns are with solvent-cast films of styrene-butadiene-styrene block copolymers.[79] No crystallites were observed in the sample. All the scattering lobes were thought to be due to strained regions about the hard domains of styrene in this case.

This aspect of light scattering patterns will be further discussed in the later section.

The orientation of scattering lobes in H_v pattern due to crystallites may be well predicted by the theory developed by Stein,Erhardt, Aartsen, Clough and Rhodes.[74]

The amplitude of scattering from a rod of length L and infinitesimal thickness may be expressed as follows.

$$E = C \left(\underset{\sim}{M} \cdot \underset{\sim}{O} \right) L \frac{\sin(kaL/2)}{(kaL/2)} \qquad (51)$$

where C is a constant, k is $2\pi/\lambda$, λ is wave length in the

medium, $\underset{\sim}{M}$ is the induced dipole moment, $\underset{\sim}{O}$ is a unit vector in the polarization and a is given as follows.

$$a = (1-\cos\theta)\sin\gamma\cos\phi - \sin\gamma\sin\phi\sin\theta\sin\mu - \cos\gamma\sin\theta\cos\mu \quad (52)$$

where γ and ϕ are the angular coordinates of the rod axis and θ and μ are the scattering angles as shown in Figure 25.

For anisotropic rods with the optic axis lying along the rod axis $\underset{\sim}{M}$ is given as follows.

$$\underset{\sim}{M} = \frac{\delta(\underset{\sim}{E}\cdot\underset{\sim}{r})\ \underset{\sim}{r}}{r^2} + \alpha_2\ \underset{\sim}{E} \quad (53)$$

where $\underset{\sim}{r}$ is a vector along the rod to the scattering element and expressed as follows.

$$\underset{\sim}{r} = r\ (\underset{\sim}{i}\sin\gamma\cos\phi + \underset{\sim}{j}\sin\gamma\sin\phi + \underset{\sim}{k}\cos\gamma) \quad (54)$$

where $\underset{\sim}{i}$, $\underset{\sim}{j}$ and $\underset{\sim}{k}$ are the unit vectors along x, y and z directions. δ is the anisotropy given by

$$\delta = \alpha_1 - \alpha_2 \quad (55)$$

where α_1 and α_2 are the polarizabilities parallel and per pendicular to the rod.

For a distribution of rods where $N(\gamma,\phi)d\gamma\ d\phi$ in the angular interval $d\gamma$ and $d\phi$ with no phase coherence among them, the total scattered intensities will be given by the

following equation.

$$I = KL^2 \int_0^{2\pi}\int_0^{\pi} (\underset{\sim}{M}\cdot\underset{\sim}{Q})^2 N(\gamma,\phi) \quad \frac{\sin^2(kaL/2)}{(kaL/2)^2}\, d\gamma\, d\phi \qquad (56)$$

where K is a constant.

In case of V_v scattering $\underset{\sim}{E}$ and $\underset{\sim}{Q}$ will be given as follows.

$$\underset{\sim}{E} = E\,\underset{\sim}{k} \qquad (57)$$

$$\underset{\sim}{Q} = \underset{\sim}{k} \qquad (58)$$

By substituting Equations (57), (58) into (53), one could obtain $\underset{\sim}{M}$. The value of $(\underset{\sim}{M}\cdot\underset{\sim}{Q})$ for V_v scattering will then be given by

$$(\underset{\sim}{M}\cdot\underset{\sim}{Q})_{Vv} = E\,(\delta\cos^2\gamma + \alpha_2) \qquad (59)$$

For H_v scattering

$$\underset{\sim}{Q} = \underset{\sim}{j} \qquad (60)$$

so that the $(\underset{\sim}{M}\cdot\underset{\sim}{Q})$ in this case is given by

$$(\underset{\sim}{M}\cdot\underset{\sim}{Q})_{Hv} = \delta E \sin\gamma\cos\gamma \qquad (61)$$

The intensities of H_v and V_v scattering are then found by substituting Equations (61) and (59) into Equation (56) respectively.

If the deformation is well described by affine transformation, one could determine the distribution function of

rod. The distribution function would be given by Equation (46) as discussed previously. By substituting Equation (46) into Equation (56) one could calculate the H_v and V_v scattering patterns. The resulting equations are not analytically integrable but could be evaluated numerically by computer. The computation was done assuming that $C^2L^2/4\pi = 1$, $E = 1$, $\delta = 4$, $\alpha_2 = 1$ and $kL/2 = 20$. The computer program for the calculation is given in Appendix VI. The calculated results are shown in Figure 35 and Figure 36.

General features of scattering patterns obtained by theory agree rather well with that obtained by experiment. However, they are not successful to predict the direction of scattering lobes in H_v pattern. As shown in Figure 37, the angles at which scattering lobes orient with respect to the stretching direction do not agree very well. This may partly be attributable to the values of constants used in the calculation.

The V_v scattering patterns of unstretched specimen has almost spherically symmetric shape. With increasing elongation, the shape changes to elliptical whose major axis lies perpendicular to the stretching direction. At the same time, new scattering lobes parallel to the stretching direction appear. This new lobes increase their intensity with increasing elongation and decrease with decreasing elongation. One might attribute these scattering lobes to the anisotropy caused by strain field in the amor-

phous phase. This change of V_v light scattering patterns could be explained as follows. Because of the strong scattering from density fluctuations, the V_v patterns of unstretched samples were almost spherical, but with stretching, crystallites are oriented to the direction of stretching. That enhanced the scattering to the horizontal directions. General features of V_v scattering calculated by the theory agree very well with the observed patterns at bigger extension ratio.

5. The Emerging Scattering Lobes under Deformation

As has been described briefly in the previous section, the scattering patterns emerging under deformation are thought to be attributable to anisotropy caused by strain field in the amorphous phase around the crystallites. The origin of these light scattering patterns has been studied using polycarbonate film containing voids,[80] swollen filled rubber,[81] and sulphur-cured 1,4-cis-polybutadiene.[82,83] It was very firmly confirmed that the anisotropy around the voids or fillers are the scatterer in these polymers.

In Figure 38 and Figure 39, the light scattering patterns of 1248B at various strain and the micrographs of the polymer at the same strain and approximately the same place where light scattering was observed are shown. The micrographs are taken with crossed polaroids and with the

stretching direction being oriented parallel to the polarizer direction.

In the smaller strain range than 20 %, one could see some crystallites or bright part in the sample. But at bigger strain than that, there appear streaks on the surface. These streaks are predominant structures especially at high elongations. At the same time, new scattering lobes emerge in the H_v and V_v patterns. As is seen in the micrographs of elongated samples, these streaks are brighter than the surroundings. This means that the optic axis of this streaking structure lies in a somewhat different direction from that of the analyzer and polarizer direction.

The angle that these streaks make with the stretching direction decreases with increasing elongation, that is, the streaks orient more toward the stretching direction with increasing elongation. On the other hand, the light scattering lobes in H_v pattern orient more toward the horizontal direction. The angles which the streaks and a H_v scattering lobe make with stretching direction are measured and are shown in Table 5.

The results at various strains show an interesting feature of the light scattering. As could be seen in Table 5, the two angles make 90° when they are added. This result could be explained very well as follows:

Suppose the optic axis of these streaks is parallel to the direction in which they orient. Assume that these

streaks are on the plane of the film. Then the intensities of the H_v and V_v components of the scattering will be given as follows.

a given by Equation (52) will reduce to the following equation in this case.

$$a = -\sin\theta\cos(\gamma - \mu) \tag{62}$$

$N(\gamma,\phi)$ in Equation (56) will be N, which is the number of the streaks orienting to the direction when γ is equal to the angle ω, which they make with the stretching direction, otherwise it may be zero. Then Equation (56) becomes

$$I_{Hv} = NkL^2(\underset{\sim}{M}\cdot\underset{\sim}{O})^2_{Hv}\ \frac{\sin^2(g(\omega))}{(g(\omega))^2} + \frac{\sin^2(g(-\omega))}{(g(-\omega))^2} \tag{63}$$

$$I_{Vv} = NkL^2(\underset{\sim}{M}\cdot\underset{\sim}{O})^2_{Vv}\ \frac{\sin^2(g(\omega))}{(g(\omega))^2} + \frac{\sin^2(g(-\omega))}{(g(-\omega))^2} \tag{64}$$

where

$$g(\omega) = \frac{kL}{2}\sin\theta\cos(\omega - \mu) \tag{65}$$

$(\underset{\sim}{M}\cdot\underset{\sim}{O})_{Vv}$ and $(\underset{\sim}{M}\cdot\underset{\sim}{O})_{Hv}$ will be given by

$$(\underset{\sim}{M}\cdot\underset{\sim}{O})_{Vv} = E(\delta\cos^2\omega + \alpha_2) \tag{66}$$

$$(\underset{\sim}{M}\cdot\underset{\sim}{O})_{Hv} = \frac{\delta E}{2}\sin(2\omega) \tag{67}$$

As one could expect from the Equation (63), the approximate value of angle μ_H at which H_v scattering lobes lie is given by the following equation.

$$\omega - \mu_H = \pm 90^\circ \quad \text{or} \quad \omega + \mu_H = \pm 90^\circ \tag{68}$$

The increase of intensity of light scattered by these streaks with increasing strain can be explained by the increase of the value of δ of the structure with increasing strain. The cause of the structure of these streaks is not certain at this stage of experiment, but it might be due to the shearing stress within the sample. Or it might be attributable to the stress concentration around the both ends of rod-like crystallites. The general feature of the experimental H_v scattering pattern agrees very well with that of the calculation. On the other hand, the V_v scattering due to the streaks dose not agree very well. This disagreement may be partly attributable to the fact that the scattering by density fluctuations could influence strongly for the scattering at the meridian. The possibility was examined by comparing H_h and V_v scattering patterns. In Figure 41, the H_h, H_v, V_v and V_h scattering patterns of 1248B elongated 78.6 % are shown. The H_v and V_h patterns are almost the same but the H_h and V_v patterns differ considerably. In H_h pattern one no longer observes broad scattering lobes in the meridian. Instead, scattering lobes orienting to the same direction as that of newly emerging lobes in the H_v

pattern are observed. These are the results expected from the theory.

The two strong scattering lobes in the horizontal direction in the H_h pattern are attributable to density fluctuations.

The results shown in Figure 41 further substantiate that the optic axis of the streaks found is parallel to their long axis.

6. Young's Modulus, Strain and Stress Optical Coefficients

(1) Young's modulus of the copolymers. In non-crosslinked amorphous polymers of low molecular weight, flow will occur after relatively short time. However in crystalline polymers, the crystalline regions or entanglements will restrict the flow process. As has been mentioned before, the copolymers used in this work show a rubbery region, especially in higher crystalline 1248B. In this region, it would be a good approximation to assume that the crystallites are acting as crosslinking points. If this is the case, one may apply the statistical rubber elasticity theory to the copolymers and could predict the mechanical and rheo-optical properties of these ethylene-propylene copolymers.

In Figure 42, the Young's moduli of both samples of the copolymers are seen to decrease with increasing tem-

perature. In the α-transition region, the moduli decrease abruptly, suggesting that not only the amorphous phase but also the crystalline phase contribute to moduli. It implies that the assumptions made here are not strictly true. In spite of these difficulties, Bueche[84] has presented a theoretical attempt to describe the mechanical properties on these bases.

He assumed that the structure of the polymers to be as follows: The crystallites are rectangular parallelepipeds of dimensions $\alpha \times \alpha \times \lambda$. The length λ is taken to be parallel to the chain axis in the crystal. All chains are assumed to enter and leave the crystal through the ends, each of area α^2. After leaving the crystal, the chains, if long enough, will enter a new crystal whose end area is a distance b from the previous crystallite. On the average, each chain emerging from the crystal will occupy an area σ^2 of the end face. The number of effective network chains coming from this single face of the crystal is then given by $(\alpha^2/\sigma^2)p$, where p is the probability that the emergent chain will continue on into another crystallite.

Since the force constant for each chain is given as $3kT/R_s^2$, from statistical theory, where R_s^2 is the mean square length of the chain between crystals and is equal to $3b^2$ in this case, k is Boltzmann constant, the Young's modulus will be given as follows.

$$E_y = pkT(b + \lambda) / \sigma^2 b^2 \qquad (69)$$

The method used by Bueche to evaluate the necessary parameters for the calculation could not be applied to the copolymers used in this study because of their low crystallinities. However if one knows the values of these parameters by other methods, Bueche's theory may be very easy to apply.

Another approach was made by Nielsen.[85] He assumed that crystallites act both as crosslinks and as a rigid filler. According to the statistical theory, the shear modulus G is given by the equation.

$$G = \rho RT / \bar{M}_c \qquad (70)$$

where ρ is the density of the polymer, R is the gas constant, and $\bar{M}_c$ is the number-average molecular weight between crosslinks. In the case of crystalline polymers one may assume that $\bar{M}_c$ is the number-average molecular weight of an amorphous sequence.

The effect of crystallites as fillers was estimated by the theory developed by Guth[86] and Smallwood.[87] It is expressed as follows.

$$F(\phi_c) = 1 + 2.5 \phi_c + 14.1 \phi_c^2 \qquad (71)$$

where ϕ_c is the volume fraction of crystallites. Then the shear modulus of a crystalline polymer becomes

$$G = \rho RT \cdot F(\Phi_c) / \bar{M}_c \qquad (72)$$

He estimated the value of $\bar{M}_c$ of copolymeric rubber as follows. If the crystallizable unit A and non-crystallizable unit B are present in a chain randomly, the fraction, $n_A(m)$, of material A contained in sequences m units long is given by[88]

$$n_A(m) = (1 - X_A) X_A^{m-1} \qquad (73)$$

where X_A is the mole fraction of unit A. The weight fraction of material A contained in sequences exactly m units long is given by

$$w_A(m) = m (1 - X_A)^2 X_A^{m-1} \qquad (74)$$

Long sequences of A units crystallize at higher temperatures than shorter sequences of A units. Assuming that at a given temperature all but only A sequences of length m_0 units or longer are contained in crystallites, the weight fraction of material A in crystallites is calculated. The resulting equation is

$$f_A(m_0) = m_0 X_A^{m_0-1} - (m_0 - 1) X_A^{m_0} \qquad (75)$$

If W_A is the weight fraction of component A in the copolymer, the crystallinity is given by

$$w^c = W_A f_A(m_0) \qquad (76)$$

The amorphous phase consists of all of the sequences of B units together with those sequences of A units that are less than m_0 long. It is thought that the relative number of amorphous sequences is equal to that of crystalline sequence. Then the relative number of network chain is given by Equation (77).

$$R' = \sum_{m=m_0}^{\infty} X_B \, X_A^{m-1} \Big/ \sum_{n=1}^{\infty} X_B \, X_A^{n-1} = X_A^{m_0-1} \qquad (77)$$

where X_B is the mole fraction of unit B.

The number average molecular weight of an amorphous chain is then given by

$$\bar{M}_c = M_A \left\{ \frac{1 - X_A^{m_0+1}}{X_A^{m_0}(1-X_A)} - m_0 - \frac{1 - M_B/M_A}{X_A^{m_0}} \right\} \qquad (78)$$

where M_A and M_B are the molecular weight of unit A and unit B respectively.

The volume fraction of crystallites will be given by

$$\Phi_c = 1 \Big/ \{ 1 + (\rho_c/\rho_a) \, R' \} \qquad (79)$$

where ρ_c and ρ_a are the densities of crystalline and amorphous phase.

If the units are not distributed randomly the probabilities p_A or p_B that an A or B units are succeeded by another A or B units should be replaced to X_A and X_B respectively.

From the shear modulus thus obtained the Young's mod-

ulus could be calculated according to the equation.

$$E_y = 2\,G\,(\,1 + \nu\,) \qquad (80)$$

where ν is a Poisson's ratio of the polymer.

The Young's moduli of the copolymers were calculated according to the theory. The calculated values are also given in Figure 42. In calculation, the Poisson's ratio is thought to be 0.5 and the densities of crystalline and amorphous parts are assumed to be the same to those of polyethylene. The specific volumes of polyethylene crystal and amorphous phase used in the calculation are given by the following equation.[50]

$$V_a = 1.1520 + 0.000780\ t \qquad (81)$$

$$V_c = 1.0020 + 0.000300\ t \qquad (82)$$

where V_a and V_c are the specific volumes of amorphous and crystalline parts of polyethylene, t is the temperature in degrees centigrade.

The calculated value of Young's modulus of 1248B agrees rather well, but in case of 1193A, the agreement is poorer. It has been reported that in case of ethylene copolymers, for example, branched polyethylene and ethylene-vinyl acetate copolymers, the calculated value is smaller than the experimental values by a factor of seven to ten.[89] Compared to those cases, the calculated Young's moduli of

the copolymers studied in this work agree very well with that of experiment. From the relatively good agreement between theory and experiment obtained in the study of the Young's modulus measurement, it was strongly suggested that the statistical rubber elasticity theory could be applied rather well to the low crystalline polymers.

Further improvement of theory could be made by introducing the non-random distribution of A and B units in a copolymer chain. It was also recognized that the morphological geometry of the individual crystallites and their distribution in the amorphous matrix radically affect the mechanical properties of crystalline polymers.[90-92]

(2) Strain and stress optical coefficients. Strain optical coefficients of the copolymers at various temperatures are shown in Figure 43. The strain optical coefficients of both polymers increase in the temperature region lower than -40°C. In the higher temperature region, the strain optical coefficients decrease with increasing temperature. Higher crystalline 1248B has larger strain optical coefficients in the temperature range studied.

The temperature at which the strain optical coefficients become maxima coincides with that of the β-transition found in the study of the viscoelastic properties of the polymers. The increase of the strain optical coefficient in this temperature region is attributable to the transition from glassy state to rubbery state. The decrease in the

higher temperature region may be due to the decrease of the amount of anisotropic crystallites. Also because of that very destruction of crystallites, which act as crosslinks, the effective number of network chains decrease and the anisotropy induced in the amorphous phase is thought to decrease.

In the temperature region at which the substantial number of crystallites are melted, the flow process begins to occur appreciably. This is thought to be the reason for the marked decrease of the strain optical coefficient near the melting points of the copolymers.

Stress optical coefficients of the copolymers at various temperatures are shown in Figure 44. In the β-transition region, the coefficients increase very rapidly with increasing temperature. They tend to level-off in the rubbery region. In the α-transition region, the coefficients increase abruptly and level-off again with increasing temperature. In the flow region they decrease with increasing temperature.

The total birefringence of semi-crystalline polymer may be resolved into three contributions[93] as shown in Equation (83).

$$\Delta = \phi_c \Delta_c + (1 - \phi_c) \Delta_a + \Delta_F \qquad (83)$$

where Δ_c is the birefringence per unit volume of crystalline material, Δ_a is the birefringence per unit volume of amor-

phous material, Δ_F is the form birefringence.

If the principal refractive indices are available, the value of Δ_c of the orthorhombic crystal system may be estimated by the following equation.

$$\Delta_c = f_a (n_a - n_c) + f_b (n_b - n_c) \qquad (84)$$

where f_a and f_b are Herman's orientation functions for the a and b crystal axes, and n_a, n_b and n_c are the principal refractive indices. If $f_a = f_b = f_{110}$, as was assumed in this work, Δ_c will be given by

$$\Delta_c = f_{110} (n_a + n_b - 2 n_c) \qquad (85)$$

where f_{110} is the orientation function of (110) normals.

The total birefringence and the crystalline contribution could be obtained by experiment. For the first approximation one may neglect the form birefringence. Then the amorphous birefringence contribution could be evaluated by subtracting crystalline contribution from the total birefringence. The amorphous contribution could be independently calculated by the statistical theory developed by Kuhn and Grün.[5]

In their treatment the actual chain is replaced by an idealized chain of m universally-jointed, randomly-oriented links, each of length l. The links are assumed to be optically anisotropic and characterized by polarizabilities α_1 along and α_2 at right angles to their length. To determine

the principal polarizabilities of the chain, and their dependence on the distance between its ends, it is required to know the angular distribution of the individual links corresponding to a given distance between the ends. The solution to this problem has been worked out by Kuhn and Grün, and is represented by the formula

$$dN = e^{\alpha} e^{\beta \cos\theta} \frac{1}{2} \sin\theta \, d\theta \qquad (86)$$

in which dN represents the number of links making an angle between θ and $\theta + d\theta$ to the line joining the ends of the chain. α and β are constants whose values depend on the distance r between the ends of the chain and are given by the relations

$$\beta = \mathcal{L}^{-1}(r/ml) \qquad (87)$$

$$\alpha = m\beta/\sinh\beta \qquad (88)$$

The function $\mathcal{L}^{-1}$ in Equation (87) is the inverse Langevin function.

If the line joining the ends coincides with the x-axis of a rectangular coordinate system, a given link of the chain make an angle θ with x-axis, and the plane containing the link and x-axis makes an angle ϕ with the plane containing x- and y-axes, the polarizabilities of the link, for fields respectively along x- and y-axes are given by the relations

$$\alpha_x = \alpha_1 \cos^2\theta + \alpha_2 \sin^2\theta \tag{89}$$

$$\alpha_y = (\alpha_1 - \alpha_2) \sin^2\theta \cos^2\phi + \alpha_2 \tag{90}$$

And the corresponding total polarizabilities of the chain will be

$$\gamma_1 = \int \alpha_x \, dN \tag{91}$$

$$\gamma_2 = \int \alpha_y \, dN \tag{92}$$

The number of links at angles between θ and $\theta + d\theta$ and between ϕ and $\phi + d\phi$ is from Equation (86)

$$dN = e^{\alpha} e^{\beta \cos\theta} \frac{1}{2} \sin\theta \frac{1}{2\pi} d\theta \, d\phi \tag{93}$$

Introducing this distribution into Equations (91), (92) and integrating, one obtains the following results.

$$\gamma_1 = m\left[\alpha_1 - (\alpha_1 - \alpha_2) \frac{(2r/ml)}{\mathcal{L}^{-1}(r/ml)} \right] \tag{94}$$

$$\gamma_2 = m\left[\alpha_1 + (\alpha_1 - \alpha_2) \frac{(r/ml)}{\mathcal{L}^{-1}(r/ml)} \right] \tag{95}$$

If the strain is not sufficiently large to cause any significant fraction of the total number of chains to assume lengths comparable with their fully-extended length, the inverse Langevin function may be represented by the first term of its series expansion and the Equations (94) and (95) reduce to the formulas

$$\gamma_1 = \frac{m}{3} (\alpha_1 + 2\alpha_2) + \frac{2}{5} m (\alpha_1 - \alpha_2) (\frac{r}{ml})^2 \quad (96)$$

$$\gamma_2 = \frac{m}{3} (\alpha_1 + 2\alpha_2) - \frac{1}{5} m (\alpha_1 - \alpha_2) (\frac{r}{ml})^2 \quad (97)$$

Suppose that the network contains N of these molecular chains, each consisting of m universally jointed links of length l. The junction points of the network will be continually fluctuating in position, on account of the random thermal motion of the chains. For the calculation of the polarizabilities of the network, they will be assumed to occupy their average positions. For simplicity, it is assumed that the distances between neighbouring junction points in the undeformed network are all equal. These restrictions were shown to be unnecessary. Finally, it is assumed that the junction points move affinely, and the volume of the network does not change during deformation.

In the unstretched network the "displacement length" of the assembly of chains may be represented by a set of vectors which are distributed randomly in direction. If the network is deformed to the extension ratio χ, the original random distribution of the vectors changes to elipsoidal distribution as shown in Figure 45. After deformation, the distribution of the vectors may be expressed by Equation (46) A given "displacement length" making an angle γ with

z-axis, and the plane containing the displacement length and z-axis makes an angle ϕ with the plane containing x- and z-axes, the polarizabilities of the displacement length for fields respectively along z and y axes will be given by

$$\beta_z = (\gamma_1 - \gamma_2) \cos^2\gamma + \gamma_2 \qquad (98)$$

$$\beta_x = (\gamma_1 - \gamma_2) \sin^2\gamma \cos^2\phi + \gamma_2 \qquad (99)$$

Then the difference of polarizabilities of the network in z and x directions will be given by

$$P_z - P_x = \int_0^{2\pi}\int_0^{\pi} N(\gamma,\phi)(\beta_z - \beta_x) \, d\gamma \, d\phi \qquad (100)$$

By substituting the Equations (98), (99) and (96), (97) into Equation (100), one can get the following result.

$$P_z - P_x = \frac{3(\alpha_1-\alpha_2)}{5ml^2} \int_0^{2\pi}\int_0^{\pi} N(\gamma,\phi) r^2 (\cos^2\gamma - \sin^2\gamma \cos^2\phi) d\gamma \, d\phi \qquad (101)$$

During the deformation the length of the displacement length will change from the original length r_0 to r. r is given by

$$r = \chi^2 \, r_0^{\,2} \, / \, (\cos^2\gamma + \chi^3 \sin^2\gamma) \qquad (102)$$

By substituting the Equation (102) and distribution function (46) into Equation (101) and performing the integration, one obtains the final result

$$P_z - P_x = \frac{Nr_0^2(\alpha_1-\alpha_2)}{5\,m\,l^2}\left(\chi^2 - \frac{1}{\chi}\right) \qquad (103)$$

If $r_0^2 = ml^2$, the equation reduces to

$$P_z - P_x = \frac{N}{5}\left(\alpha_1 - \alpha_2\right)\left(\chi^2 - \frac{1}{\chi}\right) \qquad (104)$$

From the well known Lorenz-Lorentz equation, one could calculate the refractive index from polarizabilities. The Lorenz-Lorentz equation would be given as

$$\frac{n^2 - 1}{n^2 + 2} = \frac{4}{3}\pi P \qquad (105)$$

By differentiating with respect to P, one obtains the expression

$$\Delta n = \frac{2}{9}\pi \frac{(\bar{n}^2 + 2)^2}{\bar{n}} \Delta P \qquad (106)$$

where Δn is the refractive index difference, and ΔP is the difference in polarizability, $\bar{n}$ is the average refractive index.

By substituting Equation (104) into Equation (106), one obtains the birefringence of the network as

$$\Delta n = \frac{2\pi}{45} \frac{(\bar{n}^2+2)^2}{\bar{n}} N\,(\alpha_1-\alpha_2)\left(\chi^2 - \frac{1}{\chi}\right) \qquad (107)$$

At small extension ratios, the last term of Equation (107) will be approximated in the following manner.

$$\chi^2 - \frac{1}{\chi} = 3\alpha \qquad (108)$$

where α is the strain.

By substituting Equation (108) into Equation (107) one obtains

$$\Delta n = \frac{2\pi}{45} \frac{(\bar{n}^2+2)^2}{\bar{n}} N(\alpha_1-\alpha_2)\cdot 3\alpha \qquad (109)$$

As is seen in Equation (109), it is expected that the amorphous contribution is proportional to strain.

The orientation function of the (110) normal was shown to increase nearly linearly with strain in this case. One therefore expects the linear increase of birefringence with increasing strain in small strain region, and that was found in our experiments. The peculiar decrease of birefringence in the small strain range found in polyethylene was not found in the polymers used in this work. The main reasons for the above mentioned behavior of the samples are thought to be attributable to the low crystallinity and the lack of strong interactions between crystallites.

From the statistical rubber elasticity theory, one could know the stress at a given extension ratio. The result obtained on the same assumption made to calculate the birefringence is given in the following equation.

$$\sigma = NkT\left(\chi^2 - \frac{1}{\chi}\right) \qquad (110)$$

where σ is the stress.

Then the stress optical coefficient is given as follows.

$$\frac{\Delta n}{\sigma} = \frac{2\pi}{45kT} \frac{(\bar{n}^2+2)^2}{\bar{n}} (\alpha_1 - \alpha_2) \qquad (111)$$

The stress optical coefficient is a function only of the anisotropy of the chain link and the mean refractive index of the polymer. In case of rubber, the validity of Equation (111) was confirmed by Treloar.[14]

For the low crystalline polymers like ethylene - propylene copolymers used here, the amorphous contribution to birefringence may be analyzed by the same method as that of rubber.

Because the crystalline phase is polyethylene, the principal refractive indices could be assumed to be equal to that of polyethylene crystals. By substituting the values of refractive indices reported by Bunn[94] into Equation (85) and using the experimentally obtained values of initial slopes in Figure 28, the strain optical coefficients at various temperature were resolved into crystalline (K_{cr}) and amorphous (K_{am}) contributions. Form birefringence was neglected.

The result of the resolution is shown in Figure 46. The crystalline contributions of both samples decrease with increasing temperature as well as the amorphous contribu-

tions.

As has been pointed out previously, the variation of the crystalline modulus in the α-transition region affects the Young's modulus of the polymer, but the agreement between the theoretical and the experimental results were rather good. One may therefore assume that all the stress is arising from the rubbery elastic origin. If this is the case one could calculate the anisotropy of the statistical unit of the polymer according to Equation (109).

The anisotropies of the statistical units are calculated from the contributions of amorphous phase to strain optical coefficient and Young's modulus of the copolymers. As the mean refractive index of the copolymer, the experimental value of the polymers determined by an Abbe refractometer was used. The anisotropy of the copolymers are shown in Figure 47. They are bigger than that of polypropylene reported by Samuels[95] and by Tsvetkov[96] and almost the same or bigger in the higher temperature region to the value of 5.6 Å^3, reported for polyethylene.[97]

The anisotropy of the copolymers is thought to depend on the contents of the comonomer. The calculation of the anisotropy of the copolymer was reported by Sindo and Stein. They have shown[98,99] that for the copolymer which consists of i comonomers each of them has the statistical unit length of L_i and anisotropy $(\alpha_1-\alpha_2)_i$, the average anisotropy of them are given by

$$\overline{(\alpha_1-\alpha_2)} = \sum_i N_i(\alpha_1-\alpha_2)_i L_i^2 / \sum_i N_i L_i^2 \qquad (112)$$

where N_i is the number of statistical units of type i per chain.

From the study of viscosity measurement, it is known that the lengths of the statistical units of polypropylene and polyethylene do not differ very much.[100] In this work therefore, the average anisotropy of the copolymer will be calculated according to the following equation.

$$\overline{(\alpha_1-\alpha_2)} = X_E(\alpha_1-\alpha_2)_E + (1-X_E)(\alpha_1-\alpha_2)_p \qquad (113)$$

where X_E is the mole fraction of ethylene in amorphous phase, $(\alpha_1-\alpha_2)_E$ is the anisotropy of polyethylene's statistical unit and $(\alpha_1-\alpha_2)_p$ is that of polypropylene. For the calculation, the anisotropies mentioned previously[95,97] were used. The value of X_E is obtained by subtracting the mole of ethylene units in crystalline phase from the total.

The calculated values are also shown in Figure 47. As could be seen in the figure, calculated anisotropies of the chains increase only slightly with increasing temperature. That means that the increase of anisotropies with increasing temperature observed in experiment can not be explained only on the bases of increase of more anisotropic ethylene units in the amorphous phase. The increase of anisotropies in the temperature region of 30°C to 50°C may mainly result from the decrease of Young's moduli of the copolymers. This

may suggest that it would be necessary to resolve the stress into entropic and internal energy contributions. If this could be performed, one could obtain more rigorous values of anisotropy of the statistical unit.

The increase of anisotropies of statistical unit at higher temperature may be due to the different dependency of stress and birefringence on temperature.

One of the encouraging aspects of this result is that in 1248B, the calculated and the experimental values agree rather well in the rubbery region, the temperature region between α-transition temperature and the temperature at which flow processes become predominant. In case of 1193A, this temperature region is very narrow and a distinct plateau region was not found in the plot. From this fact one might say that the model that the crystallites acting as crosslinks may valid in the temperature region in the copolymers.

The true value of anisotropy of the statistical unit is thought to be smaller than the values shown in Figure 47. This is because the form birefringence was negrected, and also because of the expansion of the crystal lattice. The crystal lattice expands mainly in a spacing. Thus the anisotropy of the crystal in these copolymers may be bigger than that of polyethylene. This increases the birefringence contribution of the crystallites and reduce the contribution of amorphous phase.

7. Estimation of Form Birefringence

The birefringences of copolymers elongated 50 % and swollen to 0.9 of volume fraction of polymer with various solvents are shown in Figure 48. Both copolymers have a minimum point in the plot. The minima of both samples occur when they were swollen by the solvent whose refractive index is around 1.46. The value is smaller than that found in polyethylene.[38]

Because of the low crystallinity of the copolymer, the velocity of swelling is very rapid. In this case, it would be dangerous to neglect the variation of orientation of crystallites and amorphous chains during the process. Also the contribution of strain field around the crystallites may change by swelling the polymer. Because of these reasons, one could not obtain the contribution of form birefringence simply subtracting the birefringence after swelling from the birefringence before swelling.

If it is assumed that crystallinity and strain field around the crystallites do not change during swelling, one could obtain the decrease of birefringence swollen by the solvent which give minimum in the plot shown in Figure 48 by the following equation.

$$d\Delta = \phi_c \, d\Delta_c + (1 - \phi_c) \, d\Delta_a \qquad (114)$$

where $d\Delta$, $d\Delta_c$ and $d\Delta_a$ are the variation of the total, cry-

stalline and amorphous birefringence of a polymer.

$d\Delta_c$ may be given by

$$d\Delta_c = df_{110}(n_a + n_b - 2 n_c) \qquad (115)$$

where df_{110} is the variation of (110) normal orientation function during swelling. df_{110} may be estimated from the change of extension ratio. When a polymer is swollen to the extent of its volume fraction of v_2, the extension ratio of the fastened polymer whose extension ratio is χ_0 before swelling will be changed to the following value after swelling.

$$\chi = \chi_0 \, v_2^{\frac{1}{3}} \qquad (116)$$

Treloar[13] showed that the birefringence of the swollen rubber is given by the following equation.

$$\Delta n = \frac{(\bar{n}^2+2)^2}{\bar{n}} \frac{2\pi}{45} N (\alpha_1-\alpha_2) v_2^{\frac{1}{3}} (\chi^2 - \frac{1}{\chi}) \qquad (117)$$

It is shown in the equation that the strain optical coefficient decreases with increasing extent of swelling.

From the equation, the change of birefringence of the fastened rubber will be given by the following equation.

$$d\Delta n = \frac{(v_2-1)\chi_0^{\,2}}{(\chi_0^{\,2} - \frac{1}{\chi})} \Delta n_0 \qquad (118)$$

where $d\Delta n$ is the variation of birefringence during swelling

and Δn_0 is the initial birefringence.

In case of the copolymers, $d\Delta n = (1-\phi_c)d\Delta_a$ and Δn_0 may be equal to the amorphous birefringence contribution of the unswollen sample.

The total birefringence of the unswollen polymers is also shown in Figure 48. From the results shown in Figure 46, one could resolve the total birefringence into amorphous and crystalline contributions. Substituting the values of n_a, n_b and n_c into Equation (115), one could obtain the variation of crystalline contribution during swelling. Also from Equation (118) one can estimate the variation of amorphous contribution. Once these values are known, the total variation of birefringence caused by the change of orientational state will be estimated. subtracting the variation of birefringence from the total and comparing the value with that at minimum in the plot shown in Figure 48, one can estimate the magnitude of form birefringence. In Table 6, the calculated variation of birefringence during swelling and the magnitude of form birefringence is shown.

The form birefringence of both copolymers are almost the same. But the ratio of the form birefringence to the total birefringence is bigger in lower crystalline 1193A than in 1248B.

This result seems contradictory, but if the effect of strain field was considered, this result might reversed,

because the correction might affect 1193A more than 1248B.

As is expected, the form birefringence is more significant in these copolymers than in polyethylene. This may be attributable to the rod-like superstructures of the crystallites.

IV. CONCLUSIONS AND FUTURE WORKS

1. Conclusions

The dynamic mechanical measurement revealed that there are three transition processes in the copolymers within the temperature region studied. The γ-transition occurs at about -120°C, and is thought to be of the same origin as that of polyethylene. The β-transition is the glass transition. In higher temperature region than that of the β-transition, the copolymers are rubbery and their mechanical and rheo-optical properties are well approximated by a network crosslinked by crystallites. The γ and β-transition have apparent activation energies of about 7 kcal/mol and about 11.5 kcal/mol respectively in both polymers.

Both copolymers have very small crystallinities consisting of polyethylene units at room temperature, 18 wt% and 12 wt% for 1248B and 1193A respectively. Melting points of the copolymer are higher than expected from Flory's theory. This is thought mainly due to the non-randomness of the comonomer distribution within a molecule.

The observed (110) spacings were bigger than that of polyethylene. Because of the imperfections of the unit cell the thermal expansion coefficients of (110) spacings of the polymers are bigger than polyethylene. The lower crystalline 1193A has a bigger thermal expansion coefficient than 1248B.

From the small angle light scattering studies of the copolymers, it was revealed that the crystallites in both polymers have rod-like superstructures.

In the studies of the x-ray orientation function measurement, it was found that the crystallites orient less than is expected from Kratky's "floating rod" model. The dependence on temperature is not prominent in the orientation functions of the copolymers. From those results, it was suggested that there are no such strong interactions between crystallites as is found in highly crystalline polyethylene.

The large amount of amorphous materials around crystallites seem to suppress the crystallites to orient according to affine transformation, especially at higher elongation.

The orientational behavior of the crystallites was studied by small angle light scattering method. From the H_v scattering pattern variations with strain, the qualitative orientational behavior was obtained.

In the light scattering patterns, new scattering lobes were found to emerge at strains of about 20 %. Microscopic studies of the polymer clearly showed that streaks appear when seen under crossed nichols, alining in the stretching direction parallel to analyzer or polarizer directions. Those streaks seen under the microscope were thought to be caused by the strain field around the rod-like

crystallites. Further study of light scattering suggests that the optic axis of those streaks is parallel to the long axis of the streaks.

Static mechanical properties agree rather well with the theory based on statistical rubber elasticity theory.

Resolution of the strain optical coefficient was performed according to the two phase model. From the birefringence contribution of the amorphous phase, the anisotropy of the statistical unit was calculated. The calculated anisotropy was affected by α-transition due to crystallites and flow processes at high temperatures. The results suggest that it is necessary to resolve the stress into entropic and internal energetic contributions. But, especially in 1248B in which marked rubbery region was observed, the anisotropy of the statistical unit obtained experimentally agree very well with the value calculated from the values of polypropylene and polyethylene.

Estimation of form birefringence resulted larger contributions than is found in polyethylene. But the true value may be smaller than is found, since at 50 % elongation, there may be some reductions of anisotropy caused by strain field around crystallites during swelling.

2. Future Works

As was mentioned in the study of crystallinity, the variation of crystallinity with temperature will be better

discussed if one could know the heat of fusion, or the value of p, that is the probability that a unit A succeeds the preceding one.

To know the p, one may need a rigorous experiment concerned with copolymerization kinetics or other ways to determine the distribution of the comonomers in a molecule. This sort of experiment may be difficult to do in this laboratory. So far, neither IR-spectroscopy nor NMR-spectroscopy seem satisfactory for the purpose.

An easier experiment may be the determination of heat of fusion. The direct measurement of heat of fusion by DSC was not successful because of the low crystallinity and the wide range of melting temperature. One of the possible methods may be the measurement of melting point depression by swelling. The melting point may be determined by measuring the intensities of depolarized light with crossed polaroid. From the preliminary experiment, it was known that a strong wide beam is necessary to avoid errors caused by the surface effects and weak intensities near the melting point. This could be easily done with a beam expander and a laser light source.

The dynamic birefringence measurement which was originally planned, was not done because of the lack of time. The dynamic birefringence measurement at low static strain may give informations about the orientational behavior of crystallites and amorphous chains. If performed at

larger strain, one might find a contribution from the strain field around the crystallites.

The study of the strain field around crystallites may be performed at elevated and lower temperatures. Especially in the β-transition region one might find the effects of the rigidities of amorphous phase on the strain field.

If measurements were performed along with morphological studies it might be easier to explain the results.

The resolution of the stress into entropic and internal energetic contributions may be difficult to perform, because of the melting of the crosslinking crystallites.

A P P E N D I X I

THE VALUE OF A FOR THE CALCULATION OF E

Tanδ Range or Amplitude Factor (db)	A
0	31.6
10	10.0
20	3.16
30	1.00
40	0.316
50	0.100
60	0.0316

A P P E N D I X II

THE COMPUTER PROGRAM FOR THE CALCULATION OF DYNAMIC STORAGE MODULUS AND LOSS MODULUS

```
010 PROGRAM VIBRON
020 DIMENSION AL(150),TAN(150),FORCE(150),LANGE(150)
030 DIMENSION COS(150),E1(150),E2(150)
040 DIMENSION PTO(150),TO(150),PT(150),T(150)
045 READ,K2
050 DO 060 I=1,K2,1
060 READ,PTO(I),TO(I)
070*CALCULATION OF CROSS SECTION
080 READ,W,TH,ALO,K1,TD
090 S=W*TH*6.4668*10.0**(-6.0)
100*CALCULATION OF E PRIME,AND E DOUBLE PRIME
110 DO 410 I=1,K1,1
120 READ,PT(I),FORCE(I),TAN(I),AL(I),LANGE(I)
130 IF(AL(I)) 140,190,190
140 IF(AL(I)+100.0) 150,170,170
150 AL(I)=ALO*2.543-0.3-10.0**(-3.0)*AL(I)
160 GO TO 210
170 AL(I)=2.543*ALO-0.1-10.0**(-3.0)*AL(I)
180 GO TO 210
190 AL(I)=2.543*ALO+10.0**(-3.0)*AL(I)
200 GO TO 210
210 COS(I)=1.0/(1.0+TAN(I)**2.0)**0.5
220 IF(LANGE(I)-20) 230,250,270
230 F=10.0
240 GO TO 290
250 F=3.16
260 GO TO 290
270 F=1.0
280 GO TO 290
290 E1(I)=2.0*10.0**9.0*AL(I)*COS(I)/(FORCE(I)*F*S)
300 E2(I)=E1(I)*TAN(I)
310*CALCULATION OF TEMPERATURE
320 IF(PT(I)) 330,350,350
330 T(I)=PT(I)
340 GO TO 370
350 PT(I)=PT(I)+TD
360 GO TO 370
370 J=0
380 J=J+1
390 IF(PT(I).GE.PTO(J)) 400,410
```

```
400 GO TO 380
410 T(I)=(TO(J)-TO(J-1))*(PT(I)-PTO(J-1))/(PTO(J)-PTO
411C(J-1))+TO(J-1)
420 WRITE(61,450)
430 DO 440 I=1,K1,1
440 WRITE(61,470) T(I),TAN(I),E1(I),E2(I)
450 FORMAT(3X,*TEMP(C)*,3X,*TAN DELTA*,3X,*EPRIME(
460CDYNE/CM↑2)*,3X,*EDOUBLE*)
470 FORMAT(F8.2,6X,F6.4,7X,E11.4,5X,E11.4)
480 END
490 END PROG
495 76
400 -120.0,-180.0
501 -117.5,-175.0
502 -115.0,-170.0
503 -112.4,-165.0
504 -110.0,-160.0
505 -107.5,-155.0
506 -105.0,-150.0
507 -102.6,-145.0
508 -100.0,-140.0
509 -97.0,-135.0
510 -94.2,-130.0
511 -91.5,-125.0
512 -88.8,-120.0
513 -85.8,-115.0
514 -83.0,-110.0
515 -80.2,-105.0
516 -77.5,-100.0
517 -74.3,-95.0
518 -71.2,-90.0
519 -68.0,-85.0
520 -64.9,-80.0
521 -61.5,-75.0
522 -58.3,-70.0
523 -55.0,-65.0
524 -51.7,-60.0
525 -48.0,-55.0
526 -44.1,-50.0
527 -40.2,-45.0
528 -36.6,-40.0
529 -32.5,-35.0
530 -28.7,-30.0
531 -24.2,-25.0
532 -20.0,-20.0
533 -15.3,-15.0
534 -10.7,-10.0
535 -6.0,-5.0
536 0.0,0.0
537 5.0,5.0
```

```
538 10.3,10.0
539 15.5,15.0
540 20.8,20.0
541 25.9,25.0
542 31.1,30.0
543 36.0,35.0
544 41.0,40.0
545 45.8,45.0
546 50.6,50.0
547 55.5,55.0
548 60.5,60.0
549 65.3,65.0
550 70.2,70.0
551 75.0,75.0
552 79.6,80.0
553 84.5,85.0
554 89.5,90.0
555 94.0,95.0
556 99.0,100.0
557 104.1,105.0
558 109.4,110.0
559 114.3,115.0
560 119.4,120.0
561 124.7,125.0
562 129.7,130.0
563 134.9,135.0
564 139.9,140.0
565 145.0,145.0
566 149.7+150.0
567 154.5,155.0
568 159.3,160.0
569 164.2,165.0
570 169.3,170.0
571 174.2,175.0
572 179.2,180.0
573 184.2+185.0
574 189.2,190.0
575 194.4,195.0
```

A P P E N D I X III

THE COMPUTER PROGRAM FOR CORRECTION OF THE DIFFRACTED X-RAY INTENSITIES

```
10 PROGRAM CORREN
20 DIMENSION PAG(50),SFC(50),SFH(50),ASFC(100),ASFH(100)
30 DIMENSION BAN(100),B(100)
40 DIMENSION NH(100),NA(100,3),HN(100),AN(100,3)
50 DIMENSION A(100),AAN(100),COUN(100)
60 DIMENSION AANR(100),POL(100),AU(100),ABSN(100),COU(100)
70 DIMENSION YSIN(100),FINCO(100),XIN(100),COUNT(100)
80 READ,KA
90 DO 100 I=1,KA
100 READ,PAG(I),SFC(I),SFH(I)
110 READ,KB
120 DO 130 I=1,KB
130 READ,BAN(I),B(I)
140 READ,TH,ABO
150 READ,KC
160 DO 350 I=1,KC
170 READ,AAN(I),NH(I),NA(I,1),NA(I,2),NA(I,3)
180 SA=0.
190 DO 240 J=1,3
200 AN(I,J)=NA(I,J)
210 SA=SA+AN(I,J)
220 HN(I)=NH(I)
230
240 A(I)=SA/HN(I)/3.
250
260 M=0
270 M=M+1
280 IF(AAN(I).EQ.BAN(M)) 300,290
290 GO TO 270
300 COUN(I)=A(I)-B(I)
310 AANR(I)=AAN(I)*3.1416/180.
320 POL(I)=2./(1.+COSF(AANR(I))**2)
330 AU(I)=ABO*TH*(1./COSF(AANR(I))-1.)
340 ABSN(I)=AU(I)/(1.-EXPF(-AU(I)))
350 COU(I)=COUN(I)*ABSN(I)*POL(I)
355 KD=KC-1
360 DO 480 I=1,KD
370 YSIN(I)=SINF(AANR(I)/2.)/1.5417
380 J=0
390 J=J+1
400 IF((PAG(J+1)-YSIN(I))*(PAG(J)-YSIN(I)).LE.0.) 420,410
410 GO TO 390
```

```
420 ASFC(I)=(SFC(J+1)-SFC(J))*(YSIN(I)-PAG(J))/(PAG(J+1)-
430CPAG(J))+SFC(J)
440 ASFH(I)=(SFH(J+1)-SFH(J))*(YSIN(I)-PAG(J))/(PAG(J+1)-
450CPAG(J))+SFH(J)
460 FINCO(I)=(6.-ASFC(I))/3.+2.*(1.-ASFH(I))/3.
470 XIN(I)=COU(KC)*FINCO(I)/1.4936
480 COUNT(I)=COU(I)-XIN(I)
490 WRITE(61,520)
500 DO 510 I=1,KD
510 WRITE(61,530),AAN(I),COUNT(I)
520 FORMAT(3X,*ANGLE*,4X,*INTENSITY*)
530 FORMAT(3X,F5.2,4X,F10.6)
540 END
550 ENDPROG
600 18
601 0.00,6.000,1.000
602 0.05,5.764,0.947
603 0.10,5.141,0.818
604 0.15,4.362,0.636
605 0.20,3.612,0.482
606 0.25,3.003,0.350
607 0.30,2.538,0.252
608 0.35,2.212,0.179
609 0.40,1.983,0.131
610 0.50,1.707,0.073
611 0.60,1.548,0.037
612 0.70,1.423,0.023
613 0.80,1.313,0.015
614 0.90,1.202,0.010
615 1.00,1.096,0.007
616 1.10,0.992,0.005
617 1.20,0.896,0.003
618 1.30,0.802,0.002
```

A P P E N D I X IV

THE COMPUTER PROGRAM FOR THE CALCULATION OF YOUNG'S MODULUS, STRAIN AND STRESS OPTICAL COEFFICIENTS

```
010 PROGRAM INSTRON
020 DIMENSION GL(50),WD(50),THI(50),NR(50)
030 DIMENSION BX2(50),BX1(50),BY2(50),BY1(50)
040 DIMENSION FX2(50),FX1(50),FY2(50),FY1(50)
050 DIMENSION YOUNG(50),ALPHA(50),STROP(50)
060 READ,K
070 DO 160 I=1,K
080 READ,NR(I),BX2(I),BX1(I),BY2(I),BY1(I)
090 READ,FX2(I),FX1(I),FY2(I),FY1(I),GL(I),WD(I),THI(I)
100 THI(I)=THI(I)*2.543/1000.
110 WD(I)=WD(I)*2.543/1000.
120 ALPHA(I)=104.67*10.**(-7.)*(BY2(I)-BY1(I))*GL(I)/
130C(BX2(I)-BX1(I))/THI(I)
140 YOUNG(I)=9.8*10.**5.*(FY2(I)-FY1(I))*GL(I)/WD(I)/
150CTHI(I)/(FX2(I)-FX1(I))
160 STROP(I)=ALPHA(I)/YOUNG(I)
170 WRITE(61,200)
180 DO 190 I=1,K
190 WRITE(61,220) NR(I),ALPHA(I),YOUNG(I),STROP(I)
200 FORMAT(3X,*RUN NUMBER*,8X,*ALPHA*,6X,*YOUNGS MODULUS*,
210C4X,*STRESS OPT COEFF*)
220 FORMAT(3X,I6,3X,E18.6,2X,E16.6,2X,E16.6)
230 END
240 END PROG
```

A P P E N D I X V

THE COMPUTER PROGRAM FOR THE CALCULATION OF ORIENTATION FUNCTION OF (110) NORMALS

```
010 PROGRAM ORIENT
0020 DIMENSION PAG(50),SFC(50),SFH(50)
0025 DIMENSION AZIM(50),ATIM(50),AM(50,3),CR(50,3)
0030 DIMENSION ZIM(50),AMO(50),CRY(50)
0035 DIMENSION ANGL(10),BTIM(10),BACK(10,3),BAK(10),BRAG(10)
0040 DIMENSION POL(10),B(10),ABSN(10),YSIN(10),ASFC(10)
0045 DIMENSION FINCO(10),COMP(10),AMOR(50),CRYS(50)
0050 DIMENSION XCRY(50),XBUS(50),XBU(50),ASFH(10)
0060 READ,NE
0070 DO 0080 I=1,NE
0080 READ,PAG(I),SFC(I),SFH(I)
0090 READ,NA
0100 DO 0200 I=1,NA
0110 READ,AZIM(I),ATIM(I),CR(I,1),CR(I,2),CR(I,3),AM(I,1),
0120CAM(I,2),AM(I,3)
0130 ZIM(I)=AZIM(I)*3.1416/180.
0140 AMS=0.
0150 CRS=0.
0160 DO 0180 J=1,3
0170 AMS=AMS+AM(I,J)
0180 CRS=CRS+CR(I,J)
0190 AMO(I)=AMS/(3.*ATIM(I))
0200 CRY(I)=CRS/(3.*ATIM(I))
0210 READ,THICK,ALO,AL,ABC
0215 THIC=THICK*ALO/AL
0220 READ,NB
0230 DO 0400 I=1,NB
0240 READ,ANGL(I),BTIM(I),BACK(I,1),BACK(I,2),BACK(I,3)
0250 BAC=0.
0260 DO 0270 J=1,3
0270 BAC=BAC+BACK(I,J)
0280 BAK(I)=BAC/(3.*BTIM(I))
0290 BRAG(I)=ANGL(I)*3.1416/180.
0300 POL(I)=2./(1.+COS(BRAG(I))**2.)
0310 B(I)=ABC*THIC*(1./COSF(BRAG(I))-1.)
0320 ABSN(I)=B(I)/(1.-EXPF(-B(I)))
0330 YSIN(I)=SINF(BRAG(I)/2.)/1.5417
0335 J=0
0340 J=J+1
0350 IF((PAG(J+1)-YSIN(I))*(PAG(J)-YSIN(I)).LE.0.) 360,355
0355 GO TO 0340
```

```
0360 ASFC(I)=(SFC(J+1)-SFC(J))*(YSIN(I)-PAG(J))/(PAG(J+1)-
0370CPAG(J))+SFC(J)
0380 ASFH(I)=(SFH(J+1)-SFH(J))*(YSIN(I)-PAG(J))/(PAG(J+1)-
0390CPAG(J))+SFH(J)
0400 FINCO(I)=(6.-ASFC(I))/3.+2.*(1.-ASFH(I))/3.
0410 XIN=POL(3)*ABSN(3)*(BAK(4)-BAK(3))
0415 DO 0420 I=1,NB
0420 COMP(I)=XIN*FINCO(I)/1.4936
0430 DO 0480 I=1,NA
0440 AMOR(I)=(AMO(I)-BAK(1))*POL(1)*ABSN(1)-COMP(1)
0450 CRYS(I)=(CRY(I)-BAK(2))*POL(2)*ABSN(2)-COMP(2)
0460 XCRY(I)=CRYS(I)-AMOR(I)
0470 XBUS(I)=XCRY(I)*COSF(ZIM(I))*SINF(ZIM(I))**2.
0480 XBU(I)=XCRY(I)*COSF(ZIM(I))
0490 BUNBO=0.
0500 BUNSH=0.
0510 NC=NA/2+1
0520 DO 0630 K=1,NC
0530 IF(K.EQ.1) 0550,0540
0540 IF(K.EQ.NC) 0610,0580
0550 BUNSH=BUNSH+XBUS(2*K-1)+4.*XBUS(2*K)
0560 BUNBO=BUNBO+XBU(2*K-1)+4.*XBU(2*K)
0570 GO TO 0630
0580 BUNSH=BUNSH+2.*XBUS(2*K-1)+4.*XBUS(2*K)
0590 BUNBO=BUNBO+2.*XBU(2*K-1)+4.*XBU(2*K)
0600 GO TO 0630
0610 BUNSH=BUNSH+XBUS(2*K-1)
0620 BUNBO=BUNBO+XBU(2*K-1)
0630 CONTINUE
0640 AVSIN=BUNSH/BUNBO
0650 AVCOS=AVSIN*COSF(BRAG(2)/2.)**2.
0660 ORIF=(3.*AVCOS-1.)/2.
0670 WRITE(61,0790)
0680 DO 0690 I=1,NA
0690 WRITE(61,0800),AZIM(I),AMO(I),CRY(I),AMOR(I),CRYS(I)
0710 WRITE(61,0810)
0720 DO 0730 I=1,NA
0730 WRITE(61,0820),AZIM(I),XCRY(I),XBUS(I),XBU(I)
0740 WRITE(61,0830)
0750 WRITE(61,0840),ORIF
0760 WRITE(61,0850)
0770 DO 0780 I=1,NB
0780 WRITE(61,0860),POL(I),ABSN(I),COMP(I),ASFC(I),ASFH(I)
0790 FORMAT(3X,*AZIM(I)*,2X,*AMO(I)*,4X,*CRY(I)*,5X,
0791C*AMOR(I)*,7X,*CRYS(I)*)
0800 FORMAT(3X,F5.1,2X,F10.6,2X,F10.6,2X,F12.7,2X,F10.6)
0810 FORMAT(3X,*AZIM(I)*,2X,*XCRY(I)*,4X,*BUS(I)*,
0811C5X,*XBU(I)*)
0820 FORMAT(3X,F5.1,2X,F10.6,2X,F10.6,2X,F12.7)
0830 FORMAT(3X,*ORIENTATION FUNCTION*)
0840 FORMAT(3X,F20.15)
```

```
0850 FORMAT(3X,*POL(I)*,2X,*ABSN(I)*,4X,*COMP(I)*,5X,
0851C*ASFC(I)*,7X,*ASFH(I)*)
0860 FORMAT(3X,F10.7,2X,F10.7,2X,F10.7,2X,F10.7,2X,F10.7)
0870 END
0880 ENDPROG
1000 18
1001 0.00,6.000,1.000
1002 0.05,5.764,0.947
1003 0.10,5.141,0.818
1004 0.15,4.362,0.636
1005 0.20,3.512,0.482
1006 0.25,3.003,0.350
1007 0.30,2.538,0.252
1008 0.35,2.212,0.179
1009 0.40,1.983,0.131
1010 0.50,1.707,0.073
1011 0.60,1.548,0.037
1012 0.70,1.423,0.023
1013 0.80,1.313,0.015
1014 0.90,1.202,0.010
1015 1.00,1.096,0.007
1016 1.10,0.992,0.005
1017 1.20,0.896,0.003
1018 1.300,0.802,0.002
```

A P P E N D I X VI

THE COMPUTER PROGRAM FOR THE CALCULATION OF LIGHT SCATTERING PATTERNS FOR ROD-LIKE CRYSTALLITES

```
5 PROGRAM LIGHT
10 DIMENSION RAZ(50),AZ(50),RTH(50),TH(50)
15 DIMENSION QL(50),VI(50),VH(50)
20 READ,R
25 READ,SK
30 READ,NA
40 READ,NB
42 READ,NE
44 READ,NF
70 READ,DA,DP
72 READ,B1
74 READ,B2
80 RS=R**0.75
90 RN=R**1.5
100 DO 440 I=1,NA
110 AN=I
115 RAZ(I)=B1*(AN-1.)
120 AZ(I)=3.1416*RAZ(I)/180.
130 DO 390 J=1,NB
140 BN=J
145 RTH(J)=B2*BN
150 TH(J)=3.1416*RTH(J)/180.
160 QL(J)=TAN(TH(J))
170 YV=0.
180 YH=0.
190 DO 360 K=1,NE
195 EN=NE
200 CN=K
210 AL=(CN-1.)*3.1416/EN
220 DO 360 L=1,NF
225 FN=NF
230 DN=L
240 PH=2.*(DN-1.)*3.1416/FN
250 A=(1.-COS(TH(J)))*SIN(AL)*COS(PH)-SIN(AL)*SIN(PH)*
260CSIN(TH(J))*SIN(AZ(I))-COS(AL)*SIN(TH(J))*COS(AZ(I))
270 ASI=SIN(SK*A)**2/SK**2/A**2
280 SV=(1.+4.*COS(AL)**2)**2
290 SH=16.*(COS(AL)*SIN(AL)*SIN(PH))**2
300 DS=RS*SIN(AL)*DA*DP/(RN*SIN(AL)**2+COS(AL)**2
310C/RN)**1.5
```

```
320 SSV=SV*ASI*DS
330 SSH=SH*ASI*DS
340 YV=YV+SSV
350 YH=YH+SSH
360 CONTINUE
370 VI(J)=YV
380 VH(J)=YH
390 CONTINUE
400 WRITE(61,450)
410 WRITE(61,460),RAZ(I)
420 WRITE(61,470)
430 DO 440 J=1,NB
440 WRITE(61,480),RTH(J),QL(J),VI(J),VH(J)
450 FORMAT(3X,*AZ(I)*)
460 FORMAT(3X,F6.2)
470 FORMAT(3X,*TH(J)*,5X,*QL(J)*,10X,*VI(J)*,10X,*VH(J)*)
480 FORMAT(3X,F6.2,3X,E11.4,3X,E11.4,3X,E11.4)
490 END
500 ENDPROG
```

B I B L I O G R A P H Y

1. J. P. Joule, Trans. Roy. Soc. (London), A149, 91 (1859)
2. J. P. Joule, Phil. Mag., 14, 227 (1857)
3. R. L. Anthony, R. H. Caston, E. Guth, J. Phys. Chem., 46, 826 (1942)
4. L. A. Wood, F. L. Roth, J. Appl. Phys., 15, 781 (1944)
5. W. Kuhn, F. Grün, Kolloid-Z., 101, 248 (1942)
6. E. Guth, H. M. James, Indstr. Engng Chem., 33, 624 (1941)
7. H. M. James, E. Guth, J. Chem. Phys., 11, 455 (1943)
8. F. T. Wall, J. Chem. Phys., 10, 485 (1942)
9. F. T. Wall, J. Chem. Phys., 11, 67 (1943)
10. F. T. Wall, J. Chem. Phys., 11, 527 (1943)
11. P. J. Flory, J. Rehner, Jr., J. Chem. Phys., 12, 412 (1944)
12. P. J. Flory, J. Rehner, Jr., J. Chem. Phys., 11, 512 (1943)
13. L. R. G. Treloar, Trans. Faraday Soc., 43, 277 (1947)
14. L. R. G. Treloar, Trans. Faraday Soc., 43, 284 (1947)
15. K. Ziegler, et al., Angew. Chem., 67, 541 (1955)
16. G. Natta, et al., J. Am. Chem. Soc., 77, 1708 (1955)
17. G. Natta, et al., J. Polymer Sci., 16, 143 (1955)
18. G. Natta, et al., Angew. Chem., 68, 393 (1956)
19. C. W. Bunn, T. C. Alcock, Trans. Faraday Soc., 41, 317 (1945)

20. A. Keller, J. polymer Sci., 17, 351 (1955)

21. Y. Fujiwara, J. Appl. Polymer Sci., 4, 10 (1960)

22. A. Keller, J. Polymer Sci., 39, 160 (1959)

23. H. D. Keith, F. J. Padden, Jr., J. Polymer Sci., 39, 101 (1959)

24. F. P. Price, J. Polymer Sci., 39, 139 (1959)

25. A. Keller, Phil. Mag., 2, 1171 (1957)

26. A. Keller, Discussions Faraday Soc., 25, 114 (1958)

27. C. W. Bunn, Trans. Faraday Soc., 35, 482 (1939)

28. R. S. Stein, J. Polymer Sci., 34, 709 (1959)

29. P. R. Swan, J. Polymer Sci., 56, 409 (1962)

30. E. W. Walter, F. P. Reding, J. Polymer Sci., 21, 561 (1956)

31. S. Onogi, D. A. Keedy, R. S. Stein, J. Polymer Sci., 50, S15 (1961)

32. R. S. Stein, S. Onogi, D. A. Keedy, J. Polymer Sci., 57, 801 (1962)

33. R. S. Stein, S. Onogi, K. Sasaguri, D. A. Keedy, J. Appl. Phys., 34, 80 (1963)

34. R. S. Stein, J. Polymer Sci., 62, S1 (1962)

35. R. S. Stein, H. Kawai, T. Itoh, D. A. Keedy, Polymer Letters, 2, 1075 (1964)

36. R. S. Stein, T. Kawaguchi, T. Ito, H. Kawai, D. A. Keedy, Macromolecules, 1, 126 (1968)

37. T. Ito, T. Oda, H. Kawai, Rev. Sci. Instr., 39, 1847 (1968)

38. F. A. Bettelheim, R. S. Stein, J. Polymer Sci., 27, 567 (1958)

39. G. ver Strate, Z. W. Wilchinsky, J. Polymer Sci. A2, 9, 127 (1971)

40. R. S. Stein, J. Powers, S. Hoshino, ONR Technical Report No. 33, Project NR 356-378, Contract Nonr. 3357(00), Univ. of Mass., Amherst, Mass., July 1961

41. S. Krimm, A. V. Tobolsky, J. Polymer Sci., 7, 57 (1951)

42. A. H. Compton, S. K. Allison, X-rays in Theory and Experiment,Van Nostrand, New York, 1935, pp. 252-255

43. N. S. Gingrich, Rev. Mod. Phys., 15, 90 (1943)

44. N. S. Gingrich, Rev. Mod. Phys., 15, 781 (1943)

45. A. Weidinger, P. H. Hermans, Makromol. Chem., 50, 98 (1961)

46. P. H. Hermans, A. Weidinger, Makromol. Chem., 44-46, 24 (1961)

47. D. A. Keedy, R. J. Volungis, H. Kawai, Rev. Sci. Instr., 32, 415 (1961)

48. R. S. Stein, J. Polymer Sci., 31, 327 (1958)

49. M. B. Rhodes, D. A. Keedy, R. S. Stein, J. Polymer Sci., 62, S73 (1962)

50. L. E. Nielsen, J. Appl. Phys., 25, 1209 (1954)

51. C. A. Sperati, W. A. Franta, H. W. Starkweather, J. Am. Chem. Soc., 75, 6127 (1953)

52. R. F. Boyer, Rubber Chem. Technol., 34, 1303 (1963)

53. M. Takayanagi, K. Imada, A. Nagai, T. Matsuo, J. Polymer Sci. C, 16, 867 (1967)

54. A. H. Willbourn, Trans. Faraday Soc., 54, 717 (1958)

55. H. A. Flocke, Kolloid-Z., 180, 118 (1962)

56. L. E. Nielsen, J. Polymer Sci., 42, 357 (1960)

57. K. Schmieder, K. A. Wolf, Kolloid-Z., 134, 149 (1953)

58. R. A. V. Raff, K. W. Doak, Crystalline Olefin Polymers, Interscience Publishers, New York, 1965, pp.780

59. S. G. Turley, H. Keskkula, J. Polymer Sci. c, 14, 69 (1966)

60. E. A. Cole, D. R. Holmes, J. Polymer Sci., 46, 245 (1960)

61. P. J. Flory, Trans. Faraday Soc., 51, 848 (1955)

62. F. A. Quinn, Jr., L. Mandelkern, J. Am. Chem. Soc., 80, 3178 (1958)

63. M. J. Richardson, P. J. Flory, J. B. Jackson, Polymer, 4, 221 (1963)

64. D. C. Smith, Ind. Eng. Chem., 48, 1161 (1956)

65. F. P. Reding, C. M. Lovell, J. Polymer Sci.,21, 157 (1956)

66. R. M. Eichhorn, J. Polymer Sci., 31, 197 (1958)

67. T. Kawai, K. Ujihara, H. Maeda, Makromol. Chem., 132, 87 (1970)

68. P. J. Holdsworth, A. Keller, I. M. Ward, T. Williams, Makromol. Chem., 125, 70 (1969)

69. P. J. Hoidsworth, A. Keller, I. M. Ward, T. Williams, Makromol. Chem., 125, 82 (1969)

70. P. J. Holdsworth, A. Keller, I. M. Ward, T. Williams, Makromol. Chem., 125, 94 (1969)

71. M. Shida, H. K. Ficker, J. Polymer Sci. B, 4,347 (1966)

72. G. Bucci, T. Simonazzi, J. Polymer Sci. C, 7, 203 (1964)

73. R. S. Stein, P. R. Wilson, J. Appl. Phys., 33, 1914 (1962)

74. R. S. Stein, P. Erhardt, J. J. van Aartsen, S. Clough, M. B. Rhodes, J. Polymer Sci. C, 13, 1 (1966)

75. K. Eckling, O. Kratky, Nature, 18, 461 (1931)

76. O. Kratky, Kolloid-Z., 64, 213 (1933)

77. S. Hoshino, J. powers, D. G. Legrand, H. Kawai, R. S. Stein, J. Polymer Sci., 58, 185 (1962)

78. M. B. Rhodes, R. S. Stein, J. Appl. Phys., 32, 2344 (1963)

79. R. S. Stein, G. L. Wilkes, J. Polymer Sci. A2, 7, 1695 (1969)

80. M. B. Rhodes, R. S. Stein, ASTM Special Technical Publication No. 348, American Society for Testing and Materials, Philadelphia

81. C. Picot, M. Fukuda, C. Chou, R. S. Stein, J. Macromol. Sci-Phys. B, 6, 263 (1972)

82. W. Yau, R. S. Stein, J. Polymer Sci. A2, 6, 1 (1968)

83. W. Yau, R. S. Stein, J. Polymer Sci. B, 2, 231 (1964)

84. F. Bueche, J. Polymer Sci., 22, 113 (1956)

85. L. E. Nielsen, F. D. Stockton, J. Polymer Sci. A, 1 1955 (1963)

86. E. Guth, J. Appl. Phys., 16, 20 (1945)

87. H. M. Smallwood, J. Appl. Phys., 15, 758 (1944)

88. R. L. Miller, L. E. Nielsen, J. Polymer Sci., 46, 303 (1960)

89. L. E. Nielsen, J. Appl. Polymer Sci., 2, 351 (1959)

90. M. Takayanagi, in Fourth Int. Cong. on Rheology, Part I; ed. by E. H. Lee and A. L. Copley, J. Wiley, N. Y. (1965)

91. J. C. Halpin, N. J. Pagano, J. Comp. Mat., 3, 720 (1969)

92. J. C. Halpin, K. Jerina, J. M. Whitney, J. Comp. Mat., 5, 36 (1971)

93. R. S. Stein, F. H. Norris, J. Polymer Sci., 21, 381 (1956)

94. C. W. Bunn, R. de Daubeny, Trans. Faraday Soc., 50, 1173 (1954)

95. R. Samuels, J. Polymer Sci. A, 3, 1741 (1965)

96. V. N. Tsvetkov, O. V. Kallistov, E. V. Korneeva, I. K. Nekrasov, Visocomol. Soed., 5, 1538 (1963)

97. R. L. Volungis, T. J. Li, R. S. Stein, J. Chem. Phys., 23, 1179 (1955)

98. Y. Shindo, R. S. Stein, J. Polymer Sci. A2, 7, 2115

99. Y. Shindo, R. S. Stein, B. E. Read, Makromol. Chem., 118, 272 (1968)

100. M. Kurata, W. H. Stockmayer, Fortschr. Hochpolymer Forsch., 3, 196 (1963)

CAPTIONS FOR TABLES

1. Some properties of 1248B and 1193A samples.
2. The solvents used for form birefringence measurement and their densities and refractive indices.
3. The calculation of the activation energies of the β and γ-transitions of 1248B and 1193A samples.
4. The positions of the diffracted x-ray intensity maxima and the (110) spacings of 1248B and 1193A samples at various temperatures.
5. The angles which streaks and the H_v scattering lobes of 1193A and 1248B samples make with stretching direction.
6. The estimation of the form birefringence of 1248B and 1193A samples.

CAPTIONS FOR FIGURES

1. The variation of the x-ray diffracted intensity with Bragg angle.
2. Schematic diagram of the set-up for Young's modulus, strain and stress optical coefficient measurement.
3. The schematic diagram of the dynamic x-ray apparatus.
4. The co-ordinate system for the calculation of orientation function of the (110) normals.
5. Schematic diagram of the apparatus for photographic light scattering.
6. The sample holder and the cell for the form birefringence measurement.
7. Schematic diagram of the set-up for form birefringence measurement.
8. The variation of the birefringence of swollen samples with their volume fraction
9. The variation in E' and E" with temperature at the frequency of 3.5,11, 35 and 110 Hz for 1248B sample.
10. The variation in E' and E" with temperature at the frequency of 3.5, 11, 35 and 110 Hz for 1193A sample.
11. The variation in tanδ with temperature at the frequency of 3.5, 11, 35 and 110 Hz for 1248B sample.
12. The variation in tanδ with temperature at the frequency of 3.5, 11, 35 and 110 Hz for 1193A sample.

13. The variation of the β-transition temperatures of branched polyethylene and ethylene-propylene copolymers with their ethylene content.
14. The variation in the value of reciprocal of the β-transition temperature with frequency.
15. The variation in the value of reciprocals of the γ-transition temperature with frequency.
16. The variation of the x-ray diffraction intensities at various temperatures with Bragg angle for 1248B sample.
17. The variation of the x-ray diffraction intensities at various temperatures with Bragg angle for 1193A sample.
18. The variation of the (110) spacings of Marlex, 1248B and 1193A samples.
19. The variation of the crystallinities of 1248B and 1193A samples with temperature.
20. The variation of the melting point of ethylene-propylene copolymers with their ethylene content.
21. The variation of crystallinity of ethylene-propylene copolymers with their ethylene content.
22. The variation of the (110) spacing of various ethylene-propylene copolymers with their ethylene content.
23. The variation of $Tm/T\overset{o}{m}$ with ΔH_u.
24. The small angle light scattering patterns of undeformed 1248B and 1193A samples.
25. The co-ordinate system for the calculation of light scattering patterns.

26. The variation of the orientation functions of the (110) normals at various temperatures with strain for 1248B sample.

27. The variation of the orientation functions of the (110) normals at various temperatures with strain for 1193A sample.

28. The variation of the initial slope of the orientation functions of the (110) normals with temperature for 1193A and 1248B samples.

29. The variation in H_v and V_v light scattering patterns with strain for 1248B sample.

30. The variation in H_v and V_v light scattering patterns with strain for 1248B sample.

31. The variation in H_v and V_v light scattering patterns with strain for 1193A sample.

32. The variation in H_v and V_v light scattering patterns with strain for 1193A sample.

33. The variation in x-ray diffraction pattern with strain for 1248B sample.

34. The variation in x-ray diffraction pattern with strain for 1193A sample.

35. The variation in calculated H_v light scattering pattern with extension ratio for the rod-like crystallite

36. The variation in calculated V_v light scattering pattern with extension ratio for the rod-like

crystallite.

37. The variation of angle which a H_v scattering lobe makes with stretching direction with strain for 1193A and 1248B samples.

38. The variation in H_v, V_v light scattering patterns and in micrograph with strain for 1248B sample.

39. The variation in H_v, V_v light scattering patterns and in micrograph with strain for 1193A sample.

40. The calculated H_v and V_v light scattering patterns for the streaks in 1248B sample strained 62.6 %.

41. The light scattering patterns and a micrograph for 1248B sample strained 78.6 %.

42. The variation of Young's modulus with temperature for 1248B and 1193A samples.

43. The variation of strain optical coefficient with temperature for 1248B and 1193A samples.

44. The variation of stress optical coefficient with temperature for 1248B and 1193A samples.

45. The co-ordinate system used for the calculation of strain and stress optical coefficients of the network.

46. The variation of the total strain optical coefficient and the crystalline contribution of strain optical coefficient with temperature for 1248B and 1193A samples.

47. The variation of anisotropy of the statistical unit with temperature for 1248B and 1193A samples.

48. The variation of birefringence of the swollen samples with the refractive index of the solvent for 1248B and 1193A samples.

Table 1 Some Properties of the Ethylene-propylene Copolymers

Sample	Ethylene content (mole %)	$[\eta]$ Decalin 135 C	$\overline{Mn}$	H_f (cal/g)	Crystallinity (wt %)
1193A	68	4.1	53,000	5.1	15
1248B	77	5.0	70,000	——	21

(a) $\overline{Mn}$ by membrane osmometry

(b) All samples contain approximately 1 % calcium stearate 0.01 % catalyst residue, and 0.1 % inhibitor

Table 2 The Solvents used and their Density and Refractive Index

Solvent	Density (g/cm^3)	Refractive Index
Cyclohexane	0.7785	1.4266
Carbon Tetrachloride	1.5940	1.4607
Ethylbenzene	0.8670	1.4959
Benzene	0.8786	1.5014
Chlorobenzene	1.1058	1.5250
Tetralin	0.9702	1.5451
Trichlorobenzene	1.4542	1.5671

Table 3 The Calculation of Activation Energy

β-transition

Frequency (Hz)	1248B Transition Temperature (°C)	1248B 1000/T	1193A Transition Temperature (°C)	1193A 1000/T
110	-44	4.36	-45	4.38
35	-48	4.46	-50	4.48
11	-52	4.52	-54	4.56
3.5	-56	4.61	-63	4.76
Activation Energy	11.8 kcal/mole		11.3 kcal/mole	

(cf. Activation Energy of Polyethylene 38 kcal/mole)

γ-transition

Frequency (Hz)	1248B Transition Temperature (°C)	1248B 1000/T	1193A Transition Temperature (°C)	1193A 1000/T
110	-108	6.05	-110	6.13
35	-111	6.18	-113	6.25
11	-115	6.32	-117	6.40
3.5	-119	6.48	-120	6.54
Activation Energy	7.0 kcal/mole		7.2 kcal/mole	

(cf. Activation Energy of Polyethylene 11-15 kcal/mole)

Table 4 The Position of Peak Maxima and the (110) spacing

1 2 4 8 B

Temperature (°C)	Amorphous halo (°)	(110) Diffraction (°)	(110) Spacing (Å)
27.5	18.9	21.0	4.225
40.4	18.9	20.9	4.245
51.0	18.8	20.85	4.260
61.2	18.6	20.75	4.280
70.0	18.45	20.65	4.300
81.0	18.40		
85.0	18.45		
90.0	18.40		
95.0	18.40		
100.0	18.40		

Temperature (°C)	Amorphous halo (°)	(110) Diffraction (°)	(110) Spacing (Å)
29.5	18.85	20.80	4.260
34.0	18.85	20.80	4.260
39.5	18.80	20.75	4.280
45.5	18.70	20.60	4.310
53.0	18.60		
58.0	18.50		
63.0	18.50		
70.2	18.45		
75.0	18.40		

Table 5 The Angles which Streaks and H_v Scattering Lobes make with Stretching Direction

Strain (%)	ω (°)	μ_H (°)
39.5	63.0	31.0
62.6	54.7	33.8
79.1	50.5	37.0
105.0	47.0	40.5
154.7	42.1	51.0
101.5	45.0	46.0
50.2	55.0	33.8
27.7	60.8	29.0

Table 6 The Estimation of Magnitude of Form Birefringence

	1193A	1248B
	($\times 10^{-3}$)	($\times 10^{-3}$)
$X_c d\Delta_c$	0.25	0.34
$(1-X_c)d\Delta_a$	0.33	0.37
Total Variation	0.58	0.71
Total Birefringence	4.75	6.70
Form Birefringence	1.43	1.39
	29 %	21 %

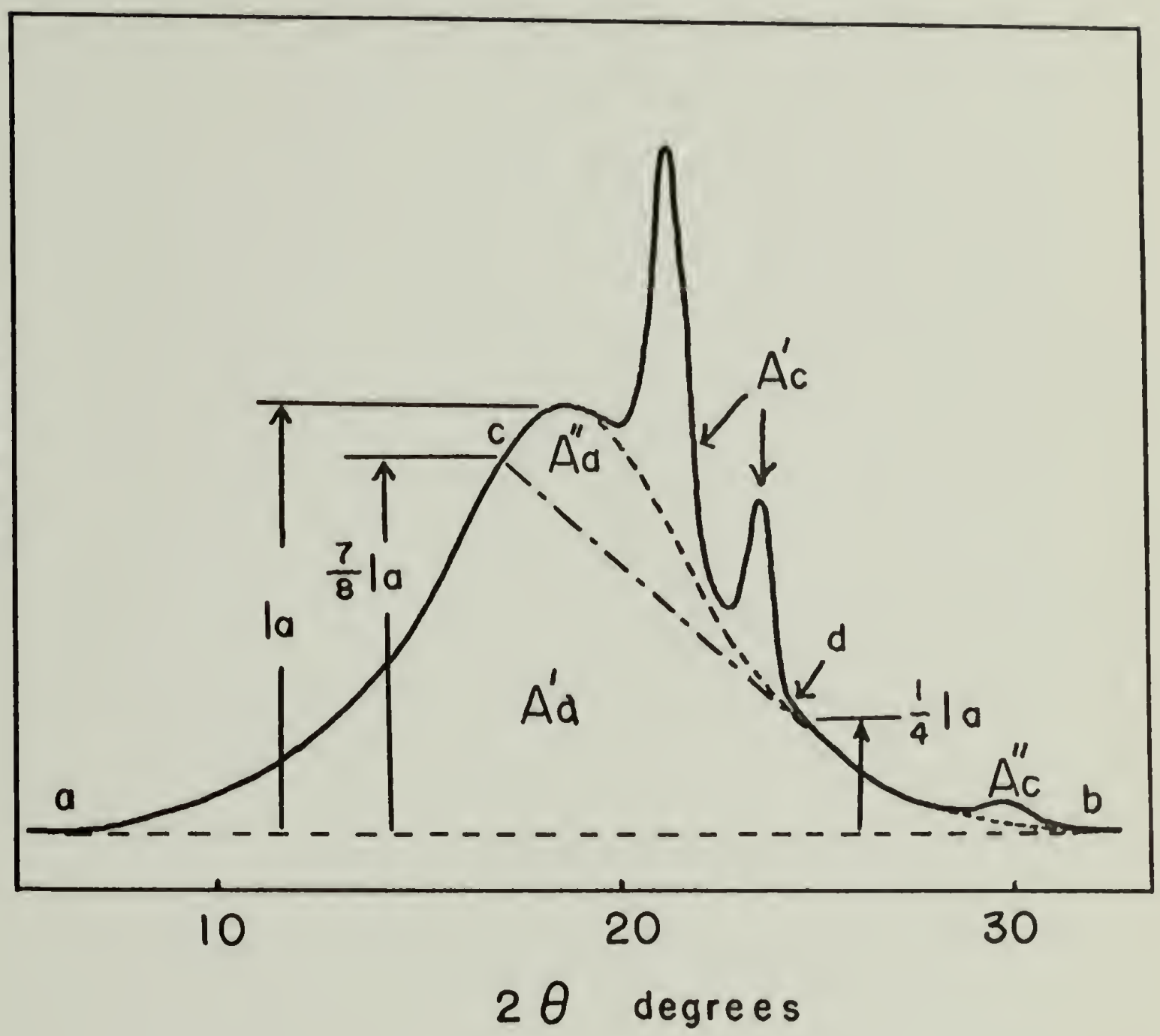

FIG. 1

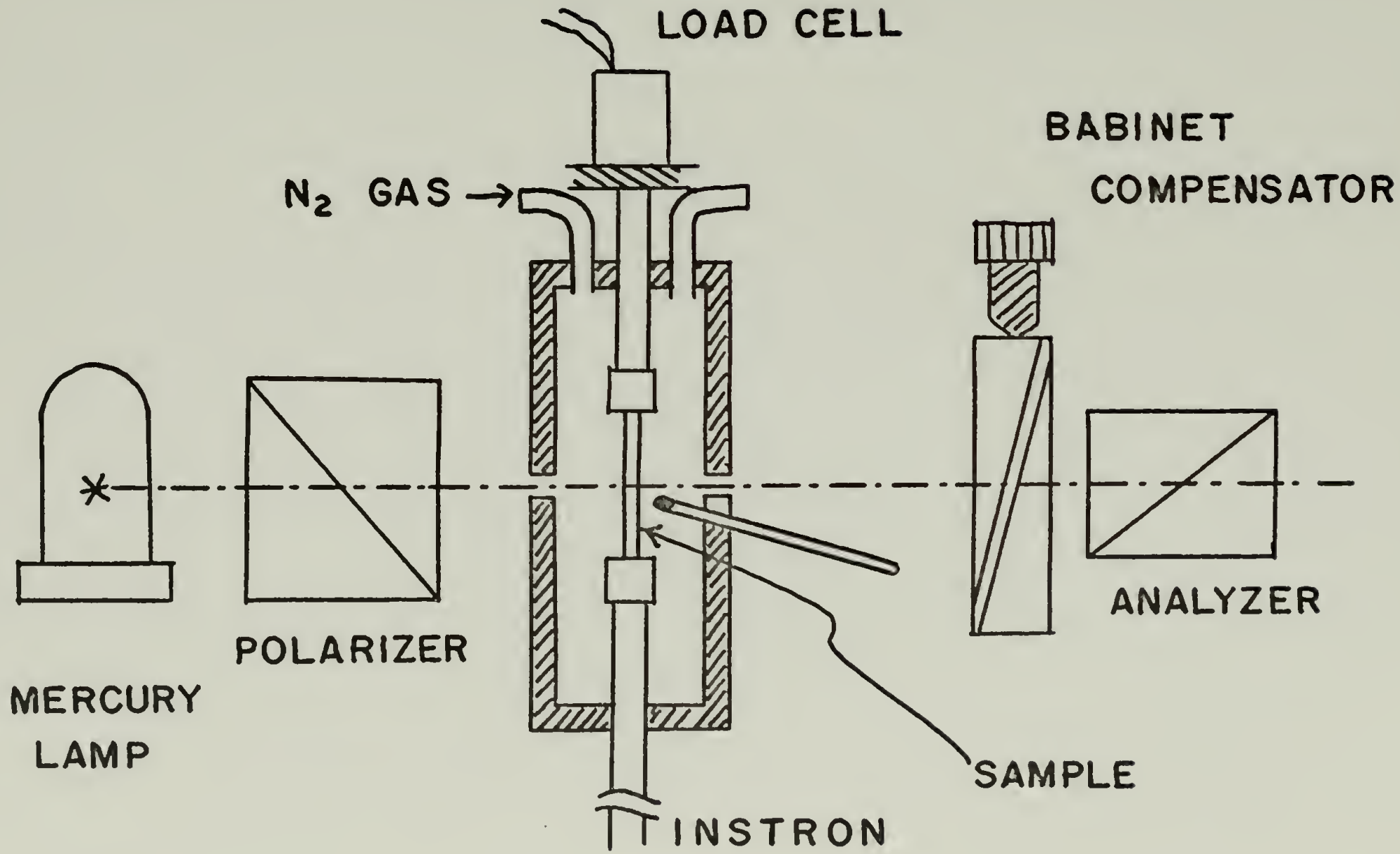
LOAD CELL
BABINET
COMPENSATOR
N_2 GAS →
ANALYZER
POLARIZER
MERCURY
LAMP
SAMPLE
INSTRON

FIG. 2

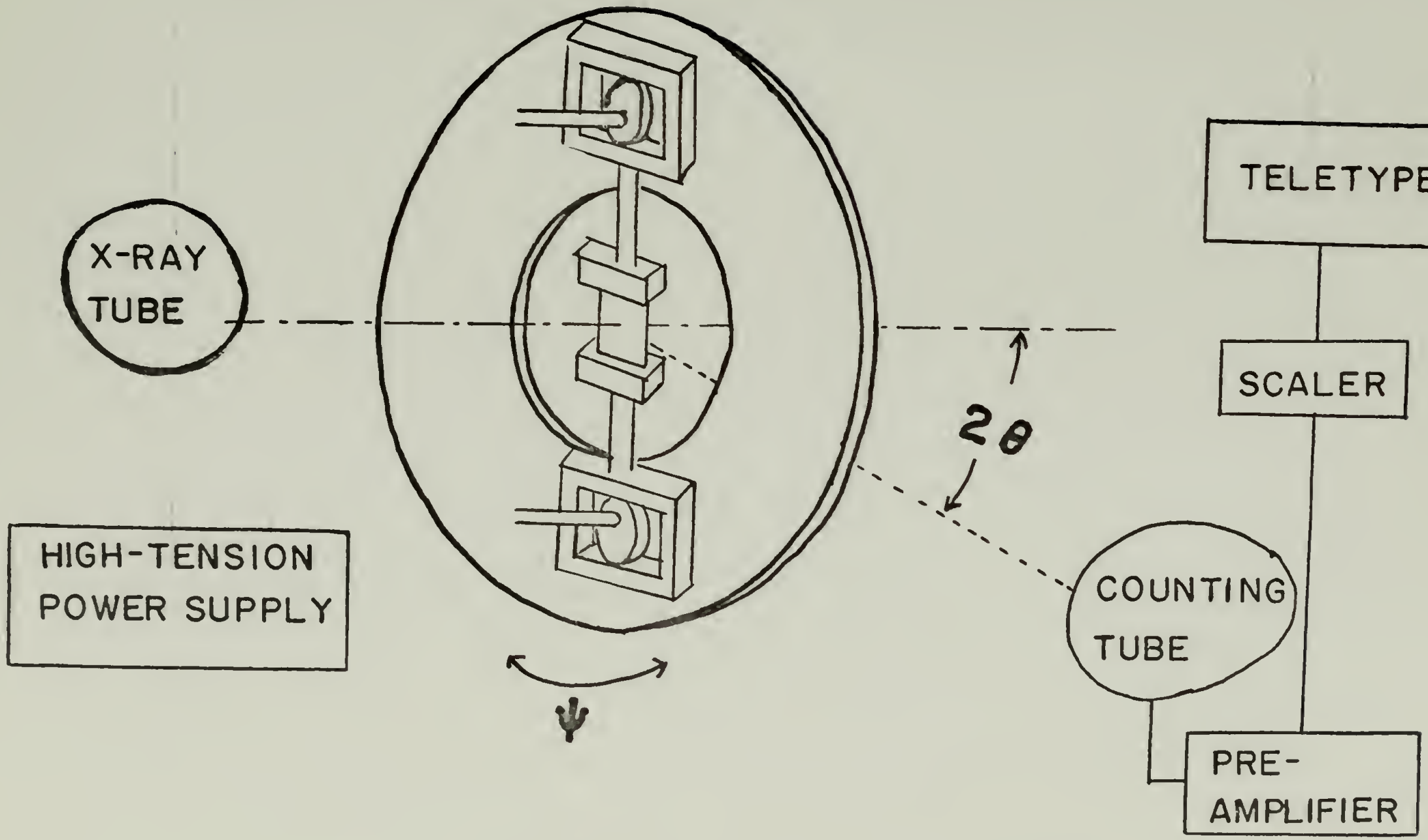
X-RAY
TUBE
HIGH-TENSION
POWER SUPPLY
2θ
TELETYPE
SCALER
COUNTING
TUBE
PRE-
AMPLIFIER

FIG. 3

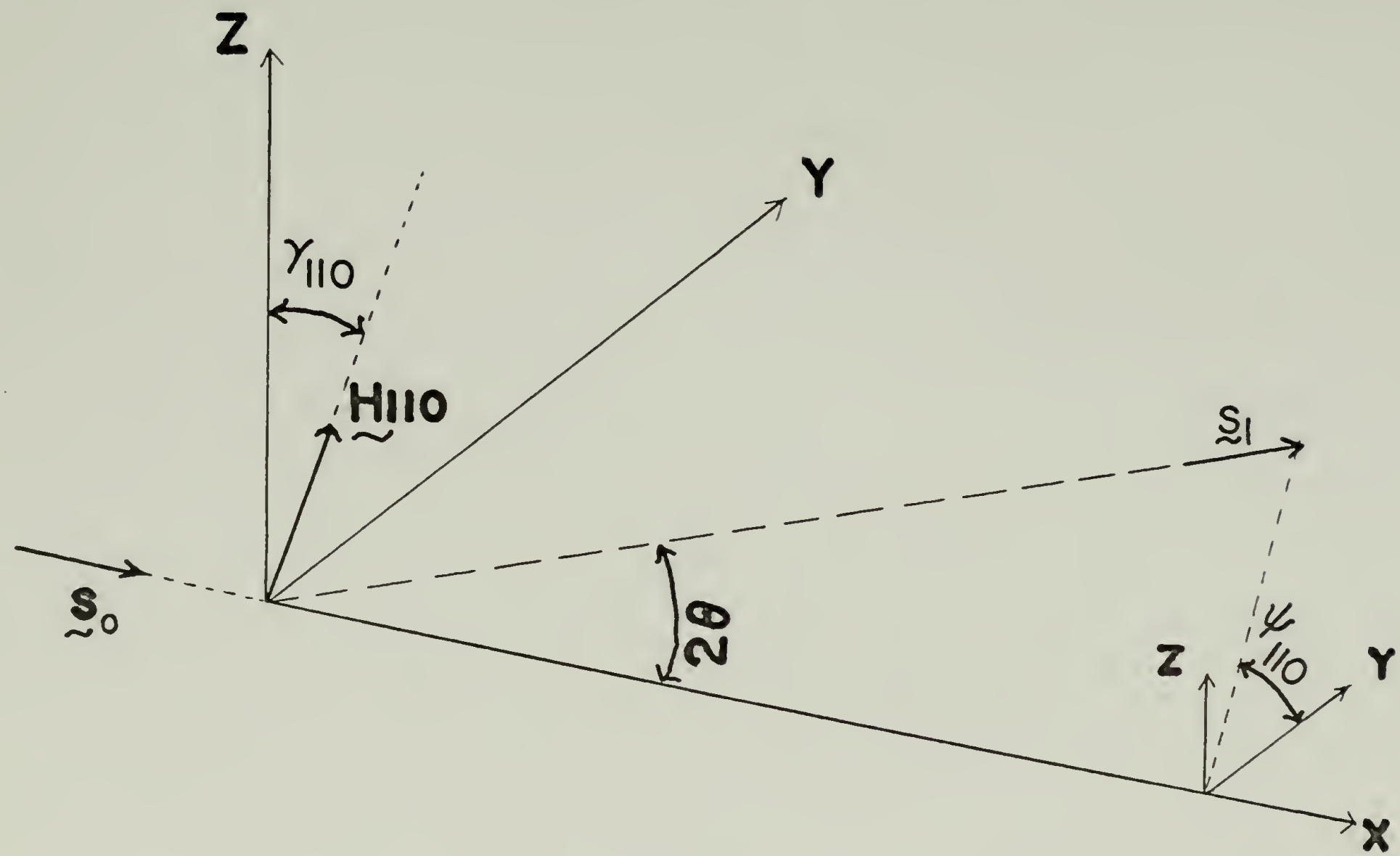

FIG. 4

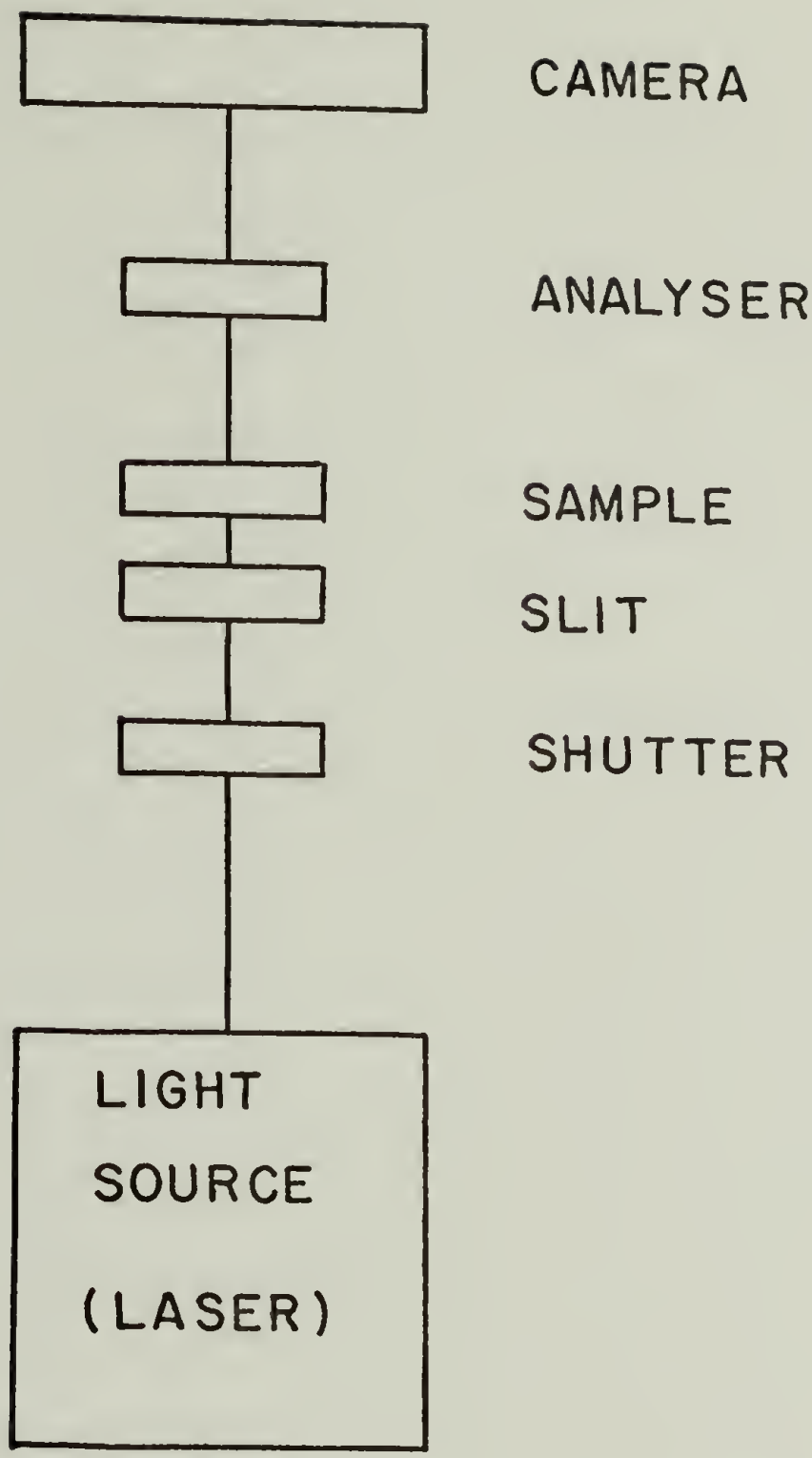

FIG. 5

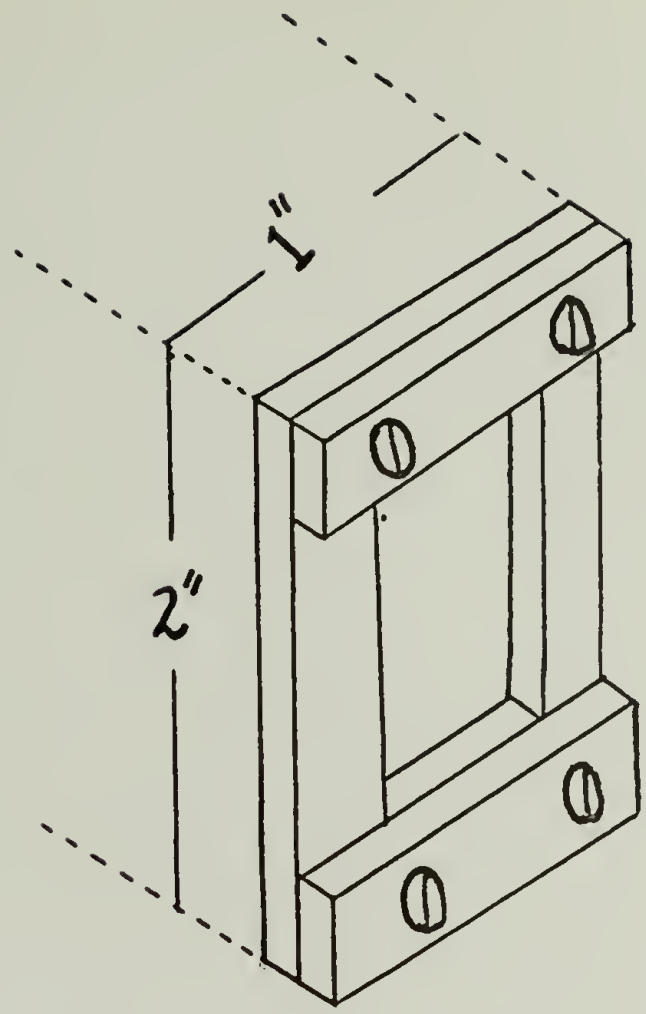

(A)

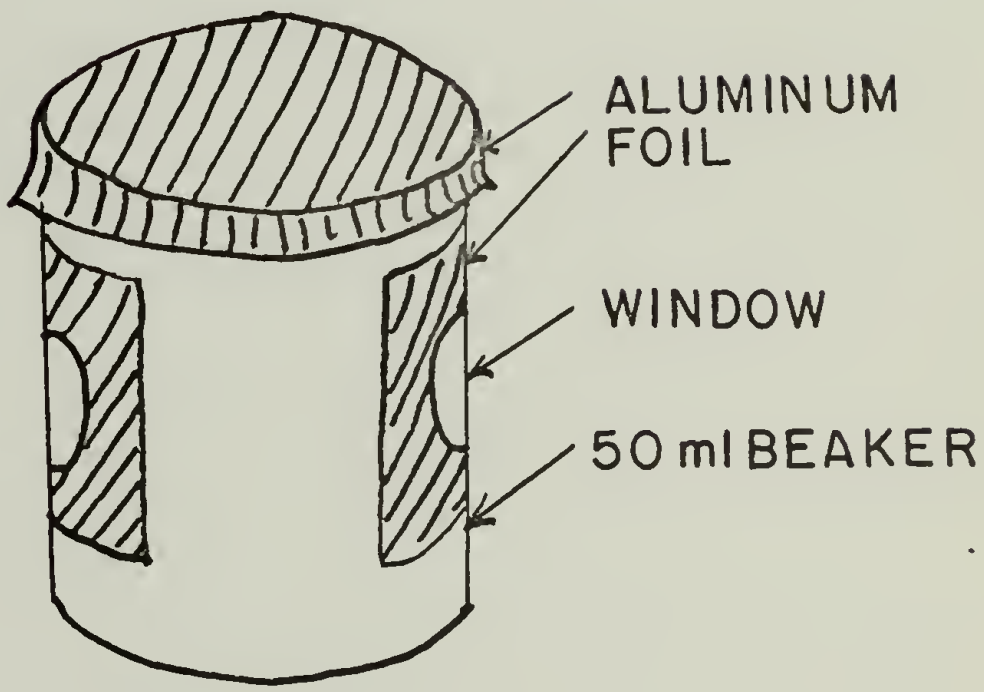

(B)

FIG. 6

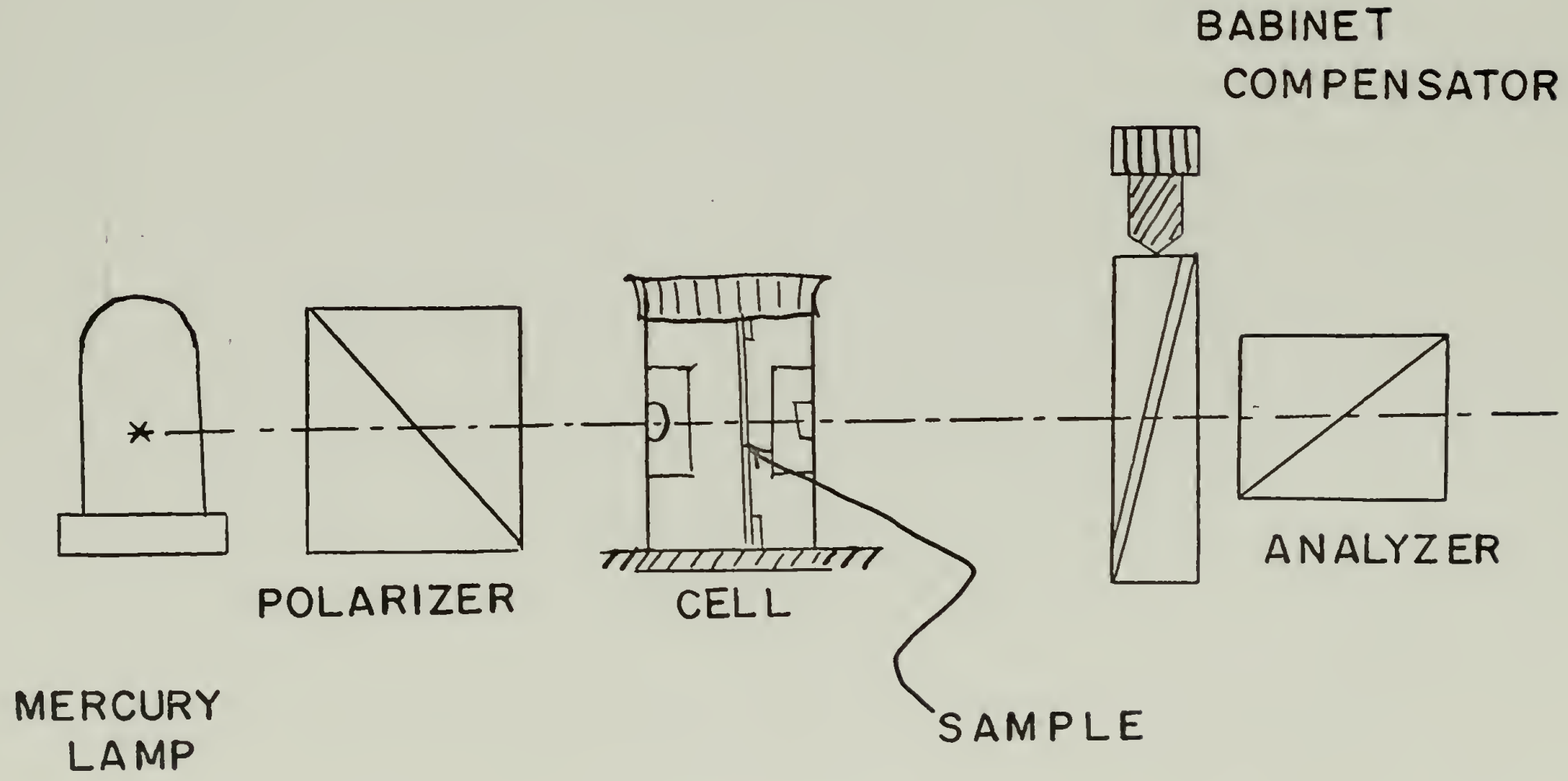
BABINET
COMPENSATOR
ANALYZER
POLARIZER
CELL
MERCURY
LAMP
SAMPLE

FIG. 7

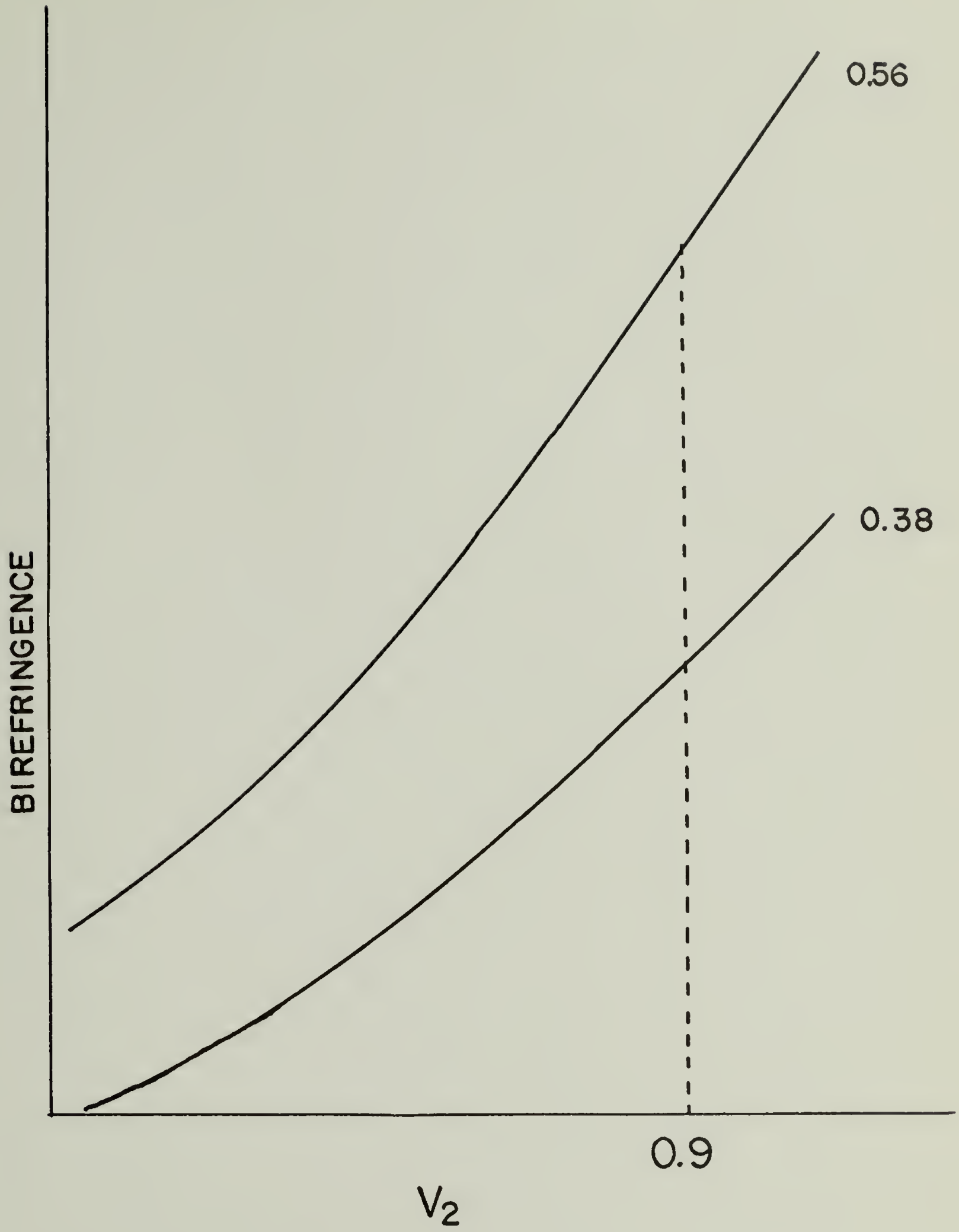

FIG. 8

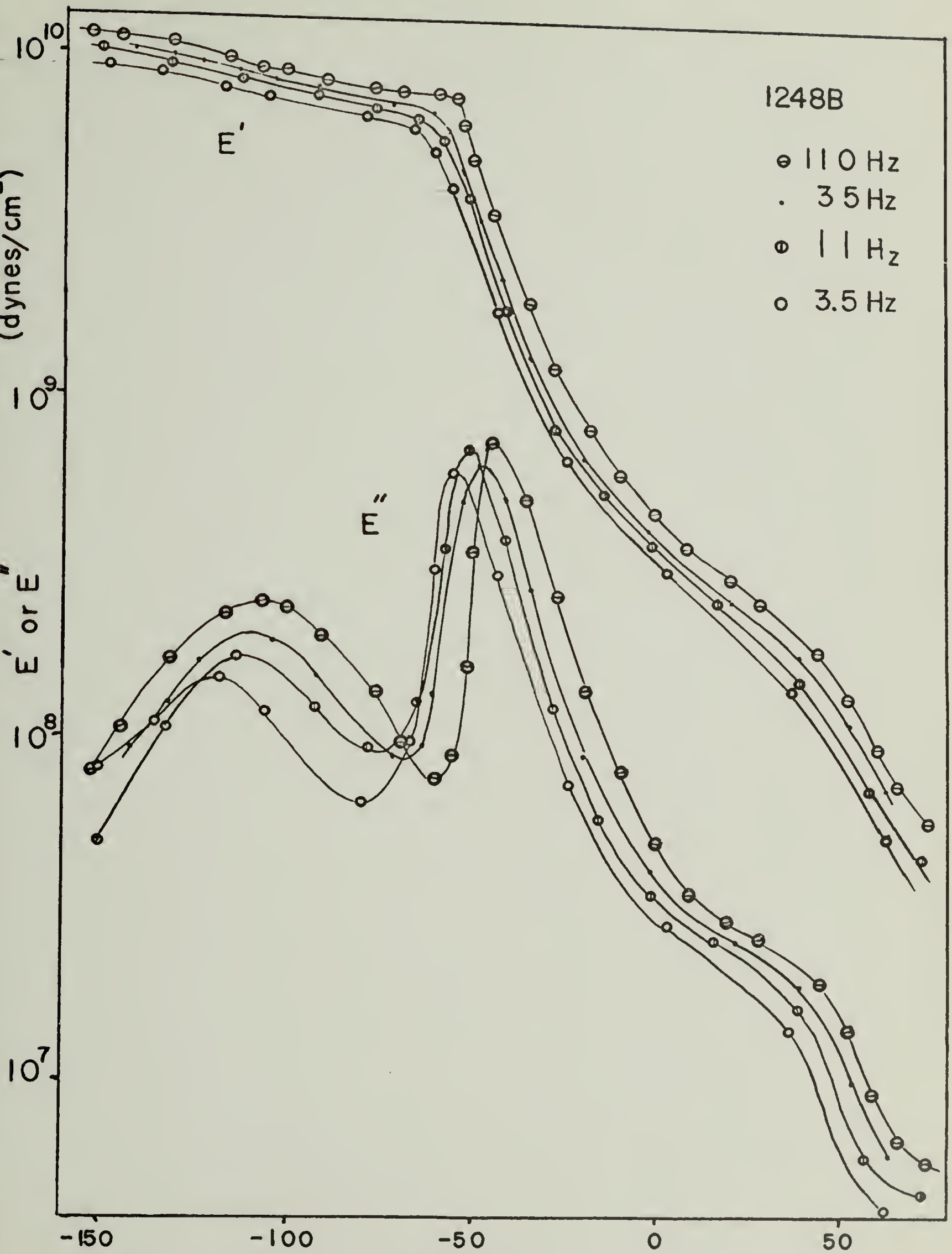
1248B
110 Hz
35 Hz
11 Hz
3.5 Hz
E'
E''
E' or E''
(dynes/cm²)
10¹⁰
10⁹
10⁸
10⁷
-150
-100
-50
0
50
TEMPERATURE (°C)

FIG. 9

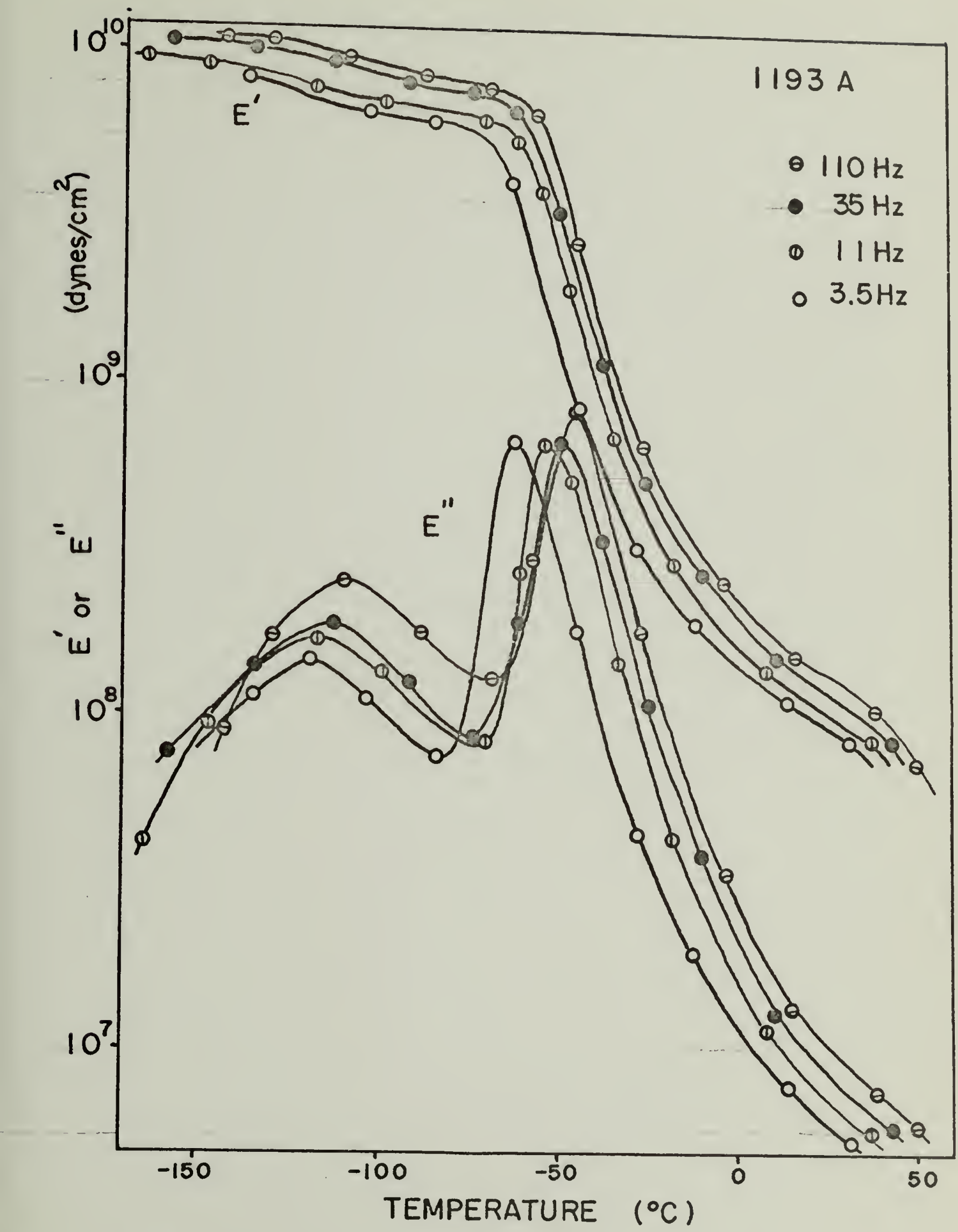
1193 A
110 Hz
35 Hz
11 Hz
3.5 Hz
E'
E''
E' or E'' (dynes/cm²)
10¹⁰
10⁹
10⁸
10⁷
-150
-100
-50
0
50
TEMPERATURE (°C)

FIG. 10

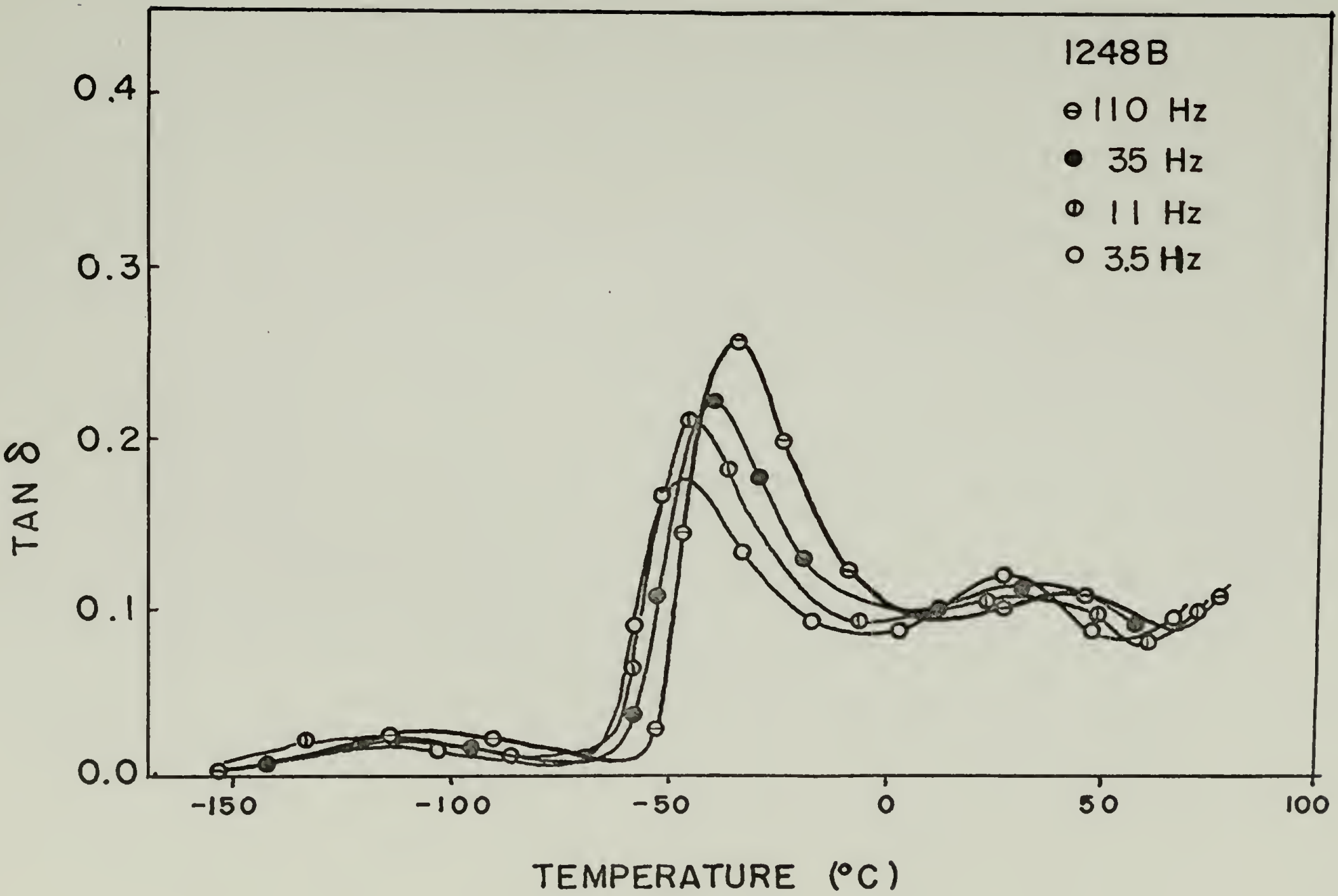
1248B
110 Hz
35 Hz
11 Hz
3.5 Hz
TAN δ
0.4
0.3
0.2
0.1
0.0
-150
-100
-50
0
50
100
TEMPERATURE (°C)

FIG. 11

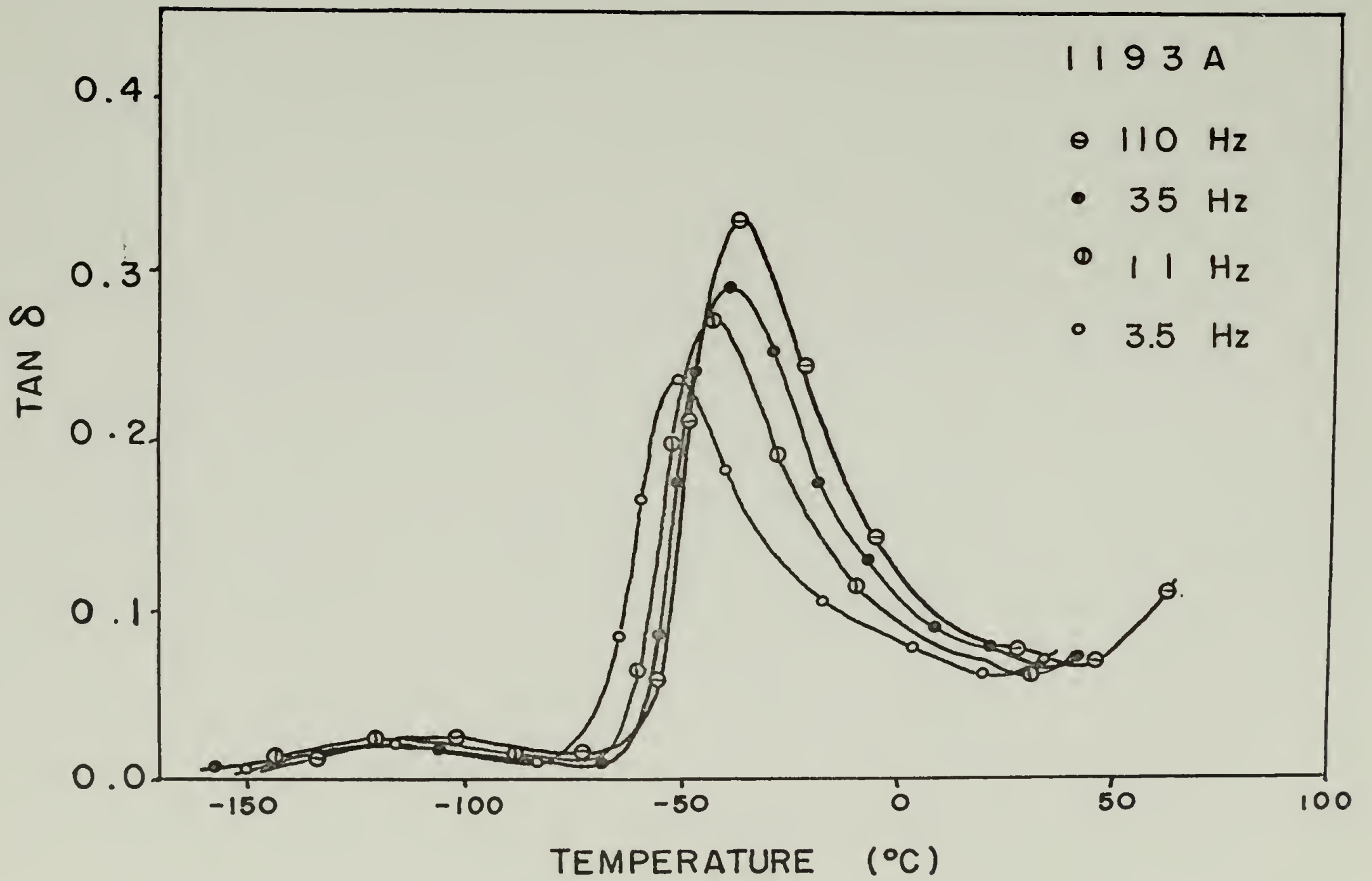
1193A
110 Hz
35 Hz
11 Hz
3.5 Hz
TAN δ
0.4
0.3
0.2
0.1
0.0
-150
-100
-50
0
50
100
TEMPERATURE (°C)

FIG. 12

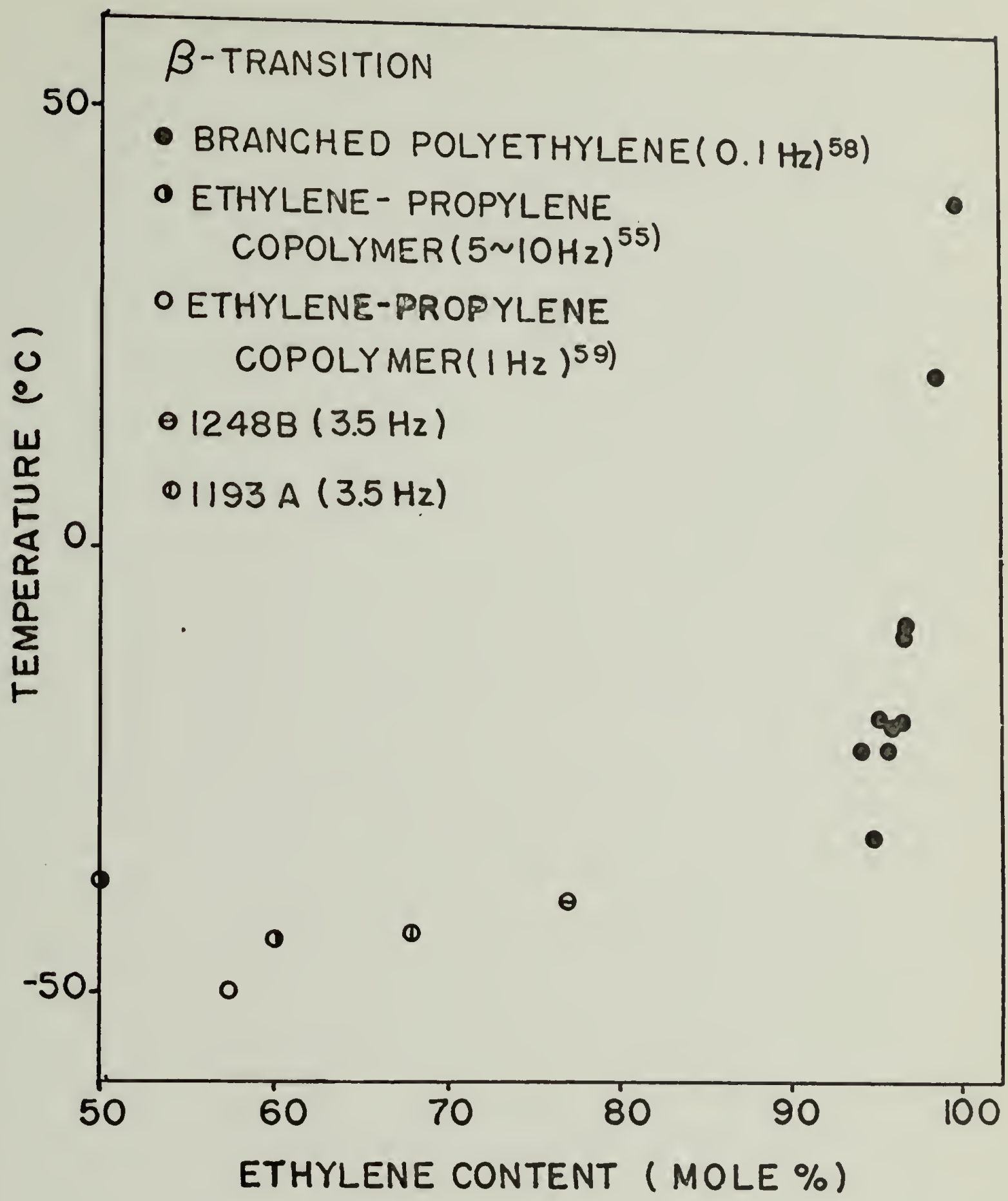
β-TRANSITION
BRANCHED POLYETHYLENE(0.1 Hz)[58]
ETHYLENE- PROPYLENE COPOLYMER(5~10Hz)[55]
ETHYLENE-PROPYLENE COPOLYMER(1Hz)[59]
1248B (3.5 Hz)
1193 A (3.5 Hz)
TEMPERATURE (°C)
50
0
-50
50
60
70
80
90
100
ETHYLENE CONTENT (MOLE %)

FIG. 13

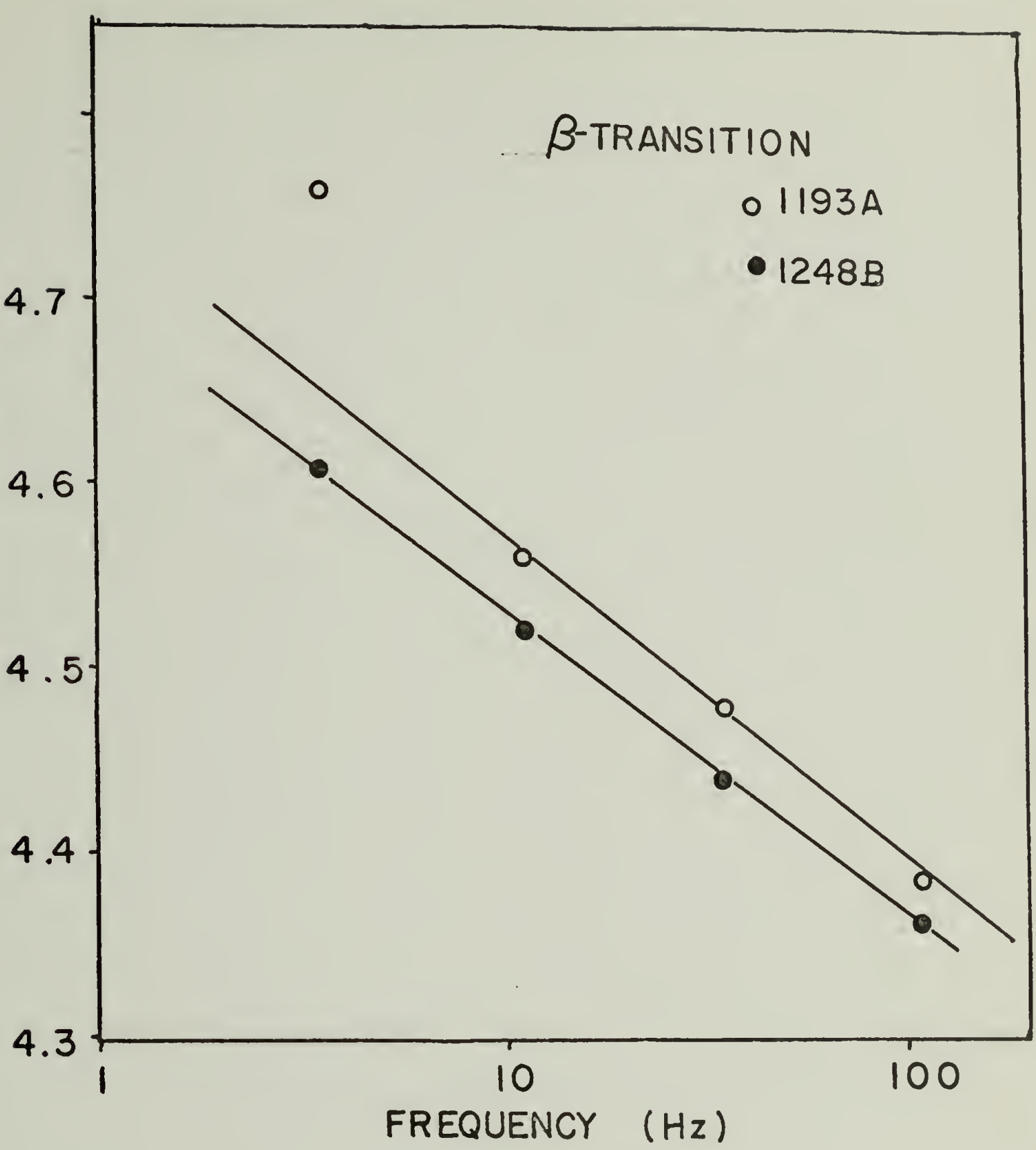
β-TRANSITION
o 1193A
● 1248B
4.7
4.6
4.5
4.4
4.3
1000/T (°K⁻¹)
1
10
100
FREQUENCY (Hz)

FIG. 14

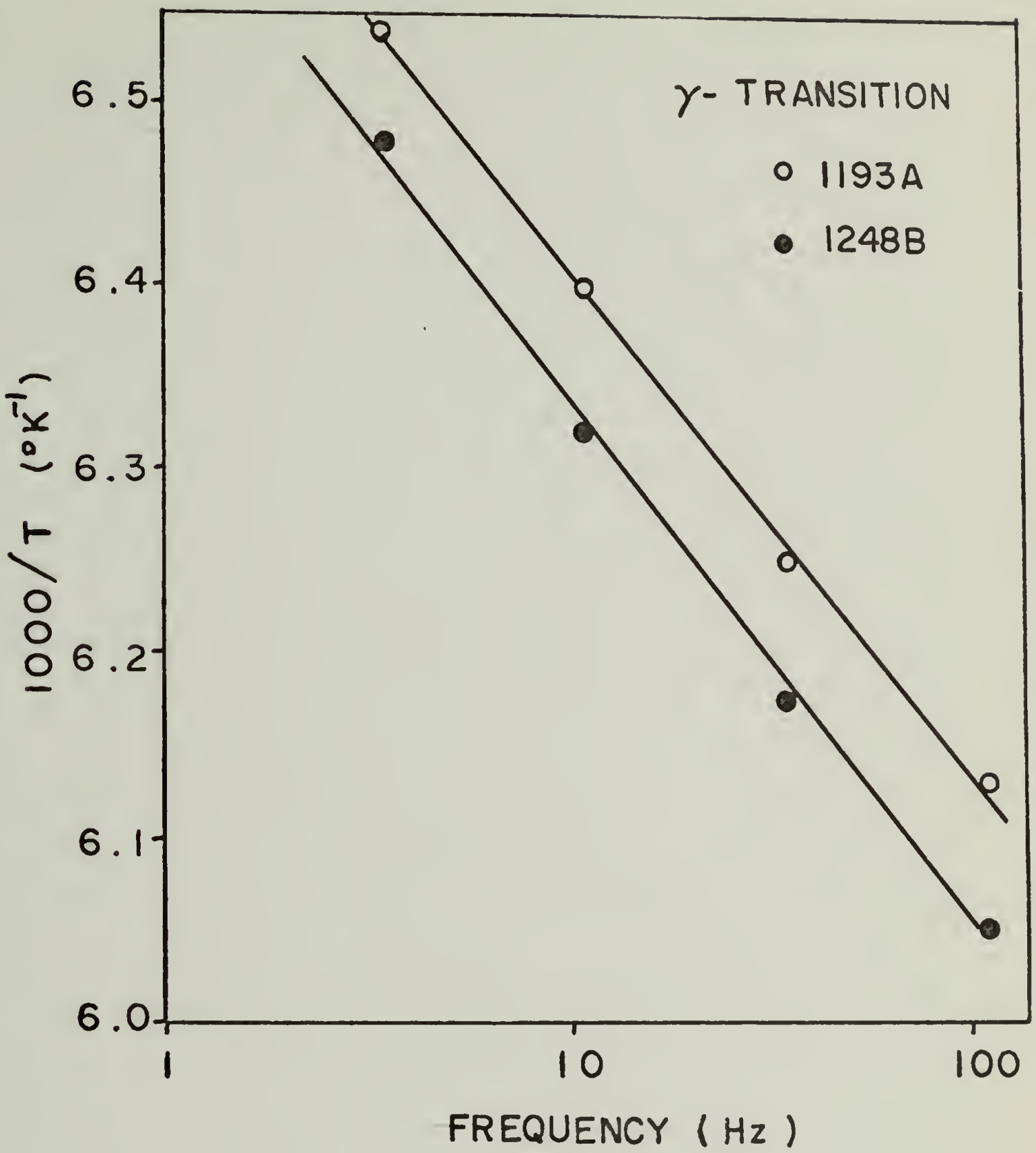
γ- TRANSITION
o 1193A
● 1248B
6.5
6.4
6.3
6.2
6.1
6.0
1000/T (°K⁻¹)
1
10
100
FREQUENCY (Hz)

FIG. 15

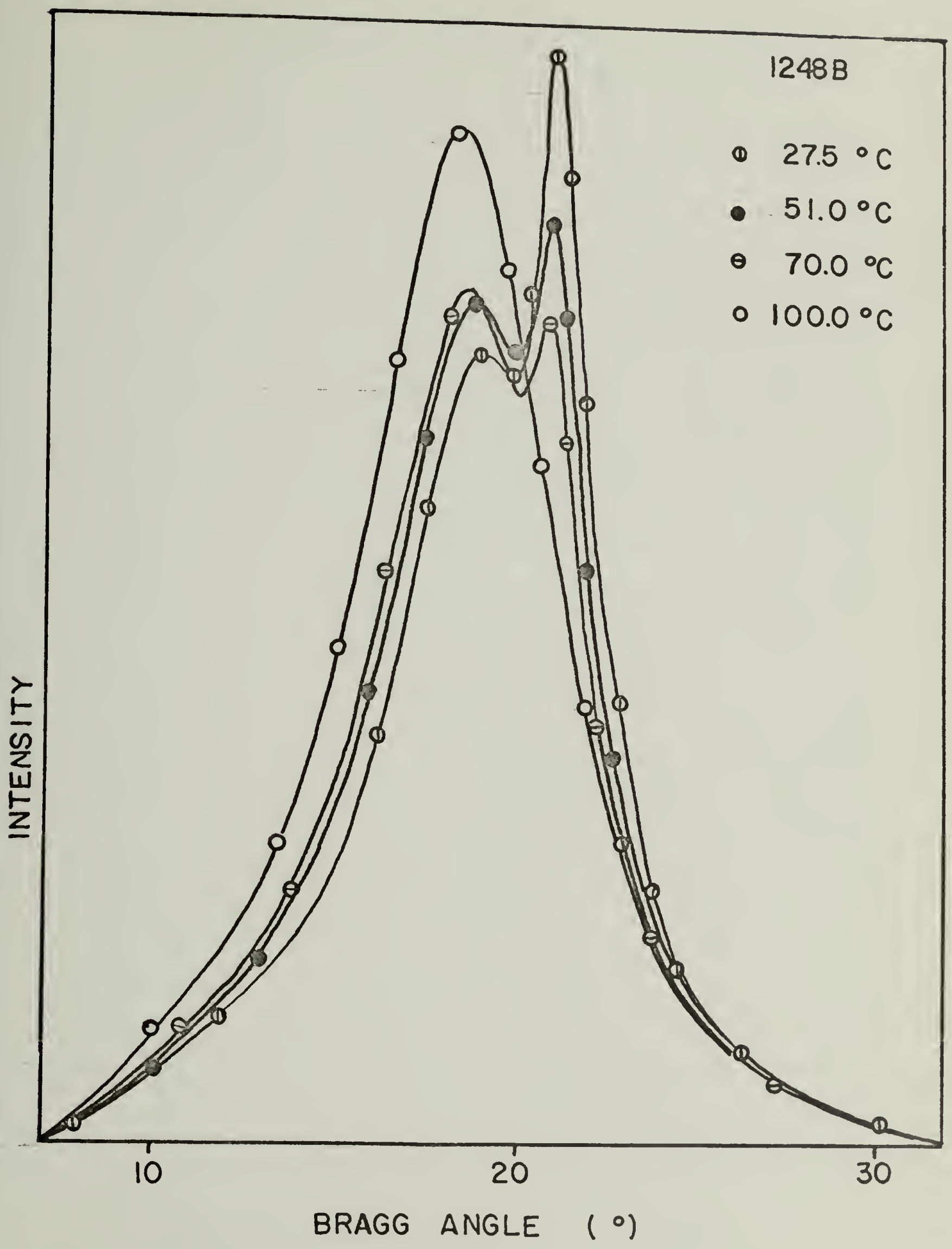

FIG. 16

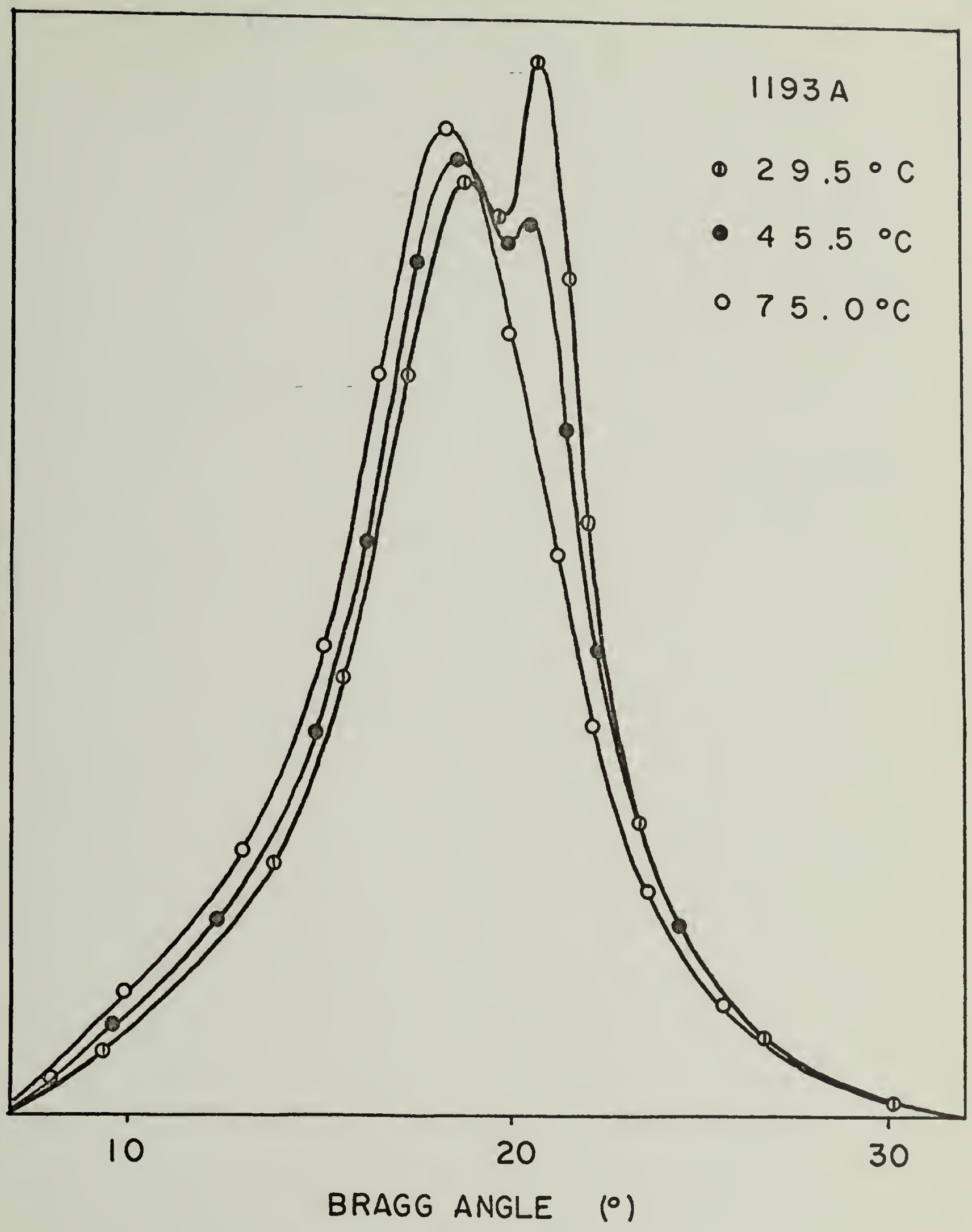

FIG. 17

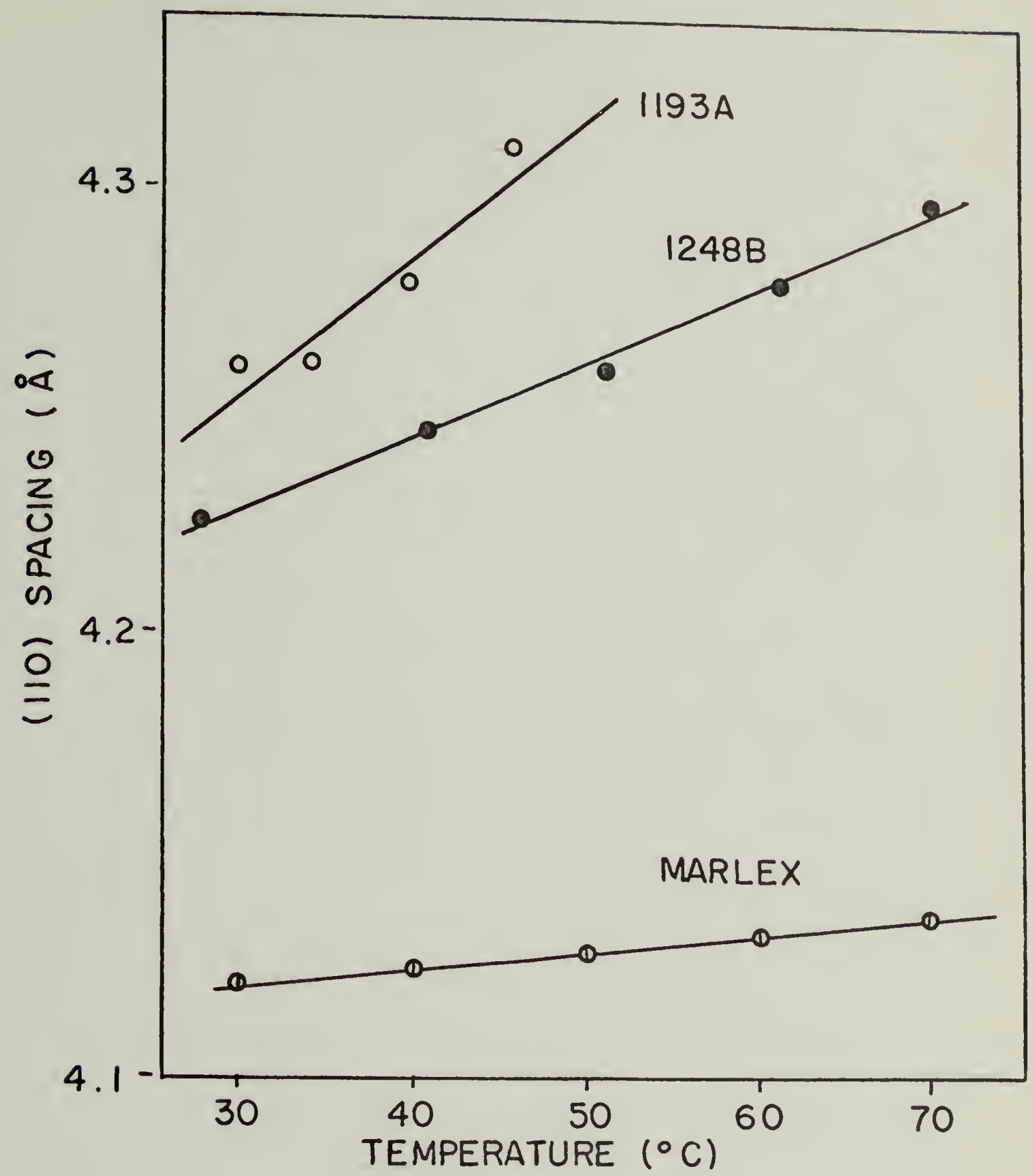
1193A
1248B
MARLEX
4.3
4.2
4.1
(110) SPACING (Å)
30
40
50
60
70
TEMPERATURE (°C)

FIG. 18

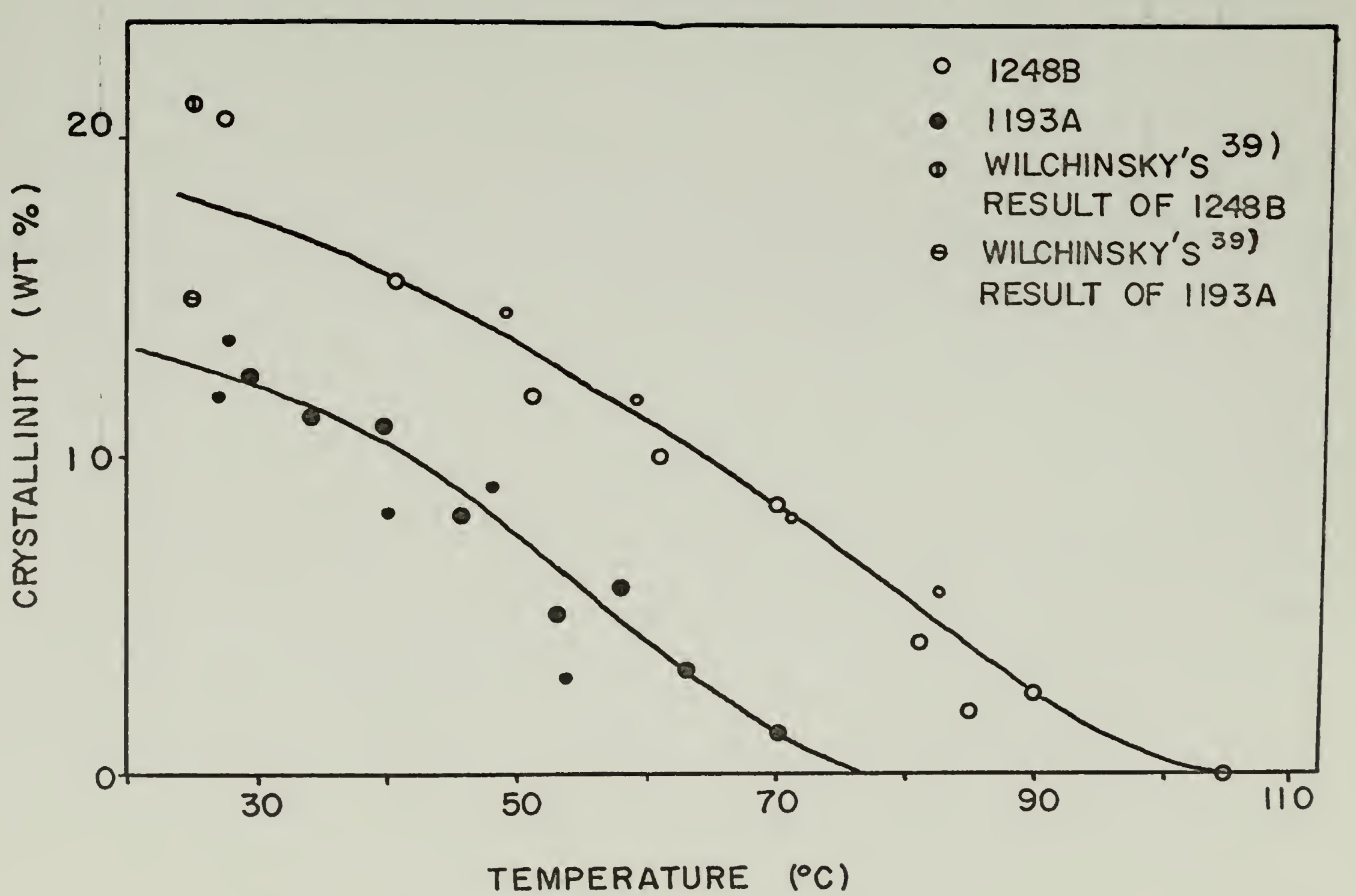
CRYSTALLINITY (WT %)
20
10
0
30
50
70
90
110
TEMPERATURE (°C)
1248B
1193A
WILCHINSKY'S 39) RESULT OF 1248B
WILCHINSKY'S 39) RESULT OF 1193A

FIG. 19

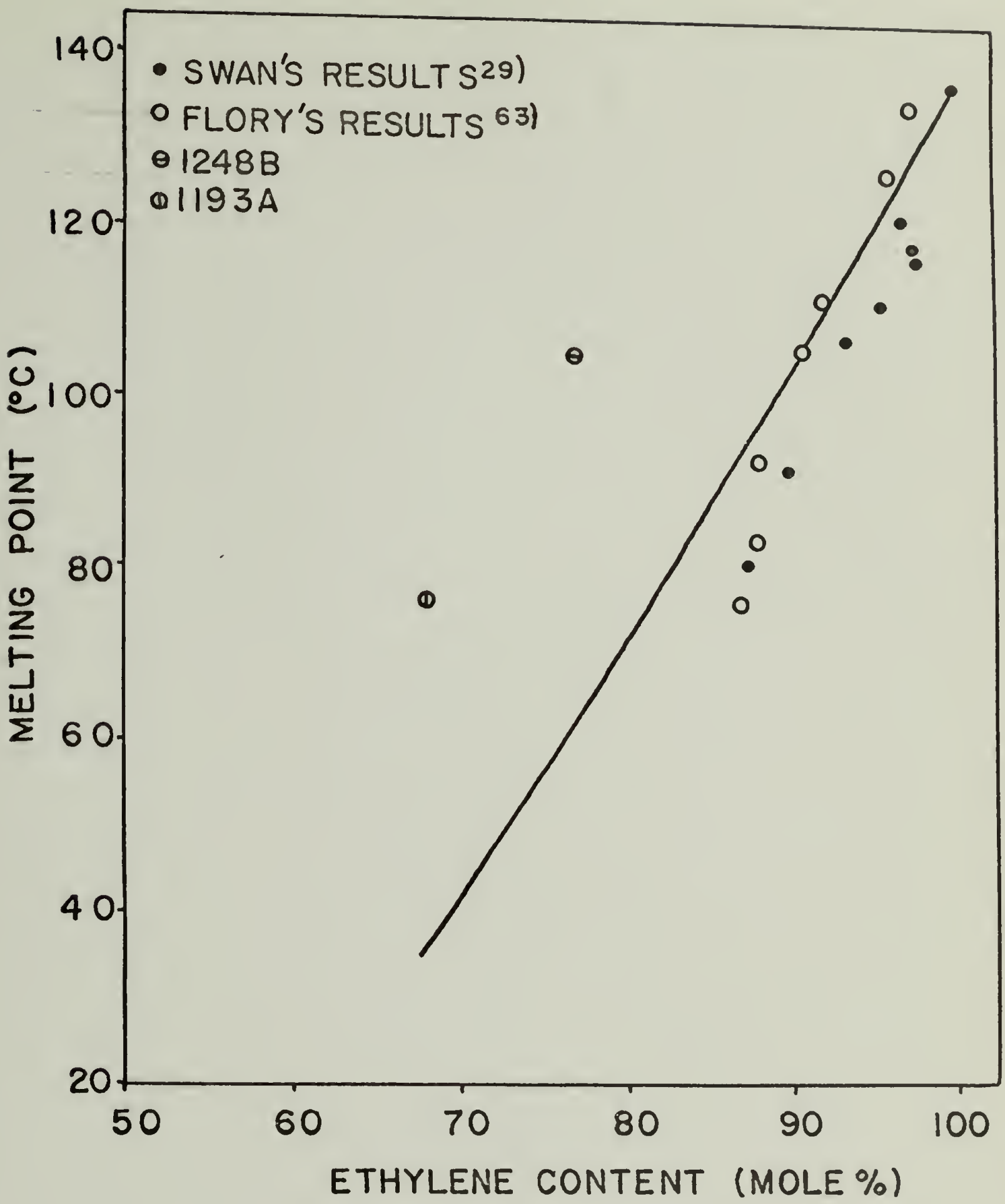
• SWAN'S RESULTS[29]
○ FLORY'S RESULTS[63]
⊖ 1248B
⊖ 1193A
MELTING POINT (°C)
140
120
100
80
60
40
20
50
60
70
80
90
100
ETHYLENE CONTENT (MOLE %)

FIG. 20

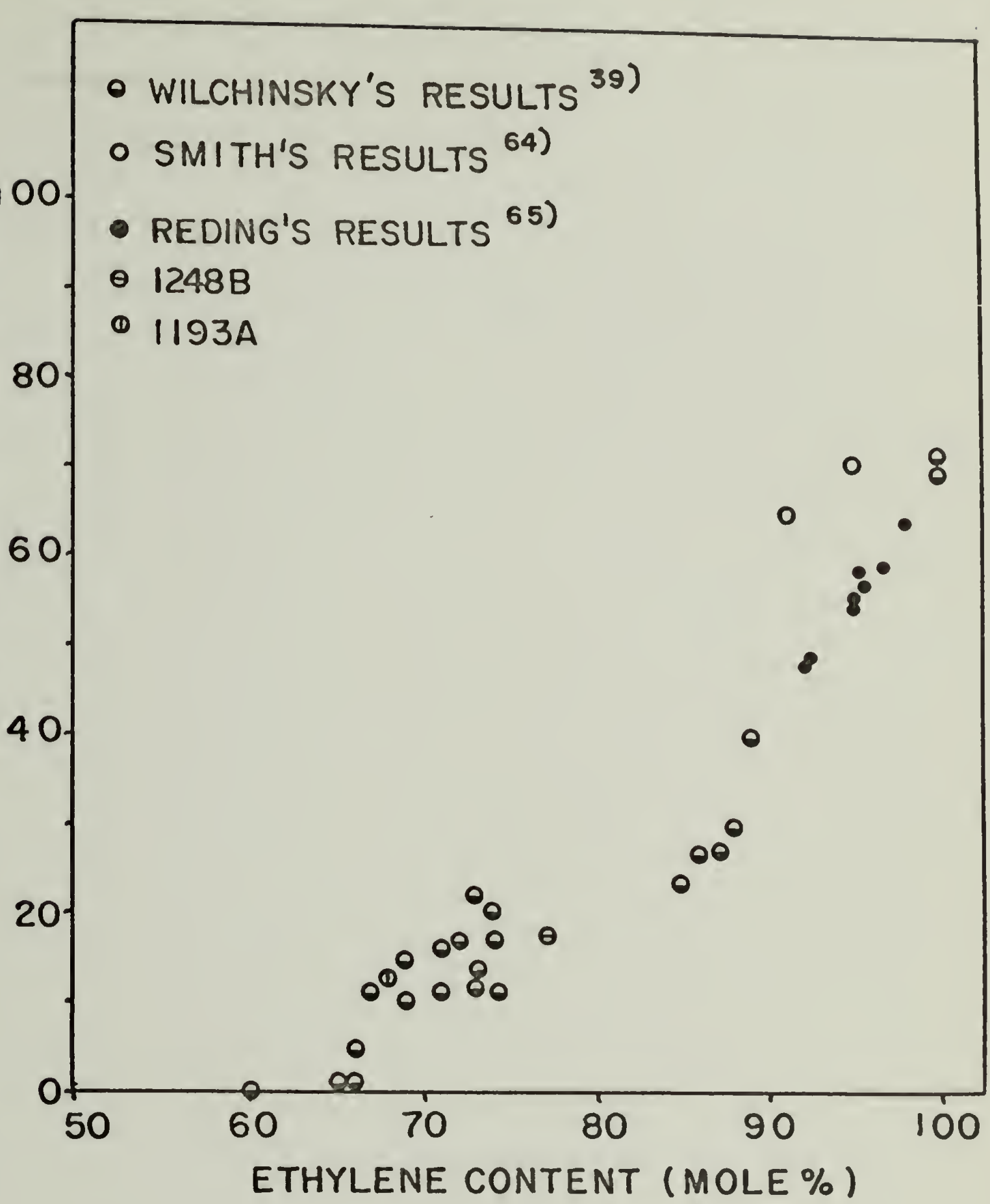
WILCHINSKY'S RESULTS [39]
SMITH'S RESULTS [64]
REDING'S RESULTS [65]
1248B
1193A
CRYSTALLINITY (WT%)
100
80
60
40
20
0
50
60
70
80
90
100
ETHYLENE CONTENT (MOLE %)

FIG. 21

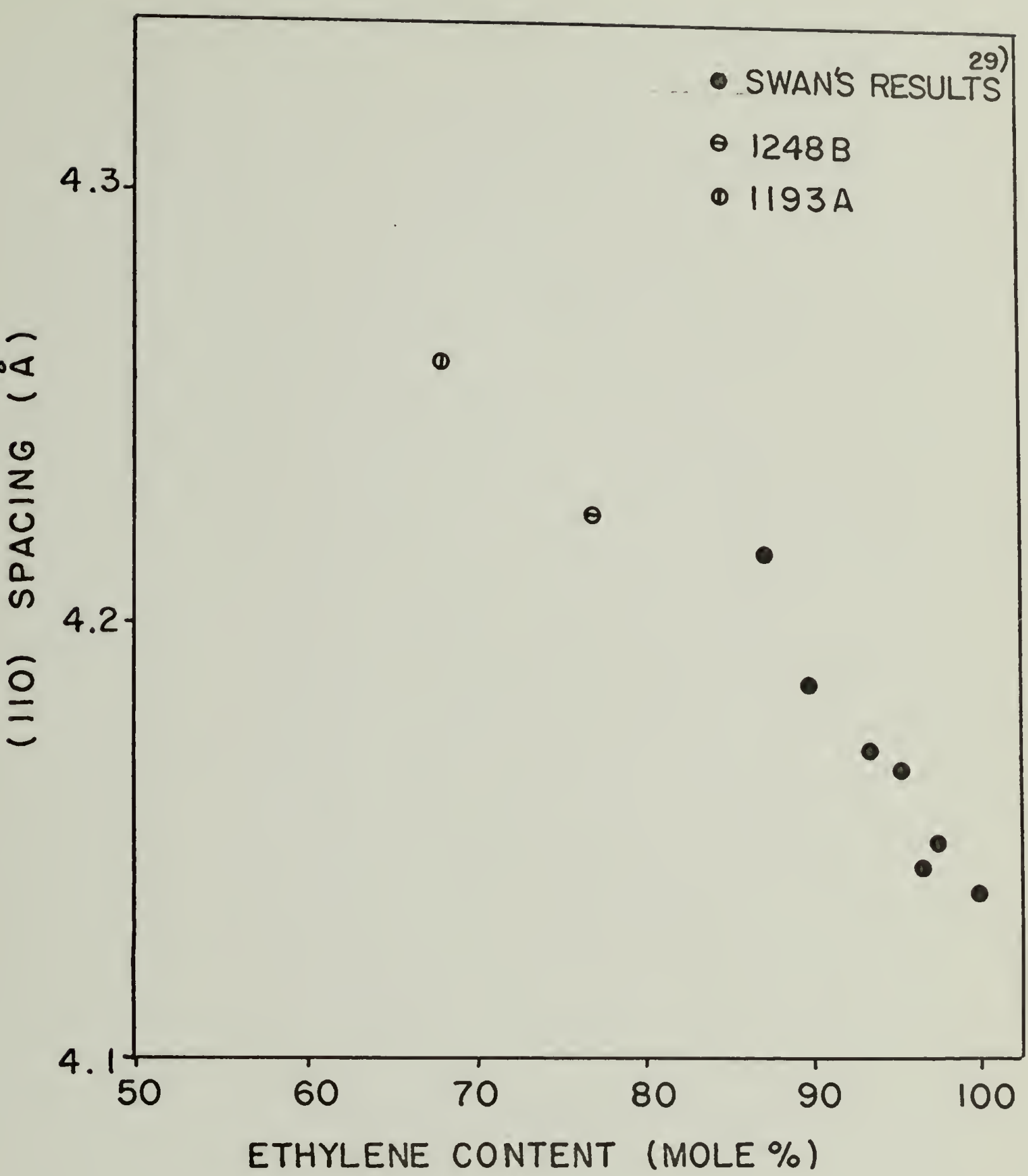
SWAN'S RESULTS 29)
1248B
1193A
4.3
4.2
4.1
(110) SPACING (Å)
50
60
70
80
90
100
ETHYLENE CONTENT (MOLE %)

FIG. 2 2

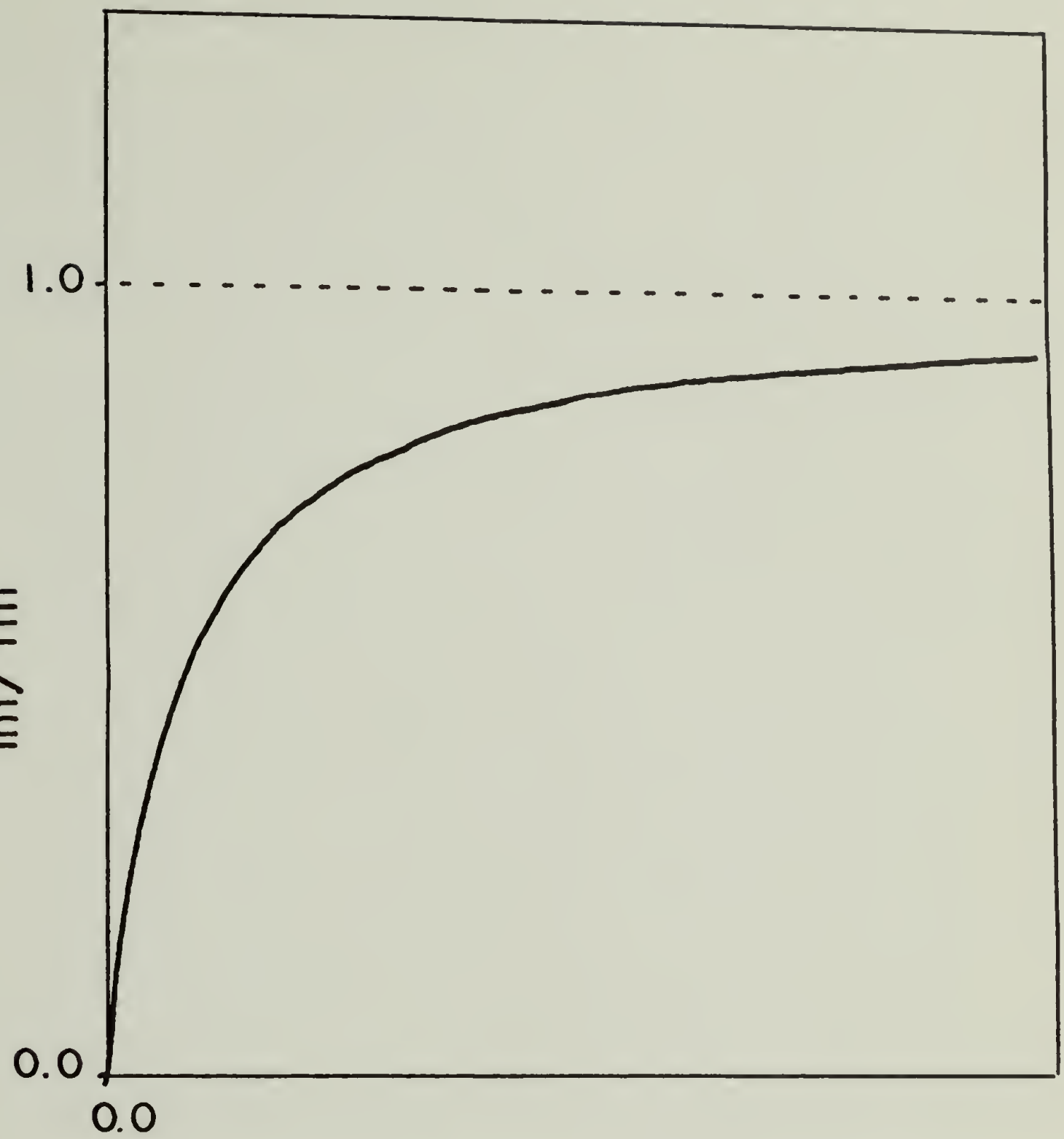

FIG. 23

1248B Vv

1248B Hv

1193A Vv

1193A Hv

FIG.24 LIGHT SCATTERING PATTERNS OF

1248B AND 1193A

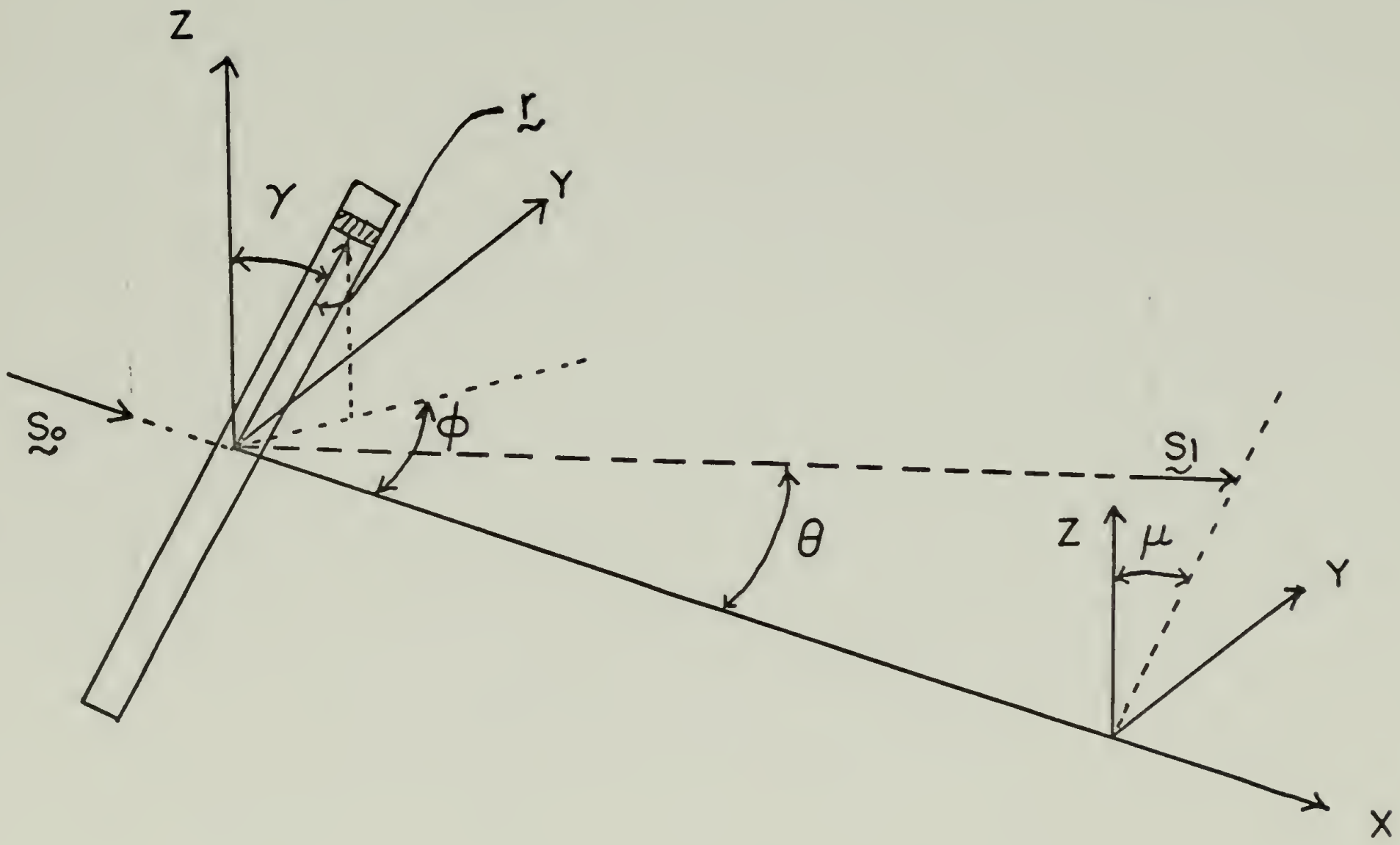

FIG. 2 5

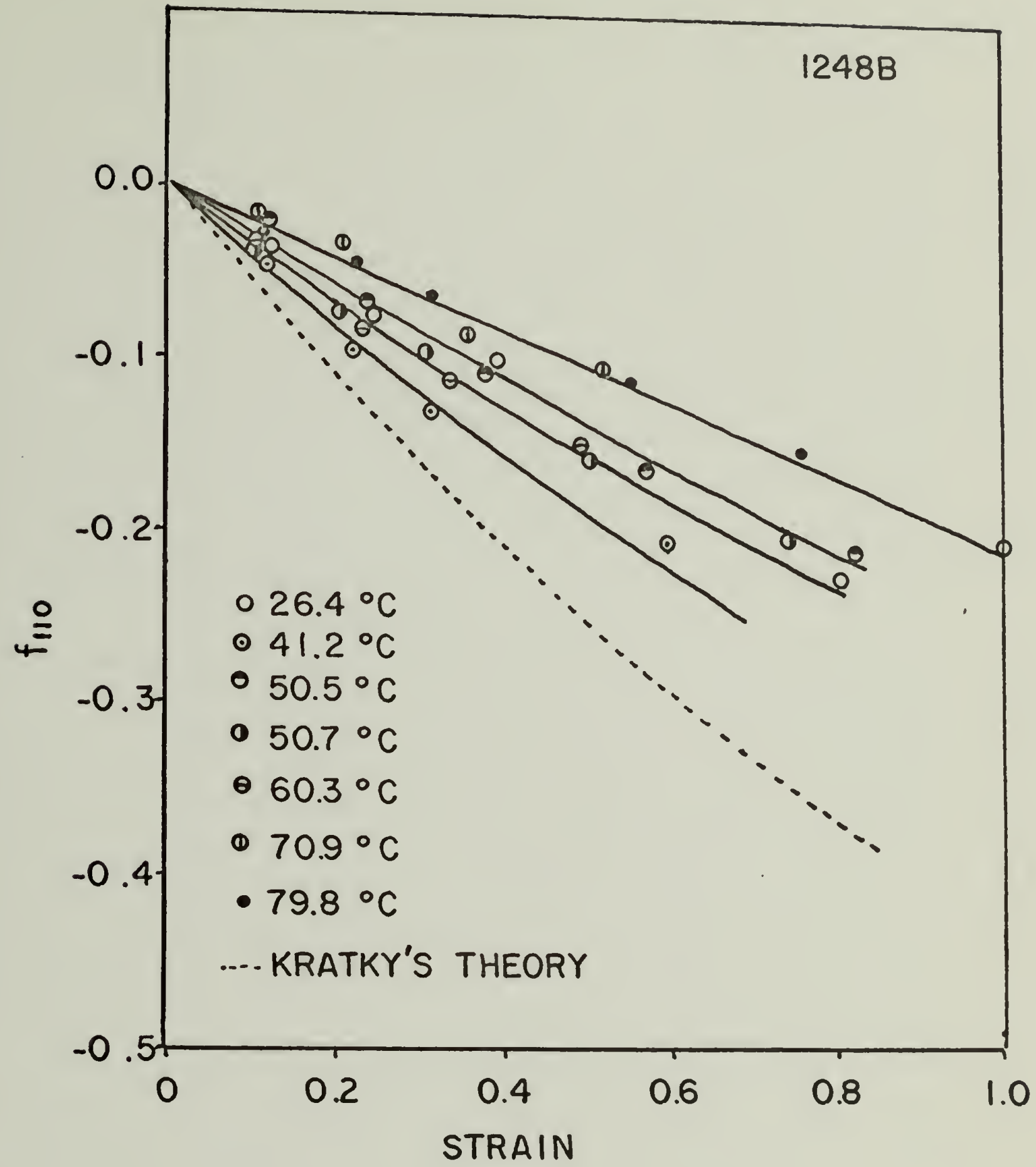
1248B
0.0
-0.1
-0.2
-0.3
-0.4
-0.5
f_{110}
o 26.4 °C
⊙ 41.2 °C
o 50.5 °C
◑ 50.7 °C
⊖ 60.3 °C
⊕ 70.9 °C
• 79.8 °C
---- KRATKY'S THEORY
0
0.2
0.4
0.6
0.8
1.0
STRAIN

FIG. 2 6

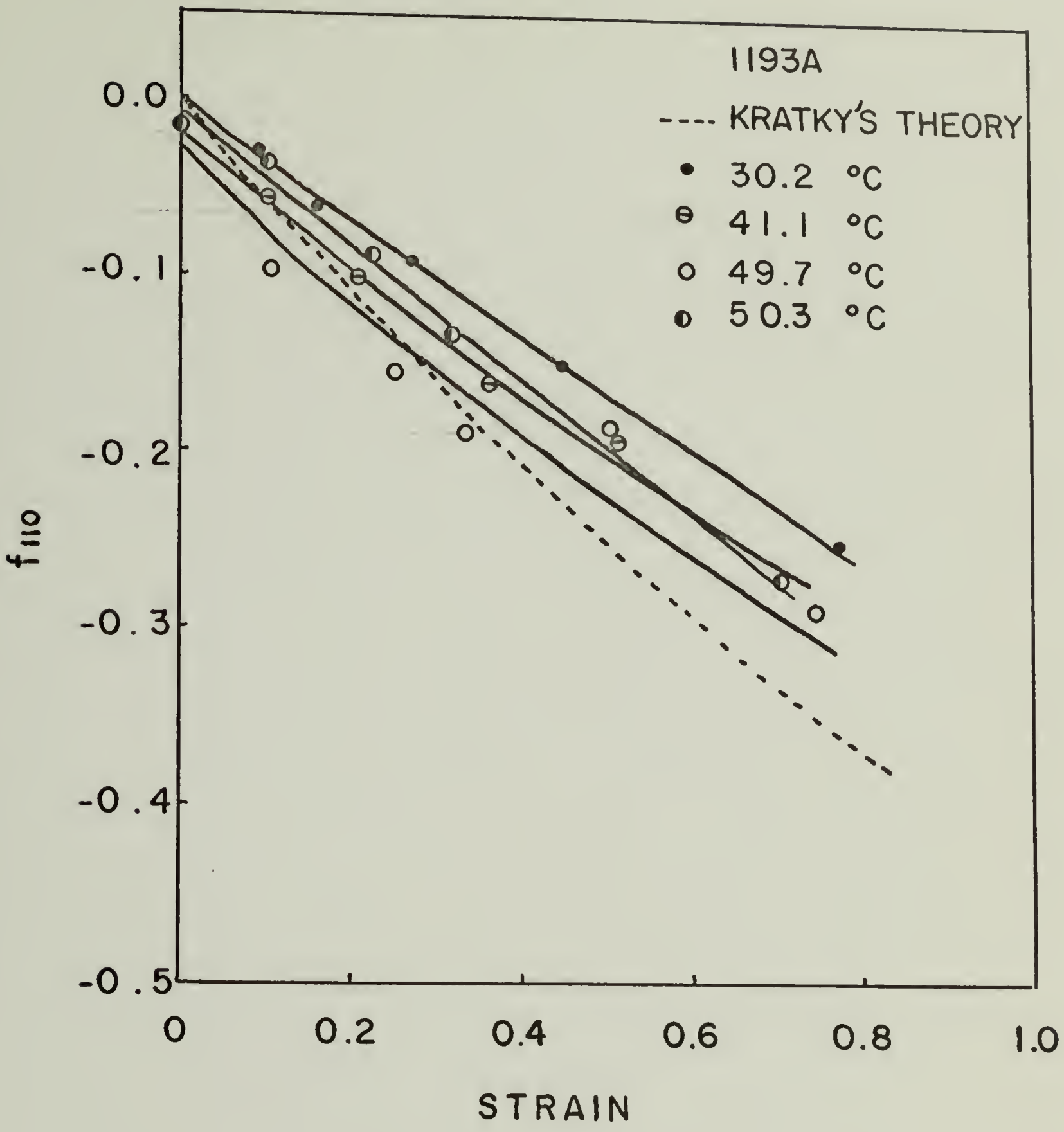
1193A
---- KRATKY'S THEORY
• 30.2 °C
⊖ 41.1 °C
o 49.7 °C
◐ 50.3 °C
0.0
-0.1
-0.2
-0.3
-0.4
-0.5
f110
0
0.2
0.4
0.6
0.8
1.0
STRAIN

FIG. 27

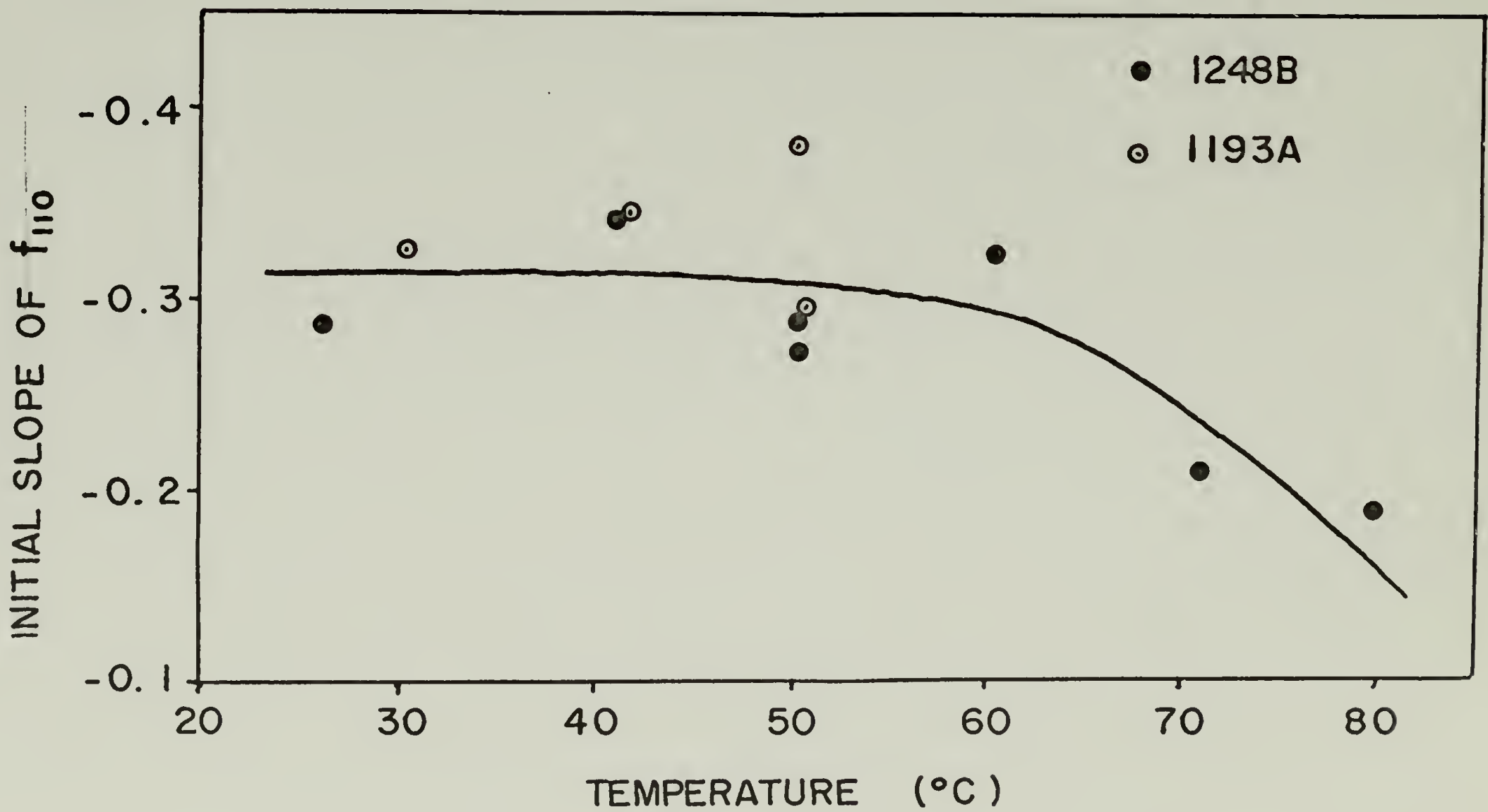
1248B
1193A
-0.4
-0.3
-0.2
-0.1
INITIAL SLOPE OF f_{110}
20
30
40
50
60
70
80
TEMPERATURE (°C)

FIG. 2 8

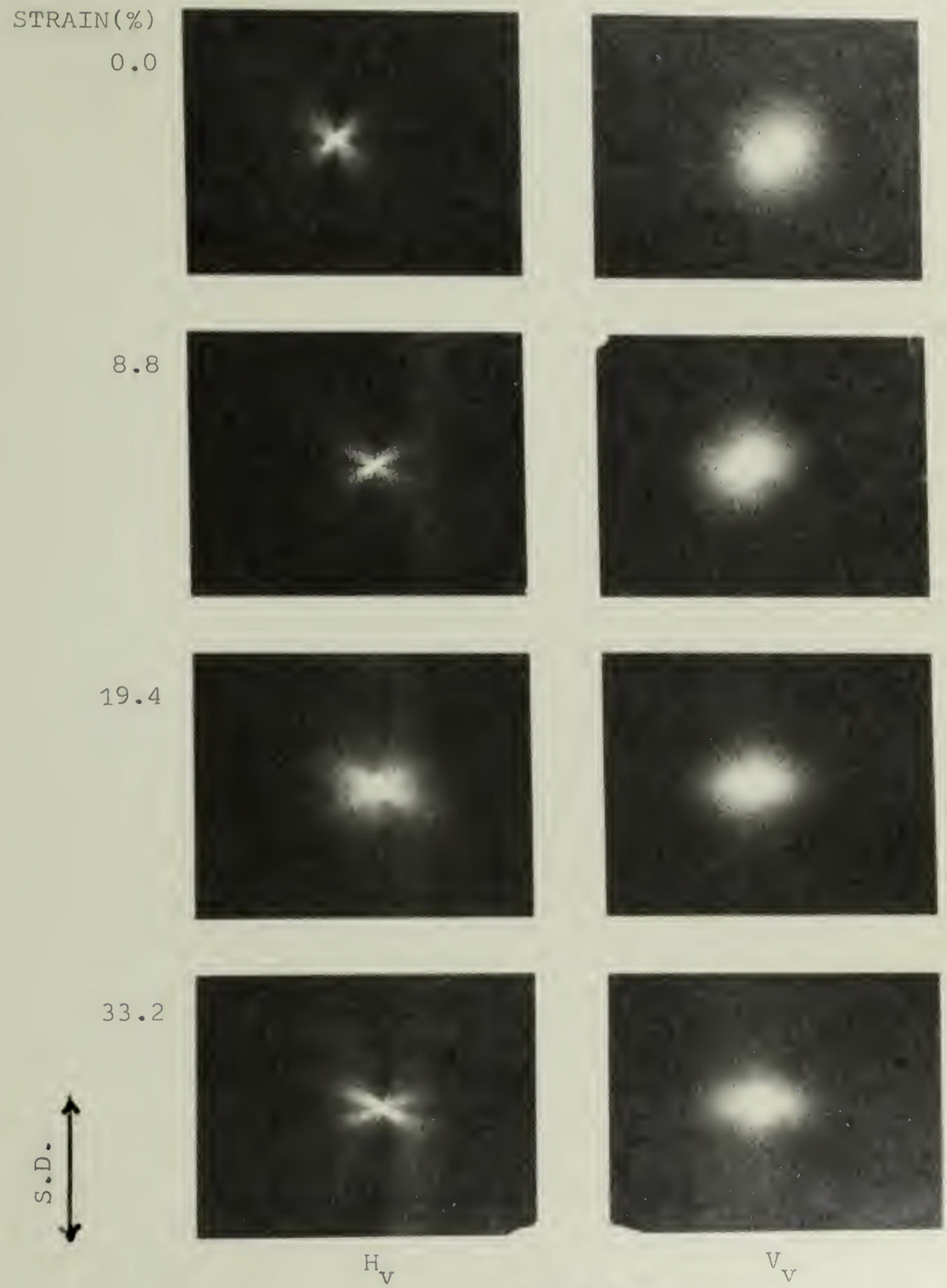

1 2 4 8 B

FIG. 29

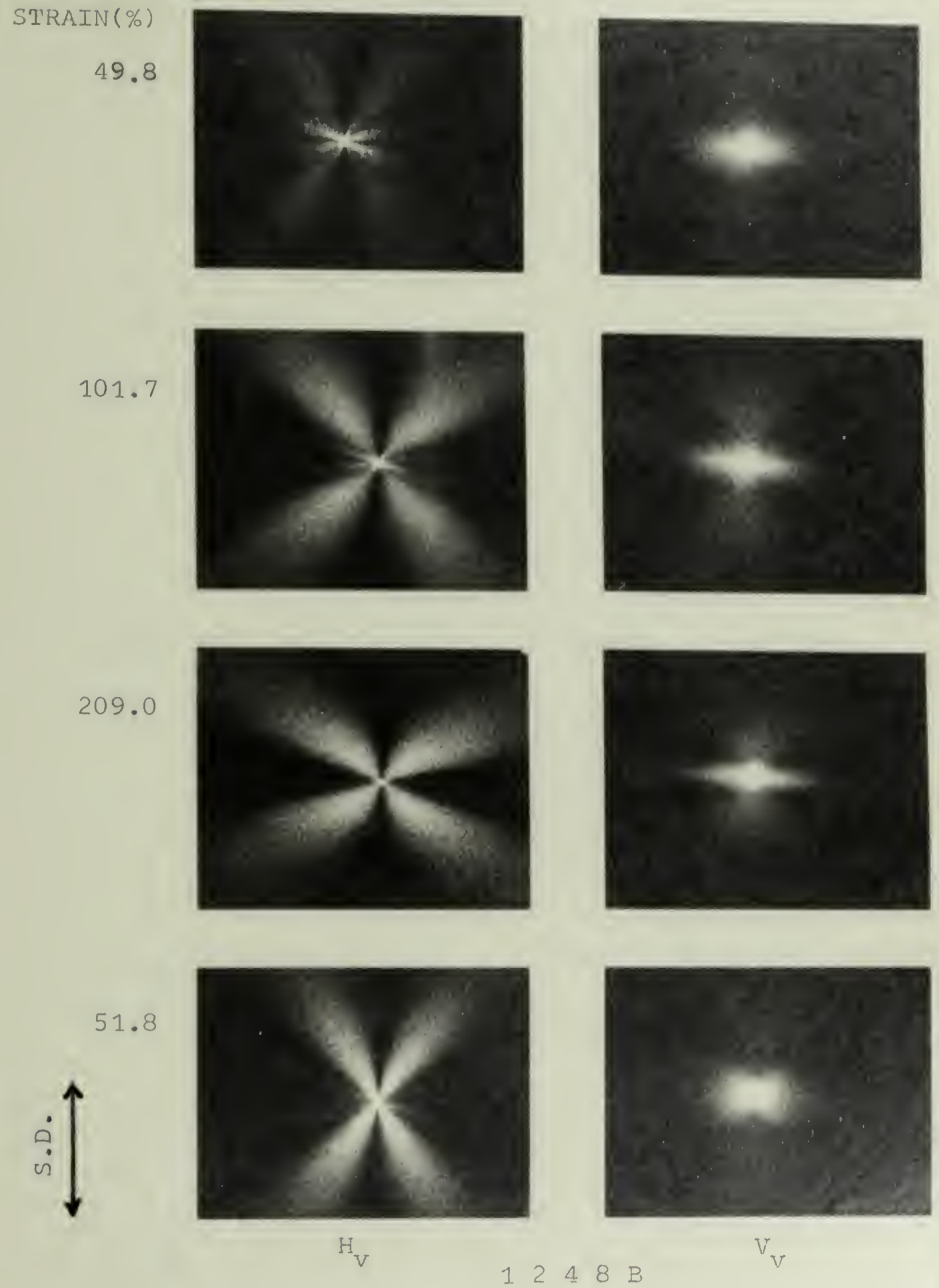

FIG. 30

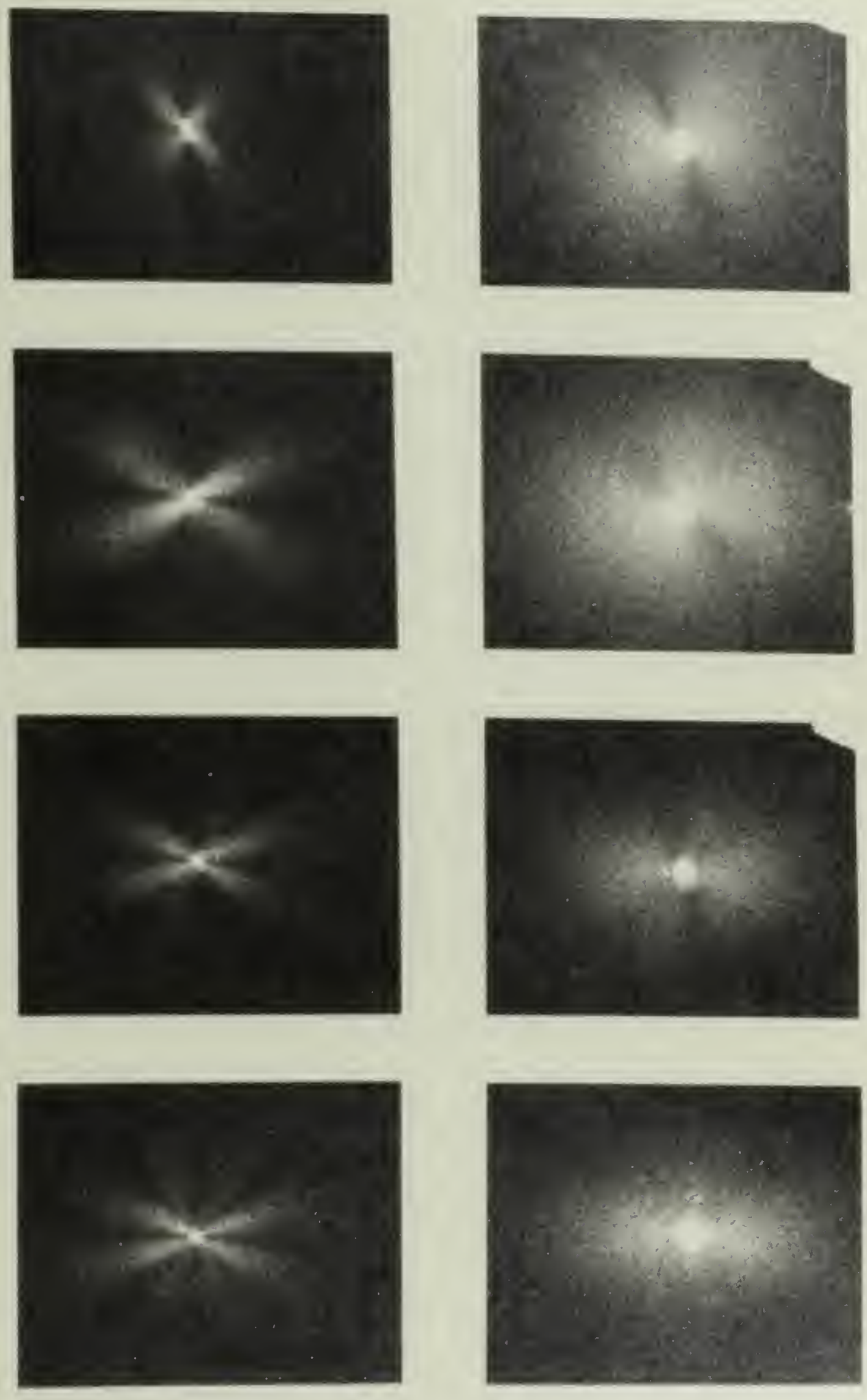

FIG. 31

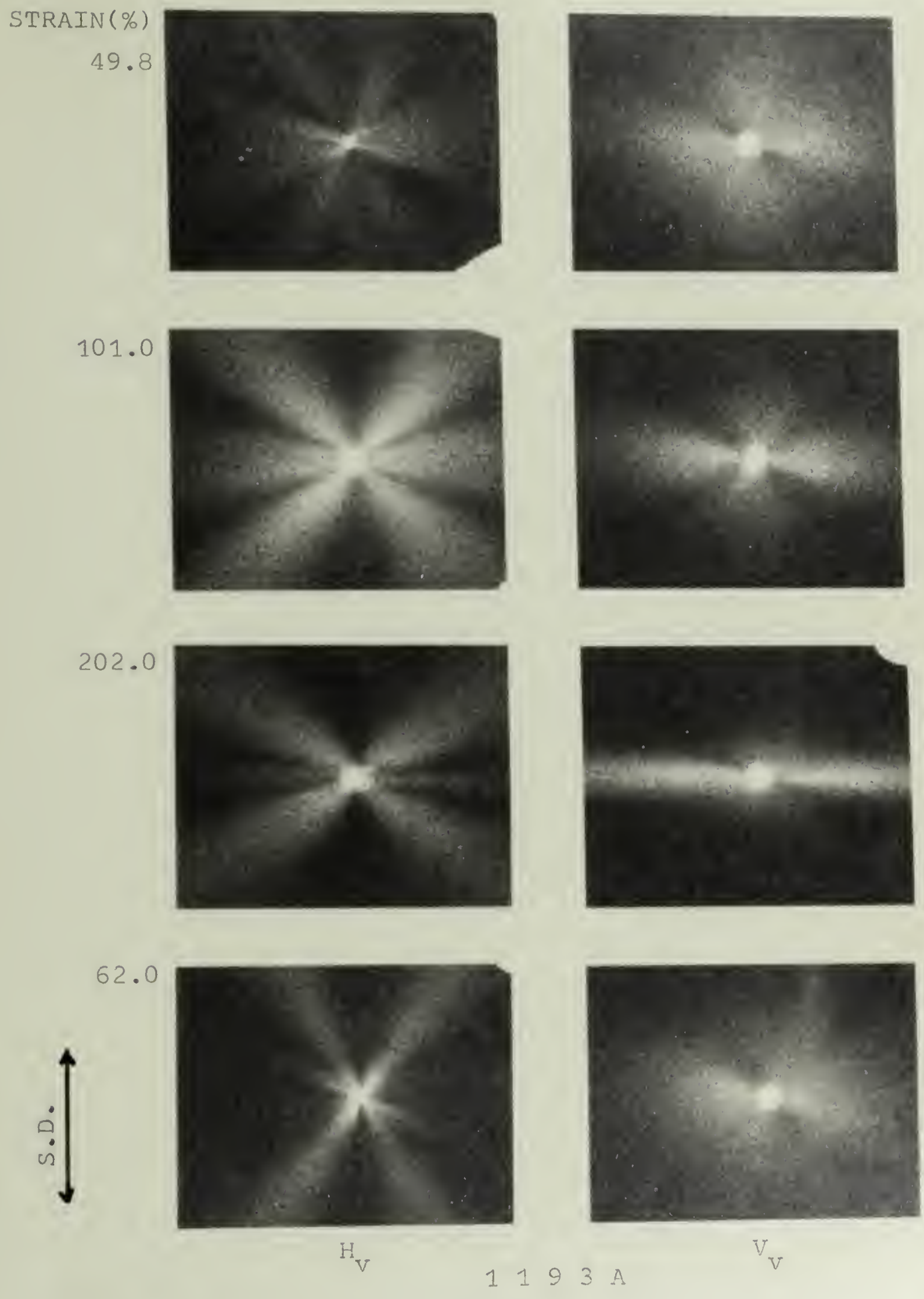

FIG. 32

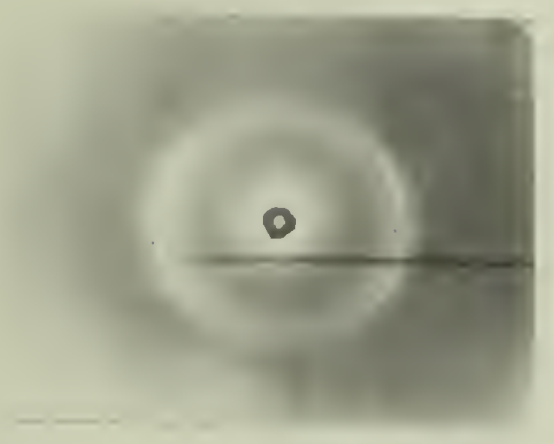

70.0 (%)

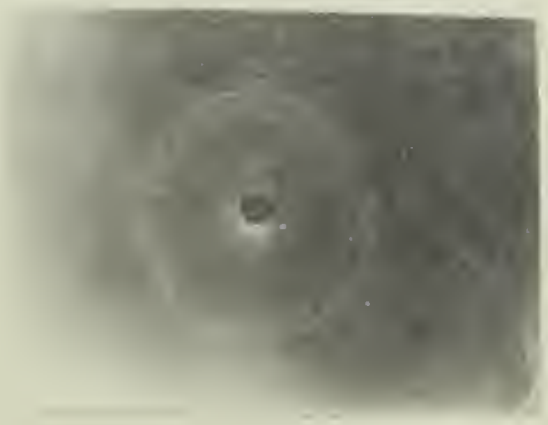

0.0 (%)

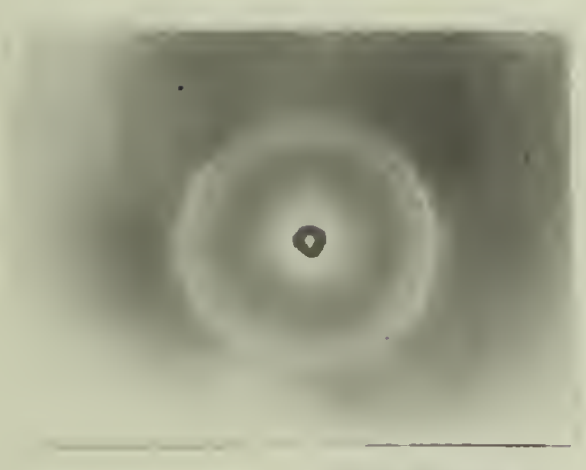

95.0(%)

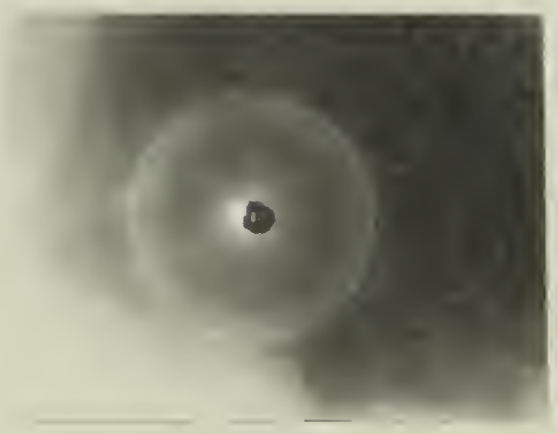

20.5 (%)

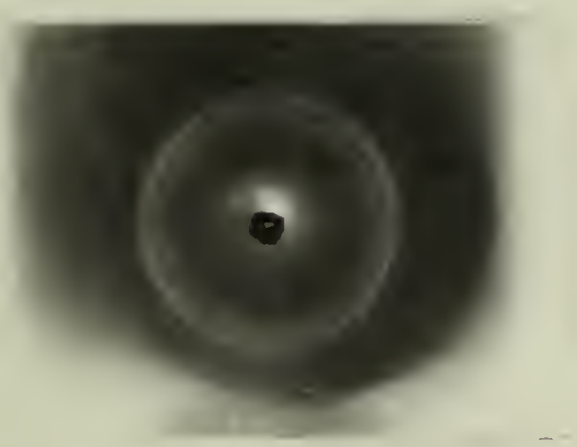

50.0 (%)

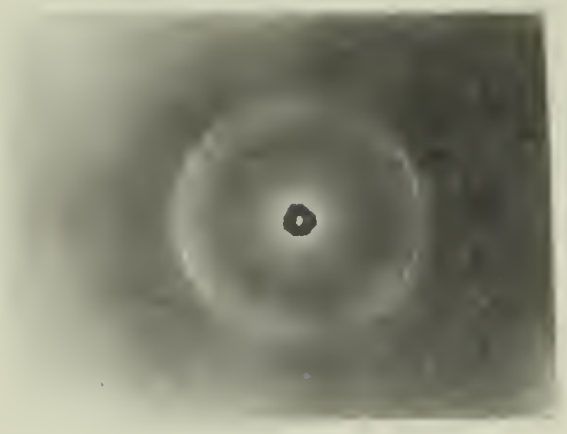

59.7(%)

S.D.

FIG. 33 X-RAY DIFFRACTION PHOTOGRAPHS FOR 1248B AT VARIOUS ELONGATIONS

62.5(%)

0.0(%)

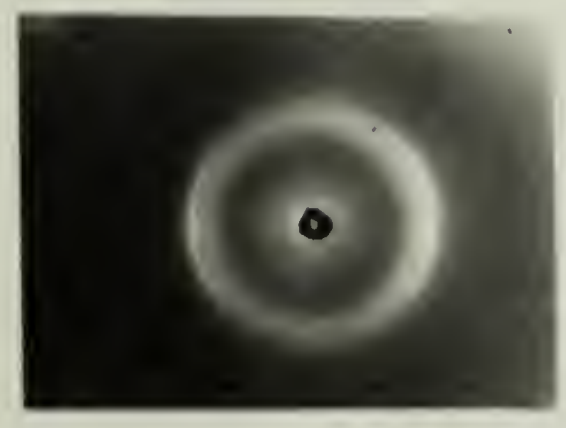

95.0(%)

20.0(%)

S.D.

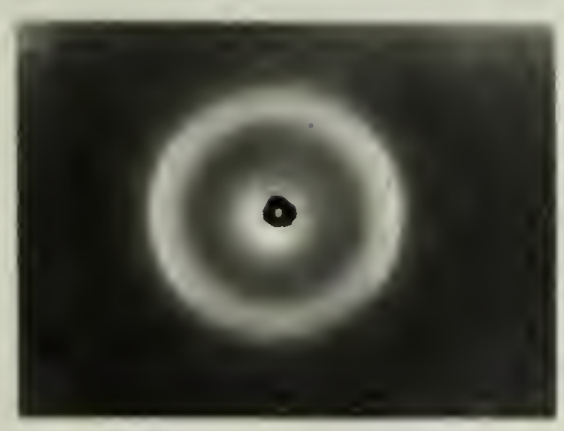

50.0(%)

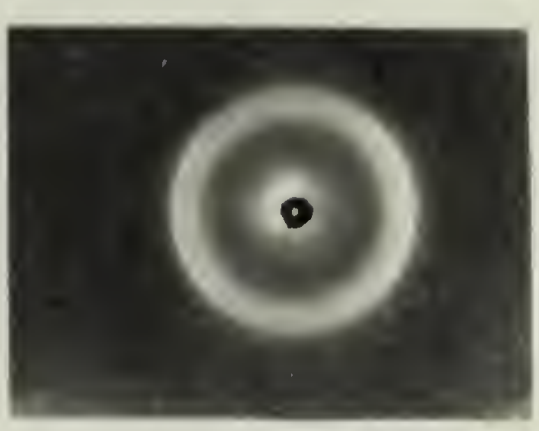

50.0(%)

FIG.34 X-RAY DIFFRACTION PHOTOGRAPHS

FOR 1193A AT VARIOUS ELONGATIONS

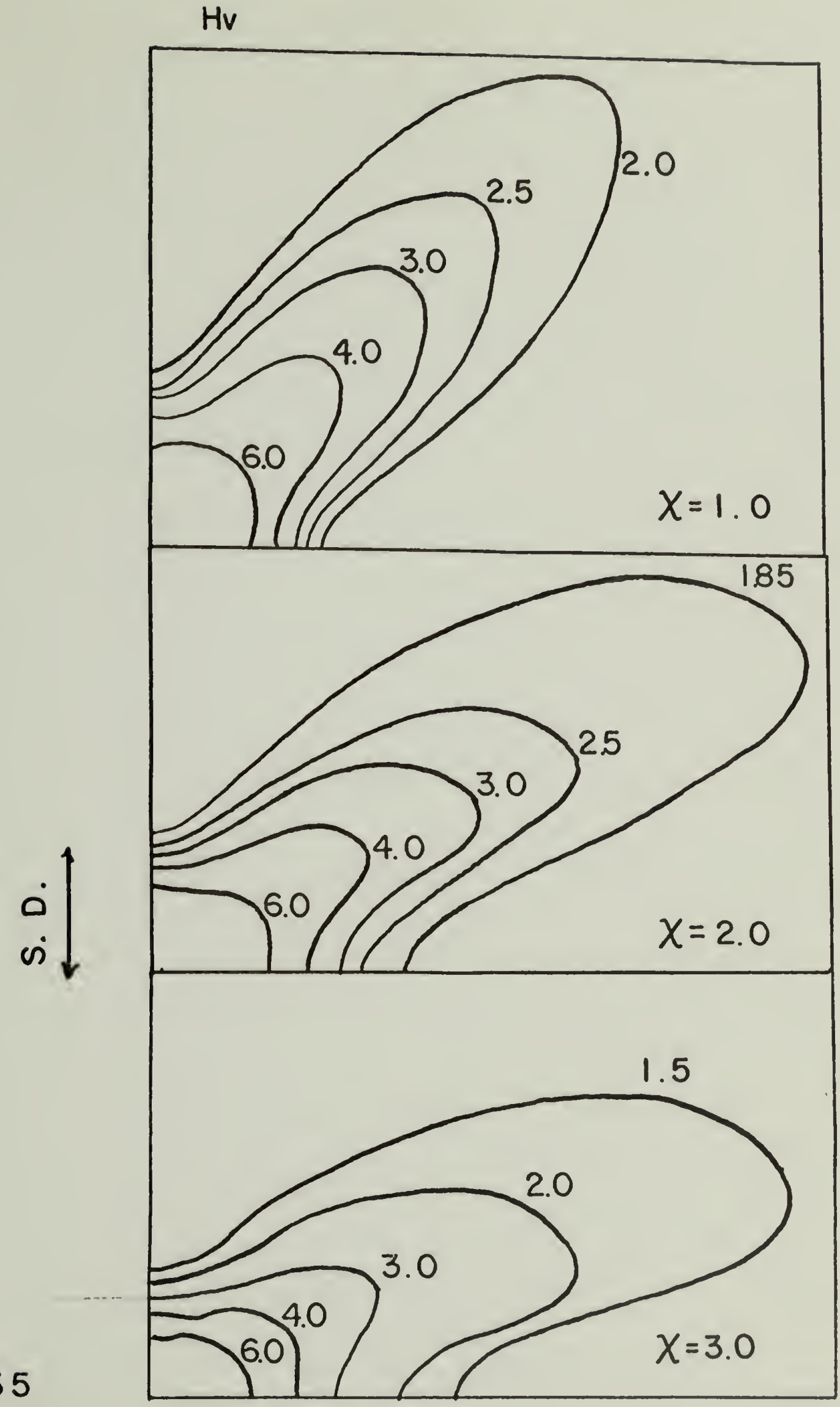

FIG. 35

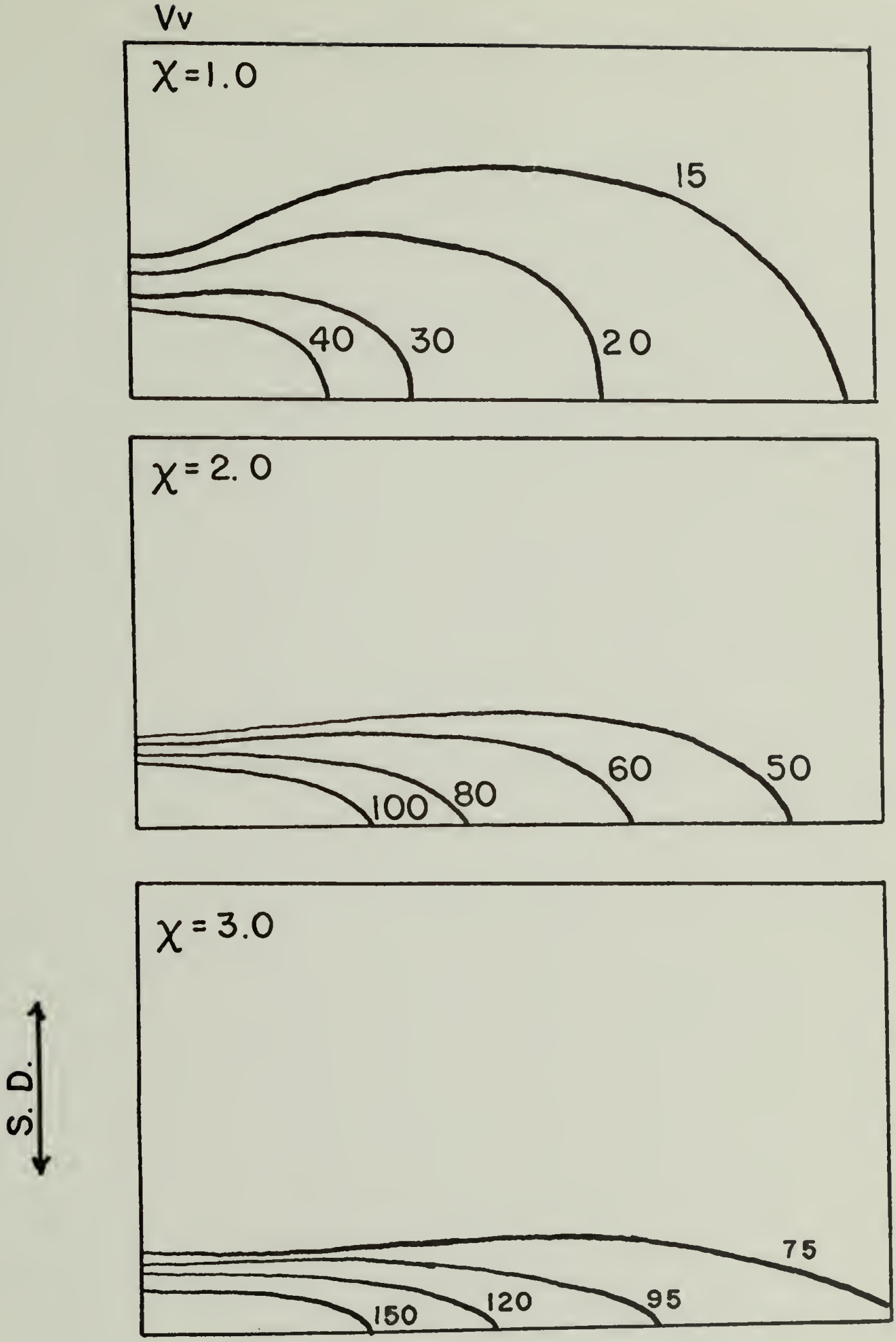

FIG. 36

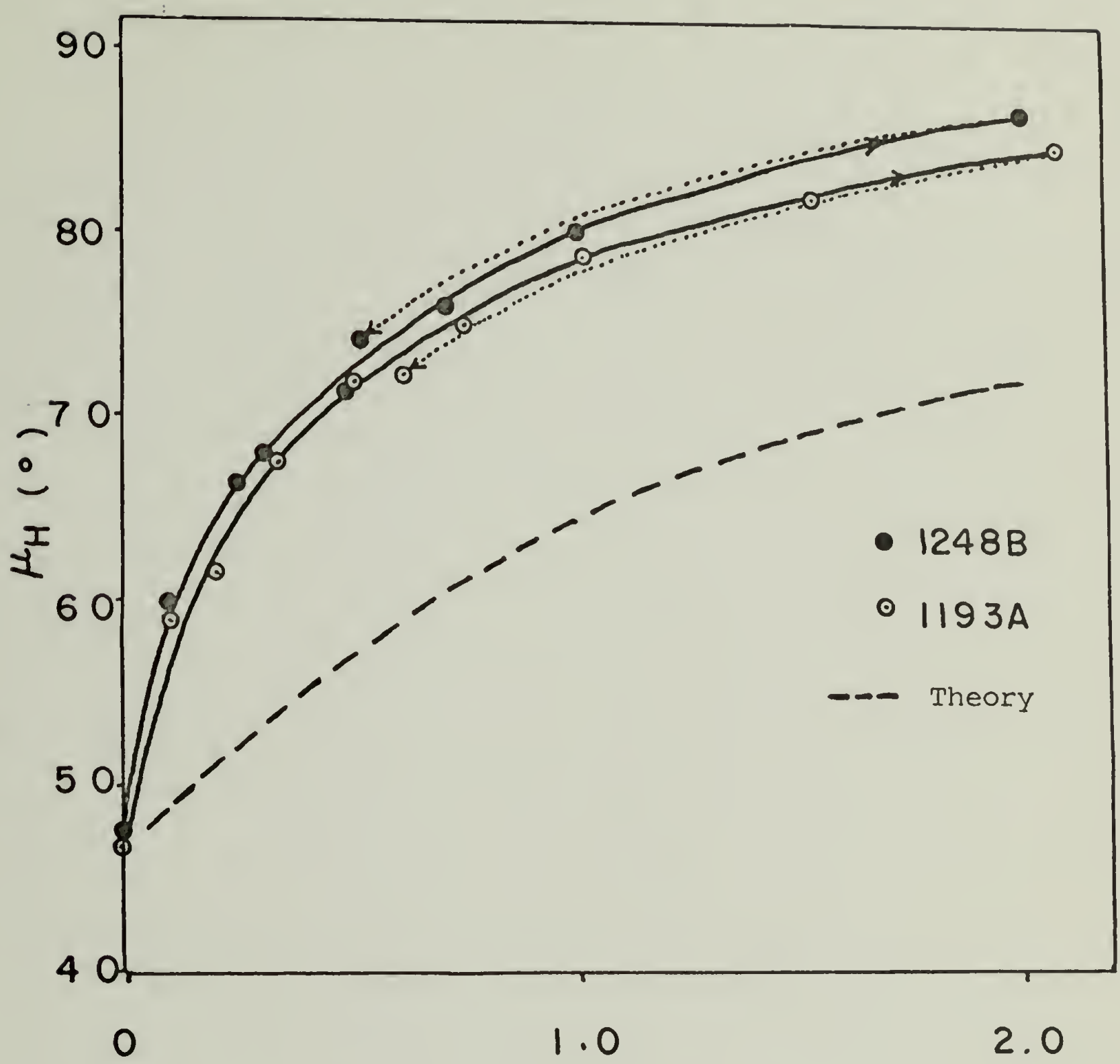

FIG. 37

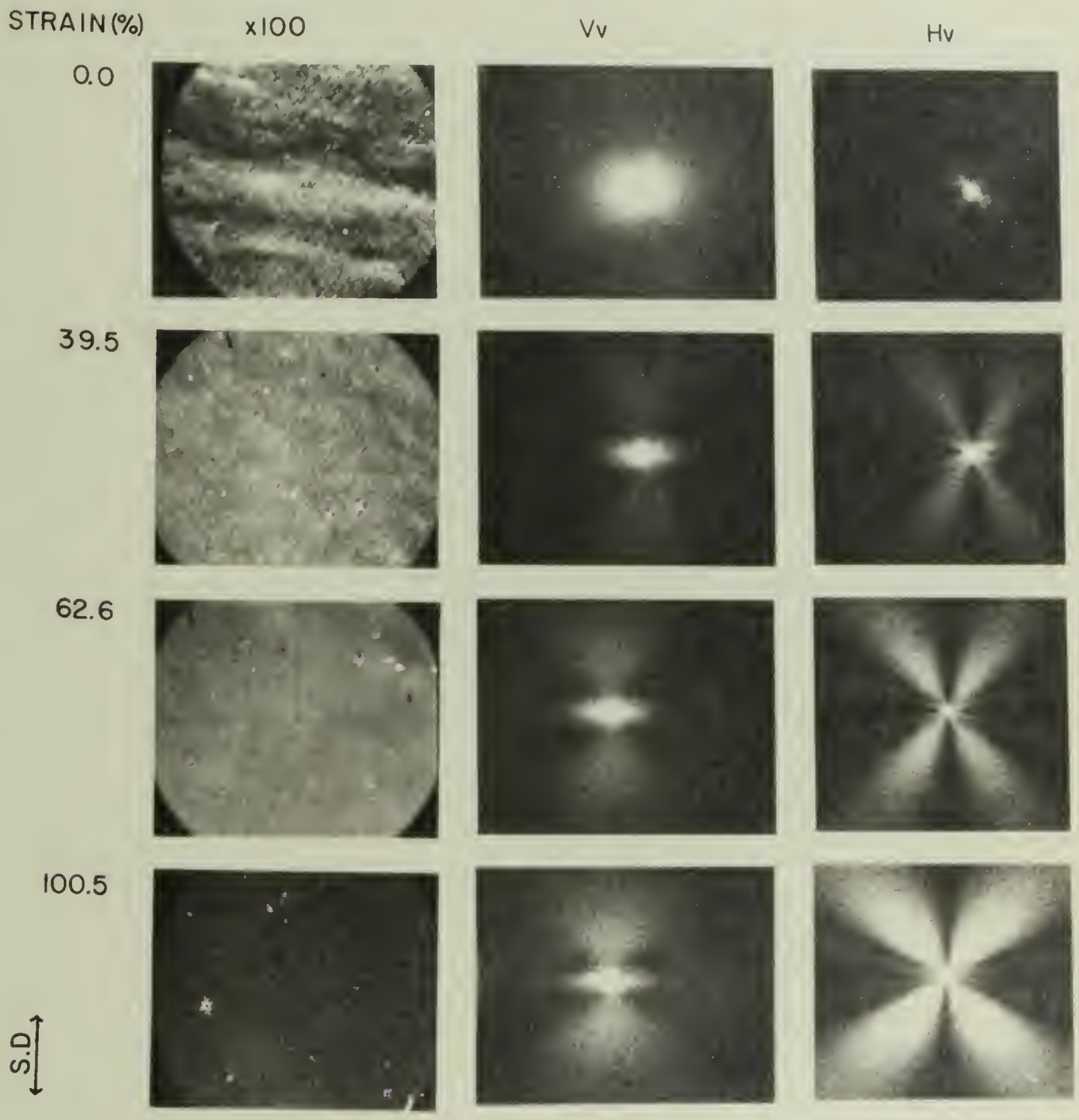

FIG. 38

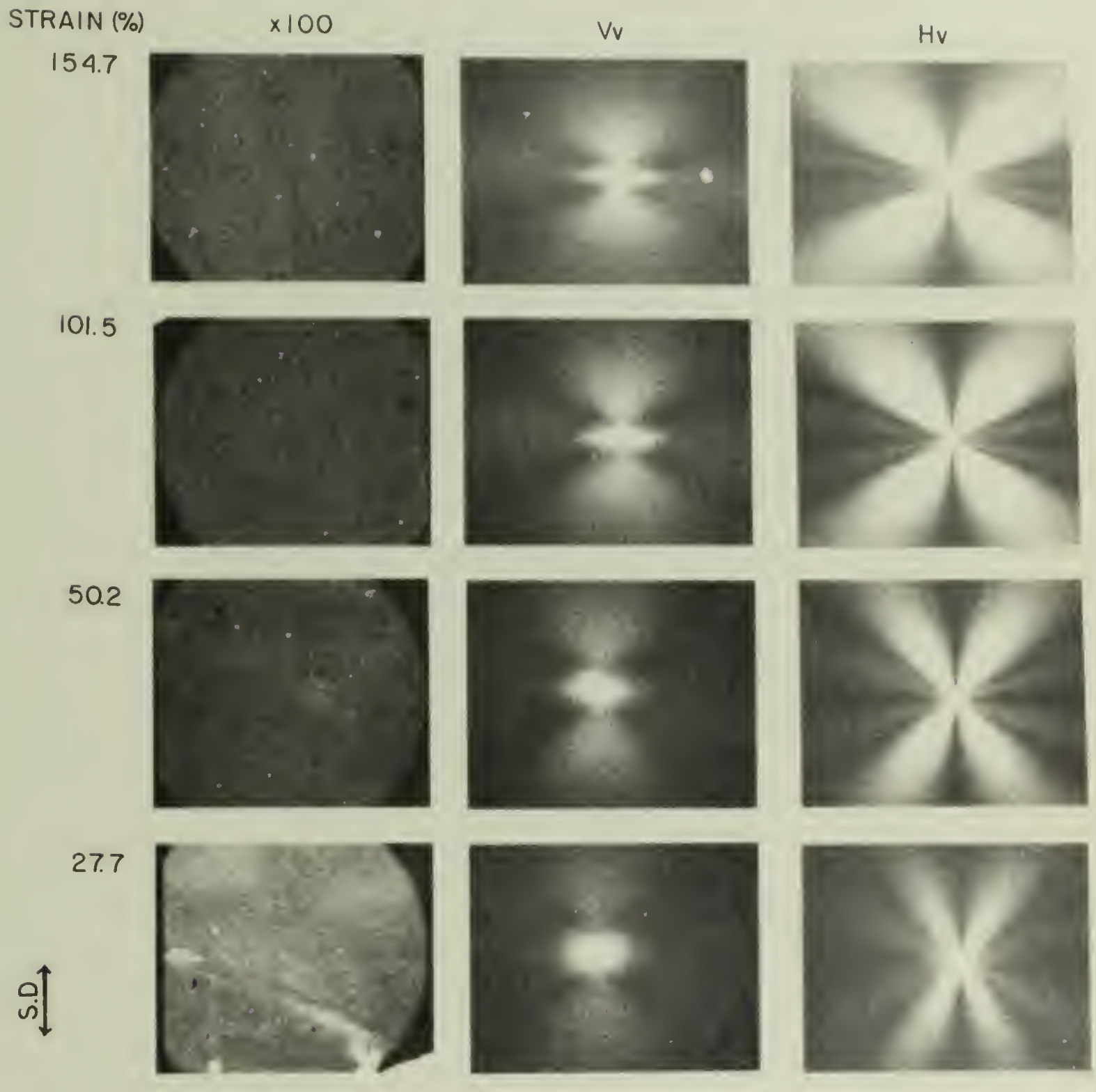

FIG. 39

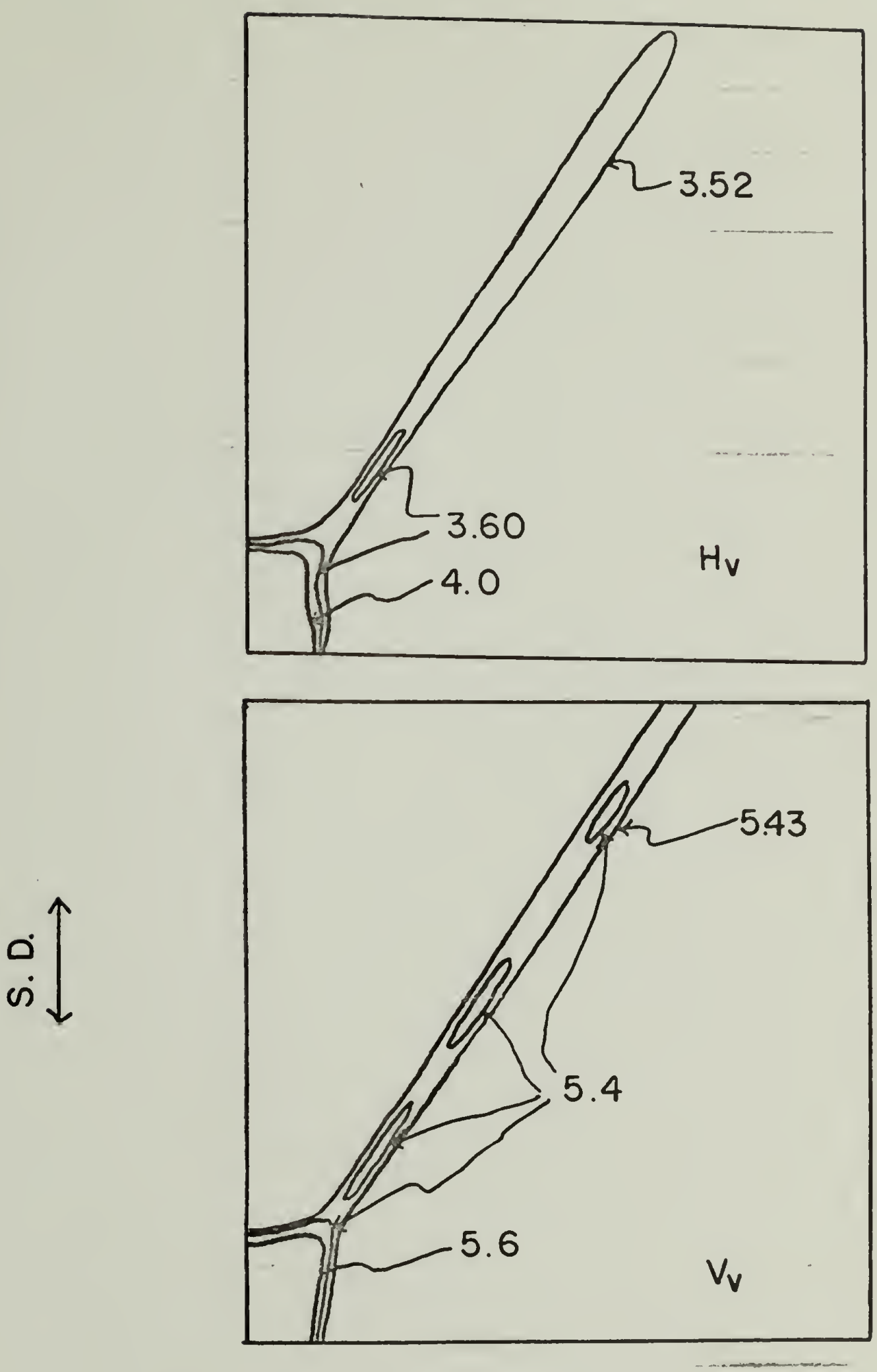

FIG. 4 0

x100

VH

HH

S.D.

HV

VV

FIG. 41

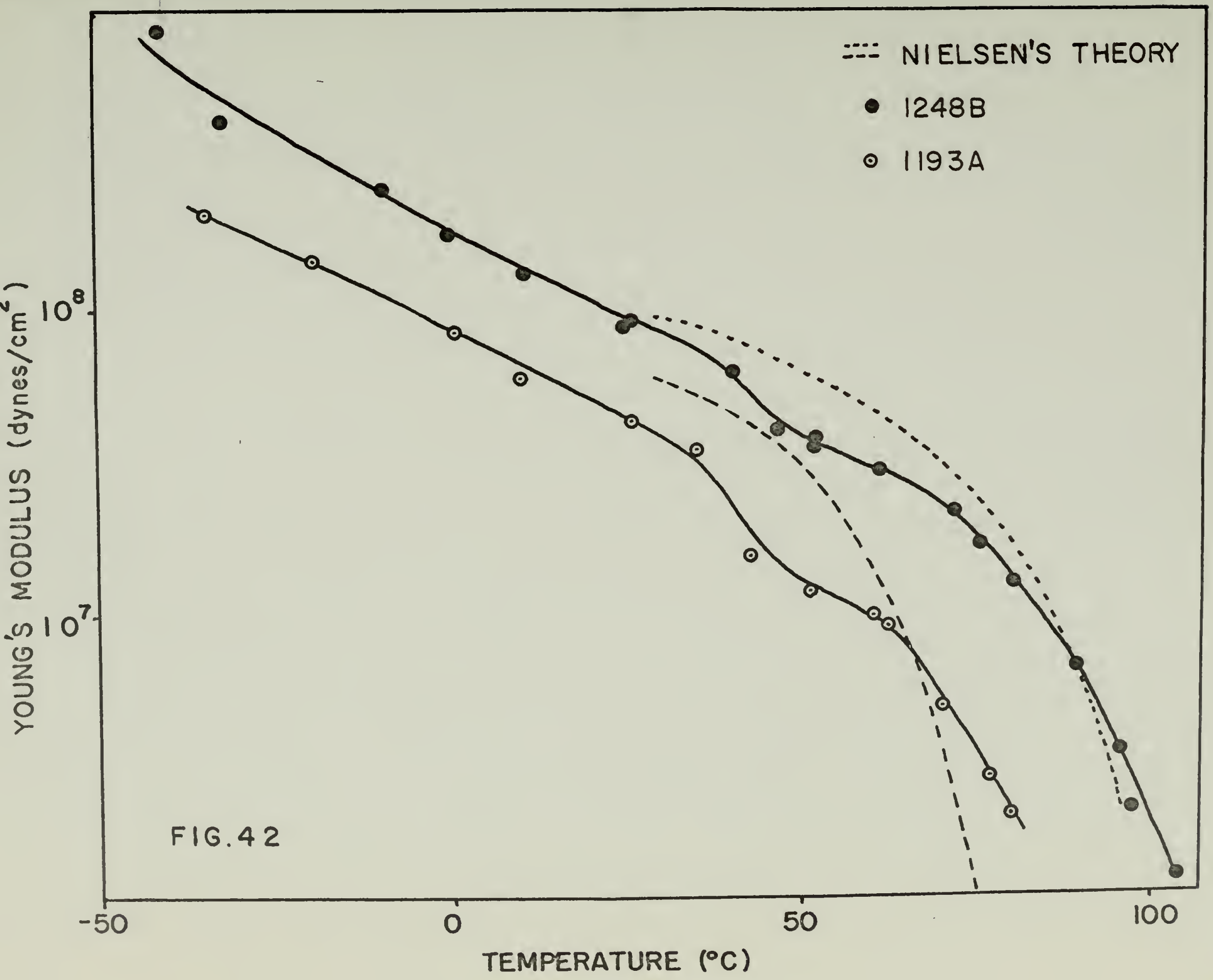
NIELSEN'S THEORY
1248B
1193A
YOUNG'S MODULUS (dynes/cm²)
10⁸
10⁷
-50
0
50
100
TEMPERATURE (°C)

FIG. 42

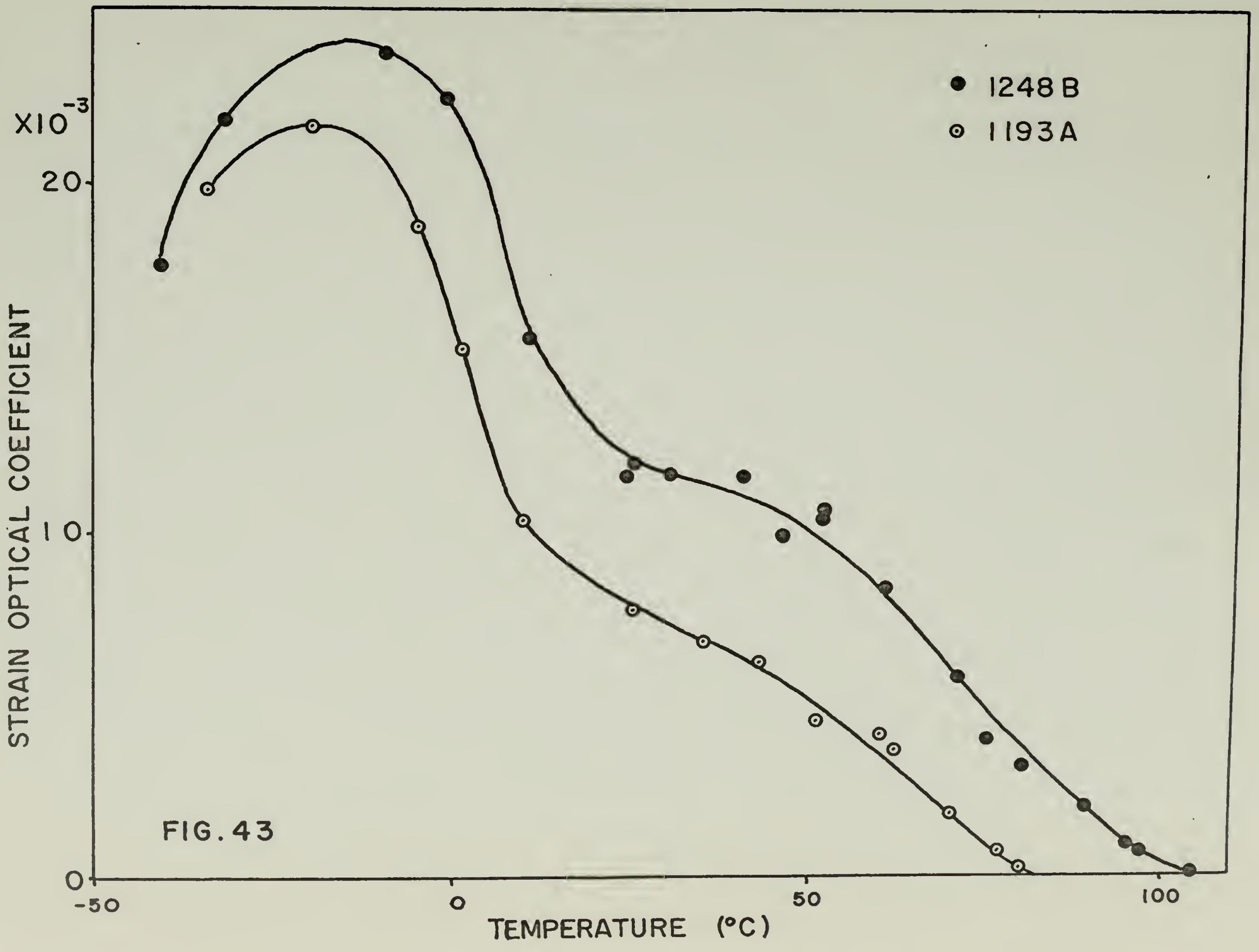
1248 B
1193 A
X10⁻³
20
0
-1
STRAIN OPTICAL COEFFICIENT
-50
0
50
100
TEMPERATURE (°C)

FIG. 43

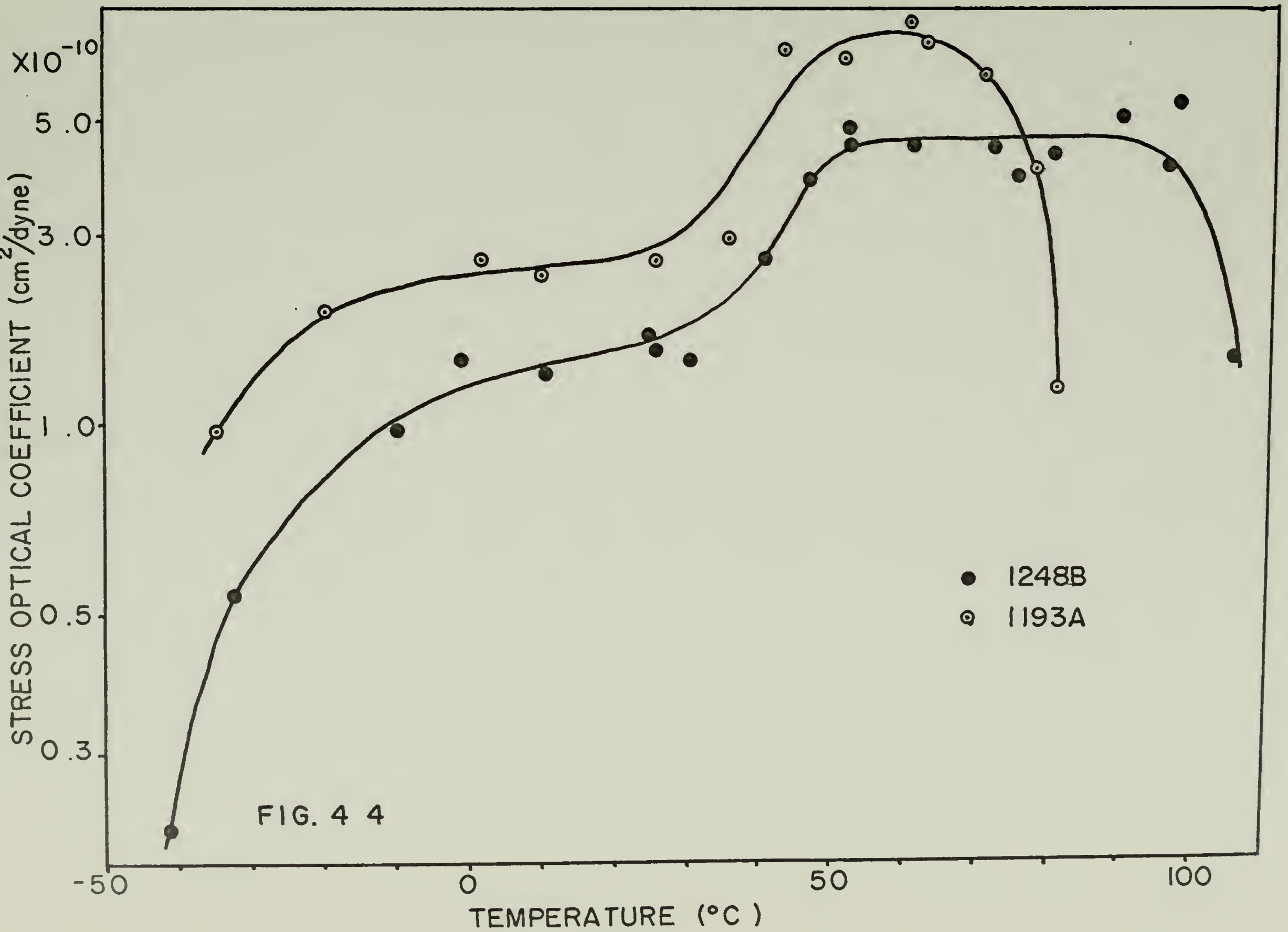
X10⁻¹⁰
5.0
3.0
1.0
0.5
0.3
STRESS OPTICAL COEFFICIENT (cm²/dyne)
1248B
1193A
-50
0
50
100
TEMPERATURE (°C)

FIG. 4 4

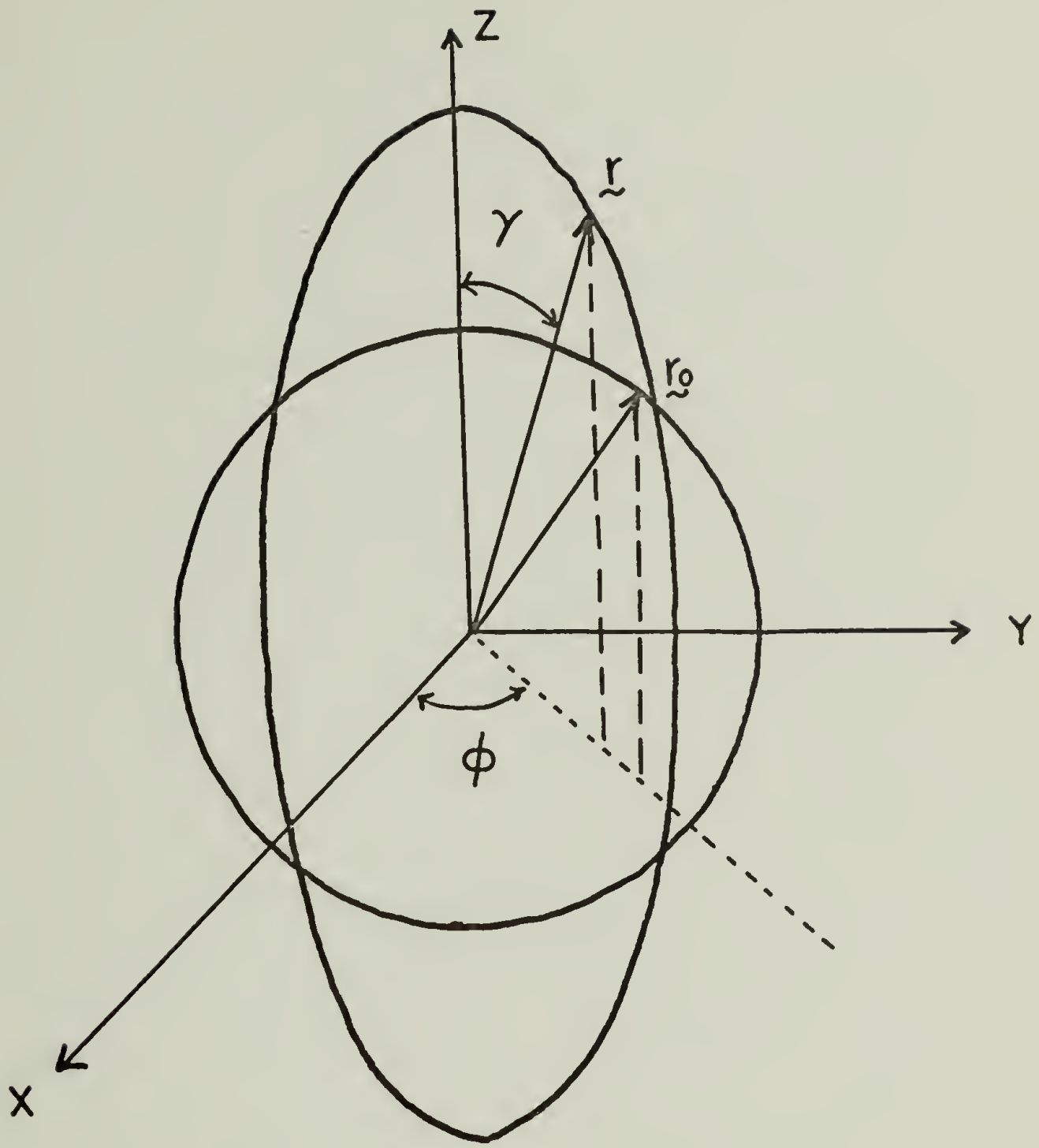

FIG. 45

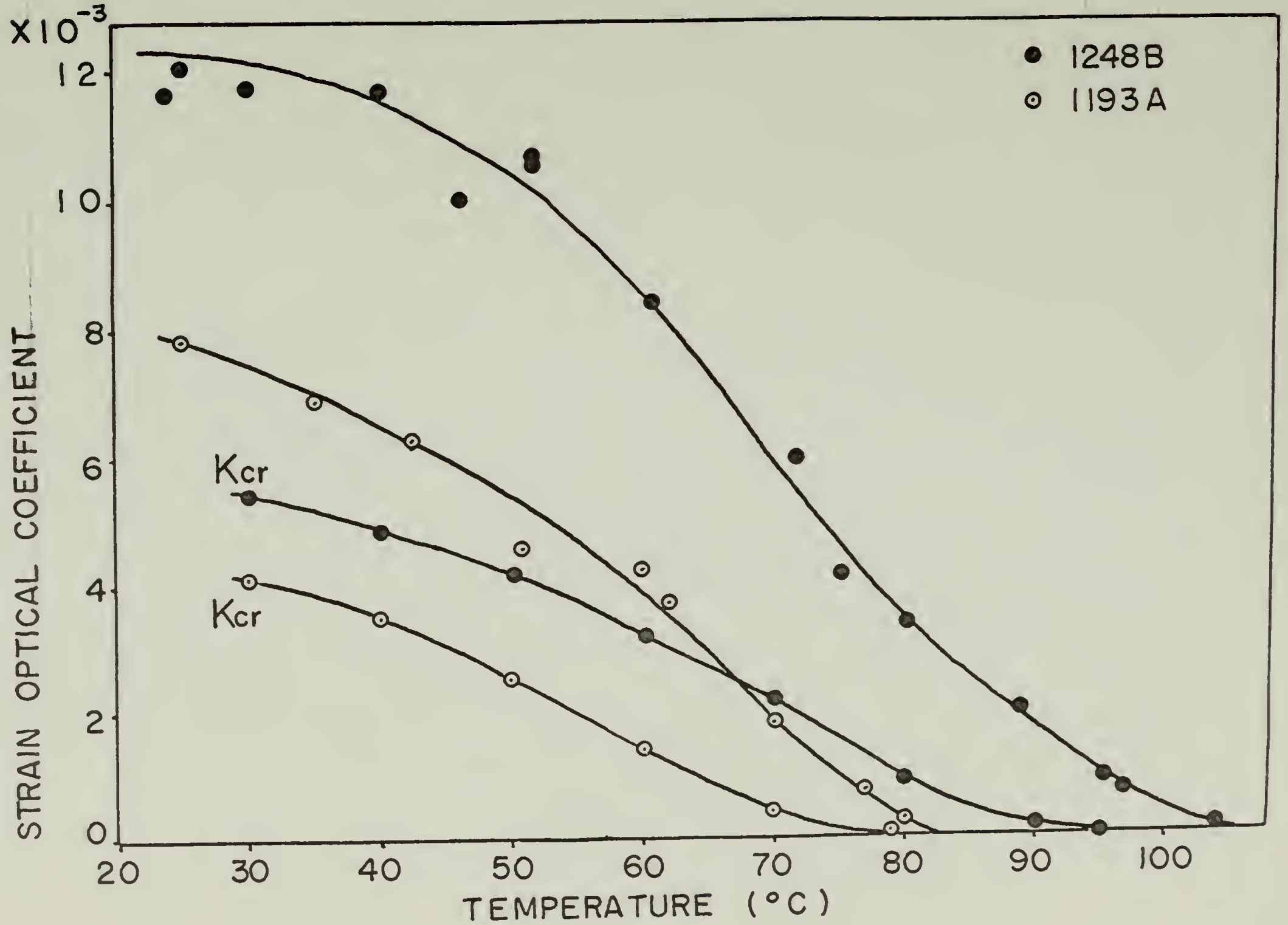
X10⁻³
12
10
8
6
4
2
0
STRAIN OPTICAL COEFFICIENT
1248B
1193A
Kcr
Kcr
20
30
40
50
60
70
80
90
100
TEMPERATURE (°C)

FIG. 46

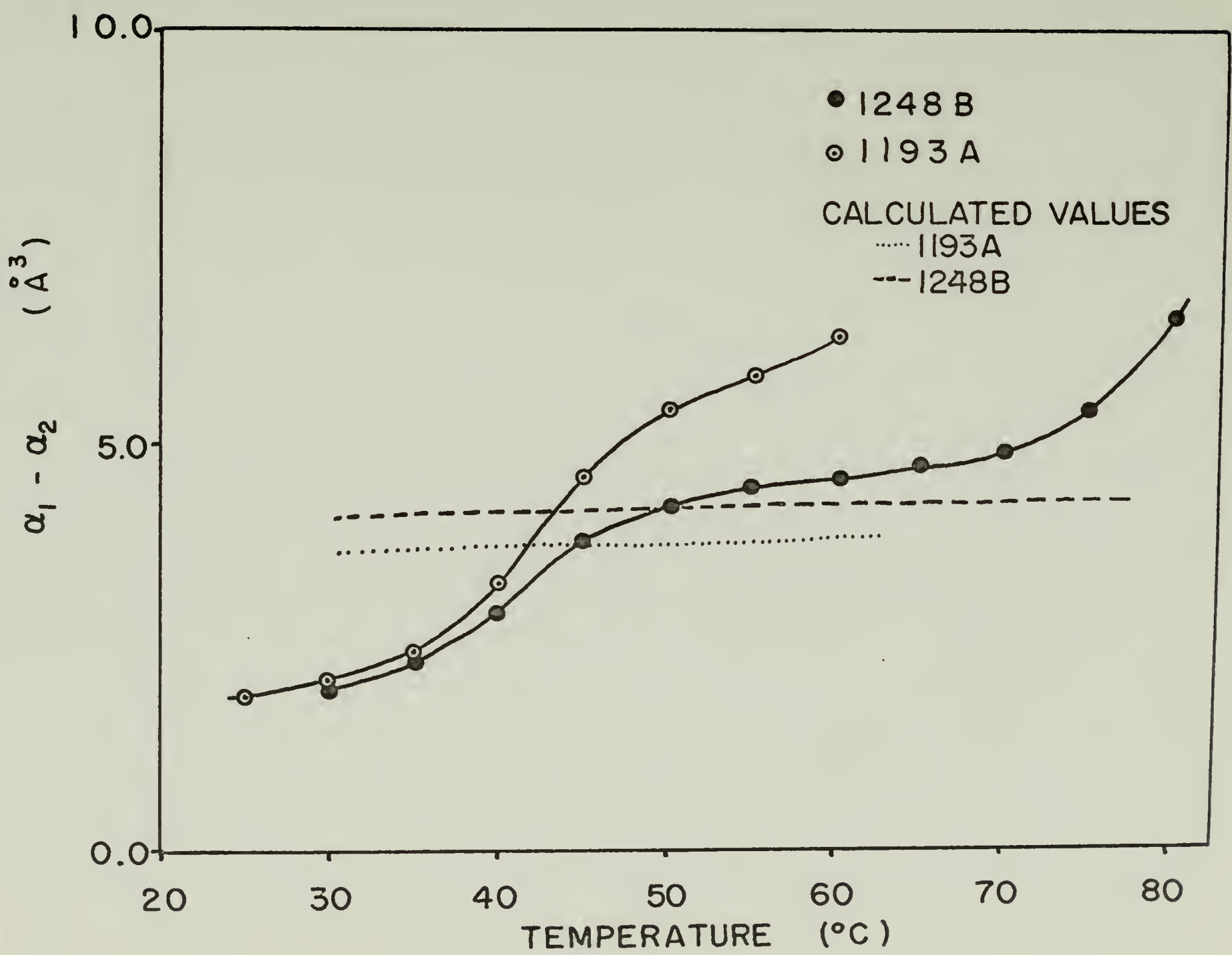
10.0
5.0
0.0
$\alpha_1 - \alpha_2$ ($\AA^3$)
1248 B
1193 A
CALCULATED VALUES
1193A
1248B
20
30
40
50
60
70
80
TEMPERATURE (°C)

FIG. 47

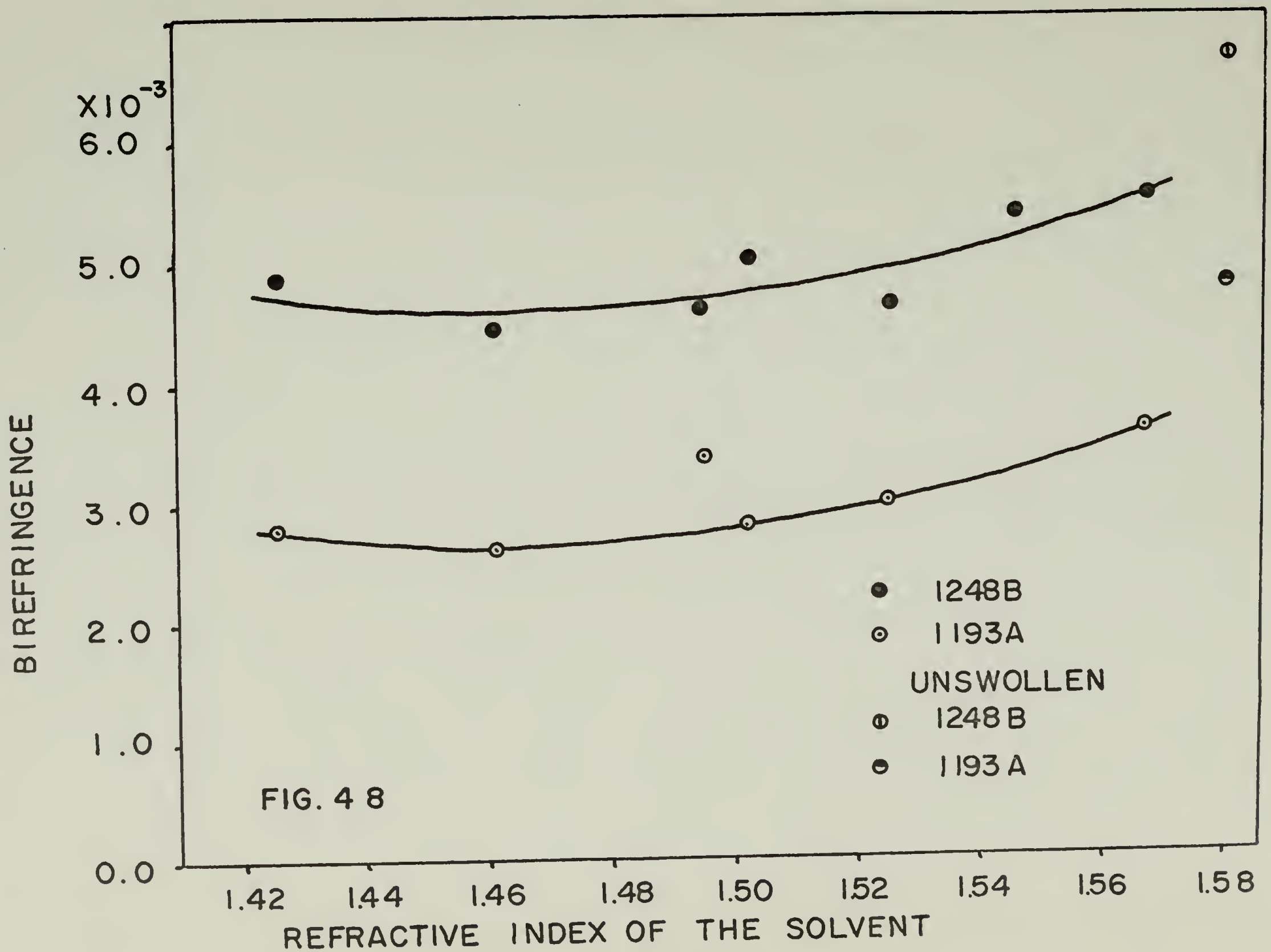
X10⁻³
6.0
5.0
4.0
3.0
2.0
1.0
0.0
BIREFRINGENCE
1.42
1.44
1.46
1.48
1.50
1.52
1.54
1.56
1.58
REFRACTIVE INDEX OF THE SOLVENT
1248B
1193A
UNSWOLLEN
1248B
1193A

FIG. 4 8